STRUCTURAL AGING OF THE UTRICULAR MACULA IN MICE

By

Jessica Pierce

November, 2012

Director of Dissertation: Sherri M. Jones, PhD

Major Department: Communication Sciences and Disorders

CBA/CaJ is a mouse strain that has no known genetic mutations affecting the inner ear, thereby serving as a control model for auditory and vestibular aging. C57BL/6J and CE/J mouse strains carry the genetic mutation *Cdh23*^{753A} (*Ahl),* which results in early-onset, age-related hearing loss. CBA/CaJ and CE/J mice both exhibit an age-related decline in gravity receptor function, with function declining at a considerably faster rate in the CE/J strain than in the CBA/CaJ strain. C57BL/6J mice exhibit minimal declines in gravity receptor function with age. The purpose of this study was to characterize the effect of age on three structures within the utricle of the inner ear; hair cells, synaptic ribbons, and post-synaptic receptor sites - all of which are critical to sensory transduction, and compare structural aging with gravity receptor functional data across the lifespan. Utricles were dissected, stained with CtBP2 (marker for hair cell nuclei and synaptic ribbons) and Shank1a (marker for post-synaptic receptor sites), and imaged using confocal microscopy. Structures were quantified and averaged over four distinct areas of the utricle at several age points across the lifespan. For the CBA/CaJ strain, the number of hair cells and CtBP2 per hair cell declined by the oldest age group while Shank1a and synaptic colocalization counts per hair cell remained relatively stable across the lifespan. All structures

measured for the C57BL/6J and CE/J strains were maintained with age. When compared with aging gravity receptor functional data, structural results for the CBA/CaJ and C57BL/6J strains were relatively consistent with their corresponding function. Maintenance of structural elements as observed for CE/J mice is disparate from severe age-related gravity receptor dysfunction observed for this strain. Overall, results suggest that presynaptic elements may play a role in normal age-related gravity receptor dysfunction while the presence of *Ahl* does not appear to result in a significant loss of vestibular structure with age. Additional influences must be responsible for age-related declines in gravity receptor function observed in the CE/J strain.

STRUCTURAL AGING OF THE UTRICULAR MACULA IN MICE

A Dissertation

Presented to the Faculty of the Department of Communication Sciences and Disorders

East Carolina University

In Partial Fulfillment of the Requirements for the Degree

Au.D/Ph.D

By

Jessica Pierce

November, 2012

STRUCTURAL AGING OF THE UTRICULAR MACULA IN MICE

by

Jessica Pierce

APPROVED BY:

DIRECTOR OF DISSERTATION/THESIS: _____

Sherri M. Jones, PhD

COMMITTEE MEMBER: _____

Timothy A. Jones, PhD

COMMITTEE MEMBER: _____

Jamie L. Perry, PhD

COMMITTEE MEMBER: _____

Xiangming Fang, PhD

COMMITTEE MEMBER

CHAIR OF THE DEPARTMENT OF CSDI: _____

Gregg D. Givens, PhD

DEAN OF THE GRADUATE SCHOOL: _____

Paul J. Gemperline, PhD

ACKNOWLEDGEMENTS

I would like to thank my parents, who have provided unending support throughout my entire life. Their dedication and confidence in me to succeed has been invaluable.

Special thanks to Dr. Teresa Lever and Dr. Sarath Vijayakumar for their wonderful guidance throughout the formulation of the confocal protocol and data gathering process. Thank you to my committee members for sharing their wealth of knowledge and expertise needed throughout this process. I would especially like to thank Dr. S. Jones for all of her dedication to helping students succeed and for her tremendous advocacy and support throughout my graduate career. This research was supported by NIH RO1 DC006443, NIH R01 DC006443-S1, and a Student Investigator Vestibular Research Grant funded by the American Academy of Audiology and the American Institute of Balance Education Foundation.

TABLE OF CONTENTS

LIST OF TABLES

LIST OF FIGURES

CHAPTER I: REVIEW OF THE LITERATURE

Introduction

Although aging and its effects on the auditory system have been studied a great deal over the past century, relatively little is known about the contribution of aging on structures in the vestibular system. Studies assessing vestibular functional aging have suggested that elderly individuals fair poorer on measures like vestibulo-ocular reflex (VOR) and optokinetic nystagmus (OKN; Baloh, Jacobson, & Socotch, 1993; Kerber, Ishiyama, & Baloh, 2006; Paige 1992, 1994) than their younger counterparts. Functional declines have also been reported in animal models (Jones et al., 2005; Jones et al., 2006; Mock, Jones, & Jones, 2011).

Vestibular functional declines with age can present significant concerns for the elderly. It is estimated that 25 to 39% of those 65 years or older fall each year (Keskin et al., 2008). Approximately 24% of individuals who fall will sustain some form of severe injury that requires medical attention or results in a fracture or restriction of activity (Means, Rodell, & O'Sullivan, 2005). Over 1.6 million older individuals are estimated to visit emergency departments for fall-related injuries each year (National Institute on Aging, 2006). For the elderly, falling may lead to extended stays in hospital settings, or even nursing homes (Means et al., 2005). This can have significant implications on quality of life, in that many of those who fall fear falling again, and therefore limit their daily activities. Balance difficulties can have detrimental effects on an individual's sense of control and independence.

In the twentieth century, the population of elderly individuals living in the United States dramatically increased. From 1904 to 1994, the number of individuals over the age of 65 grew from 3 million to 33 million. This number is projected to double to more than 80 million by the year 2030. As of 1994, about 1 in 8 Americans were elderly. By current projections, 1 in 5

Americans will be elderly by 2030 (Hobbs, n.d.). As the number of elderly individuals continues to rise, the need for care and treatment regarding conditions that the elderly face will become more relevant. In order for health care professionals to provide proper care and better intervention strategies, more research needs to be conducted to help us understand the etiology of observed declines in gravity receptor function with age.

Our ability to maintain balance is heavily influenced by the vestibular system in the inner ear, which detects and encodes head movement. In addition to the vestibular system, balance is impacted by the proprioceptive and visual systems. Together, these processes influence our overall ability to maintain proper balance. With age, degeneration of the vestibular, proprioceptive, and visual systems occurs, which can significantly impact one's ability to maintain postural control. Although numerous studies have shown that vestibular function declines with age (Baloh et al., 1993; Jones et al. 2005, 2006; Kerber, Ishiyama, & Baloh, 2006; Mock, 2008; Mock, Jones, & Jones, 2011; Shiga et al. 2005), the underlying etiology remains unclear. A few published studies have reported structural declines in gravity receptor organs from human temporal bones and animal models, including a reduction in the quantity and quality of otoconia (Jang, Hwang, Shin, Bae, & Kim, 2006), stereocilia integrity (Bloom & Hultcrantz, 1994; Rosenhall & Rubin, 1975), hair cell number and density (Park, Hubel, & Woods, 1987; Rauch, Velazquez-Villasenor, Dimitri, & Merchant, 2001; Richter, 1980; Rosenhall & Rubin, 1975), and neural components (Leonard & Kevetter, 2007; Stamataki, Francis, Lehar, May, & Ryugo, 2006;), however, data are sporadic at best. Moreover, structures have never been correlated with gravity receptor functional aging.

The current research quantified three structures of interest within and surrounding the hair cell (hair cells, synaptic ribbons, post-synaptic receptor sites) in the utricle, and correlated

structural data with vestibular functional data at various ages across the lifespan. It was hypothesized that structural aging in the utricle would correlate with gravity receptor functional aging as measured by vestibular evoked potentials (VsEPs). Specifically, it was expected that structural changes in hair cells, synaptic ribbons, and post-synaptic receptor sites would coincide with and be predicted by functional changes in vestibular evoked potentials. Better understanding of the effects of structural changes on functional aging of the vestibular system will improve knowledge regarding vestibular aging and lead to better treatment strategies for balance-related concerns. The following review will provide an overview of vestibular anatomy and physiology, general aging, and age-related declines in the vestibular system.

Vestibular Anatomy and Physiology

The inner ear is comprised of two systems; the auditory and the vestibular system. Both systems are connected by a membranous labyrinth, which contains a potassium rich fluid called endolymph, similar to intracellular fluid. The membranous labyrinth is encased in an outer, bony labyrinth. The fluid within the bony labyrinth, known as perilymph, is high in sodium and is similar to cerebrospinal fluid. The auditory system consists of the cochlea, which contains the sensory organ for hearing; the organ of Corti. The vestibular sensory system is composed of five organs; two macular organs and three semicircular canals. The macular organs are composed of the utricle and saccule and their primary purpose is to detect linear accelerations of the head. The utricle is most sensitive to linear accelerations in the horizontal plane while the saccule is most sensitive in the vertical plane, although both organs are stimulated with linear head movement in any direction. The semicircular canals consist of the anterior (superior), posterior, and horizontal (lateral) canals. When the head is in the upright position, the anterior and posterior canals are positioned vertically at an angle of 45° from one another. The horizontal

canal is positioned approximately 30° above the horizontal plane. The semicircular canals are arranged in such a way that they form coplanar pairs. The ipsilateral anterior semicircular canal forms a coplanar pair with the contralateral posterior semicircular canal while the horizontal semicircular canals form coplanar pairs with one another. Connected to each semicircular canal is an ampulla which houses the neuroepithelium for each corresponding canal. The primary purpose of the semicircular canals is to detect angular accelerations of the head. The anterior, posterior, and horizontal semicircular canals are most sensitive to angular accelerations relative to the x (naso-occipital), y (interaural), and z (rostral-caudal) axes, respectively, commonly referred to as roll, pitch, and yaw (Della Santina, Potyagaylo, Migliaccio, Minor, & Carey, 2005; Reisine, Simpson, & Henn, 1988). However, each canal may be stimulated to some extent by angular head movement in a variety of directions near its preferred axis.

Each vestibular end organ contains thousands of hair cells, which are critical to the sensory transduction process. On the apical portion of each hair cell one finds stereocilia protruding from the cell. Stereocilia are hair-like structures arranged in a staircase pattern that are sensitive to movement such that changes in head position deflect the stereocilia. Deflection of the stereocilia toward the tallest stereocilium, or kinocilium, depolarizes the hair cell. Stereocilia deflection away from the kinocilium promotes hyperpolarization. Depolarization excites the hair cell, causing neurotransmitter to be released from the base of the hair cell. Alternatively, hyperpolarization inhibits the hair cell. Contacting each hair cell at the base are afferent nerve endings, which detect the neurotransmitter released from the hair cell and produce a neural impulse, which is then sent to the brain.

Overlying the macular hair cells is the otoconial membrane. Stereocilia of the hair cells are embedded into this gelatinous meshwork. Also embedded within the otoconial membrane

are small calcium carbonate crystals known as otoconia. The otoconia add mass to the otoconial membrane, shifting in response to linear accelerations of the head. Shifting of the otoconial membrane deflects the hair cell stereociliary bundle, which depolarizes or hyperpolarizes the hair cell. In the center portion of the otoconial organs lies the striola. Stereociliary bundles are oriented relative to the striola. In the utricle, the kinocilium are oriented toward the striola while, in the saccule, the kinocilium are oriented away from the striola. In the cristae, hair cells are surrounded by a gel-like substance known as the cupula. Surrounding endolymph moves in response to rotational acceleration and shifts the cupula. The movement of the cupula is detected by the stereocilia. Hair cells are oriented in the horizontal semicircular canals so that the endolymph motion toward the utricle will result in depolarization while the anterior and posterior semicircular canals are oriented so that movement of the endolymph toward the utricle results in hyperpolarization.

Once the stereocilia detect a change in linear or rotational head position, the process of transduction begins. Transduction in the sensory cells of the vestibular system occurs after stereocilia detect motion when the force imposed by the surrounding otoconial membrane in the macular organs and cupula in the semicircular canals cause the stereocilia to deflect. Movement of the stereocilia toward the kinocilium will increase tension in stereociliary tip-links, located apically on each stereocilium. This increased tension causes mechanically-gated channels to open and allow potassium to diffuse into the cell. The influx of potassium into the hair cell will depolarize the cell; consequently, the cell's resting potential will become less negative. Once depolarization occurs, voltage-gated channels located on the lateral portions of each hair cell will open and calcium will diffuse into the cell. This increase in calcium will further depolarize the cell, and will mobilize synaptic vesicles (tethered to the synaptic ribbon) to release from the

synaptic ribbon and bind to the plasma membrane, thereby releasing neurotransmitter from the hair cell. The neurotransmitter, thought to be glutamate, will diffuse across the synaptic cleft to the primary afferent terminals of the vestibulocochlear nerve (CN VIII), and trigger an action potential. In contrast, deflection of the stereocilia away from the kinocilium promotes hyperpolarization, causing the cell to become more negative and inhibiting the release of neurotransmitter.

The vestibular end organs contain two types of hair cells; type I and type II. Type I hair cells are flask-shaped and have a cup-like structure termed a chalice or calyx-nerve terminal that envelops the basal portion of the hair cell (Eatock, Rusch, Lysakowski, & Saeki, 1998). Type II hair cells are cylindrical in shape and are normally innervated by bouton nerve terminals post-synaptically. These hair cells are slightly larger (Park, Hubel, & Woods, 1987) as well as more likely to have thinner stereocilia compared to type I hair cells (Rusch, Lysakowski, & Eatock, 1998). Type I hair cells are concentrated in the striolar region of the otoconial organs and central cristae of the semicircular canals. Type II hair cells are concentrated in the extrastriolar regions of the utricle and saccule as well as peripheral regions of the crista (Eatock et al., 1998). Most mammals also have dimorphic afferent terminals, which are composed of both calyces and bouton nerve terminals, and are found to innervate both type I and II hair cells (Eatock et al., 1998). In the utricle of the chinchilla, for example, dimorphic afferents innervate 86% of the total number of hair cells (Fernandez, Goldberg, & Baird,1990).

The cell bodies of vestibular primary afferents are contained in Scarpa's ganglia, located in the internal acoustic meatus. The vestibular organs are innervated by two branches of the vestibulocochlear nerve (CN VIII), the superior vestibular branch and inferior vestibular branch. The superior vestibular branch innervates the utricle, the anterior, and the horizontal semicircular

canal. The inferior vestibular branch innervates the posterior semicircular canal. The saccule is innervated by both branches of the vestibular nerve (Kevetter & Perachio, 1986). From the vestibular organs, the superior and inferior vestibular branches travel together to the pontomedulary junction where they bifurcate and branch to different regions of the brain. The superior branch contains axons that synapse in the superior and medial vestibular nuclei and cerebellum. Axons from the inferior branch synapse in the medial, lateral, or inferior vestibular nuclei (Naito, Newman, Lee, Beykirch, & Honsubia, 1995).

Aging

As previously suggested, aging imparts substantial changes to physical, mental, and functional states of being in both humans and animal models. Characteristics of age-related hearing loss and vestibular dysfunction provide evidence for this decline. Although changes in structure and function with age are well known among all human and animal species, the reasons behind these changes are unclear.

Aging is a complex process. There are many theories that are used to explain the aging process; however, no single theory explains the complex nature of the changes that occur with aging. Moody (2009) describes five theories of aging: 1) wear-and-tear theory, in which the body wears out over time; 2) autoimmune theory, in which the immune system weakens over time, allowing the body to be more susceptible to autoimmune diseases such as rheumatoid arthritis; 3) aging-clock theory, in which the body is programmed like a clock, and a gland (such as the hypothalamus, thalamus, or pituitary gland) regulates physiological changes that occur with age; 4) cross-linkage theory, in which cross-linking compounds accumulate in collagen (protein) and limit cell function; and 5) cellular theory, in which the cell's ability to undergo division becomes impaired, preventing cellular repair.

Aging effects on the auditory system have been widely documented. Estimates of hearing loss range from 30 to 35% of individuals between the ages of 65 and 75. Almost 50% of those individuals over the age of 75 are estimated to have hearing loss (National Institute on Deafness and Other Communication Disorders, 2010). Cochlear pathologies associated with age-related hearing loss include a decline in the number and integrity of hair cells and supporting cells (Li & Hultcrantz, 1994), spiral ganglion cell degeneration (Sha et al., 2008), endocochlear potential decline (Gratton, Smyth, Lam, Boettcher, & Schmiedt, 1997), accumulation of lipofuscin in the outer hair cells (Li & Hultcrantz, 1994), changes in vascular supply (Brown, Miller, & Nuttall, 1995; Gratton & Schulte, 1995) and giant inner hair cell stereocilia (Li & Hultcrantz, 1994). According to Schuknecht (1964), morphological changes in the inner ear which are responsible for age-related hearing loss, or presbycusis, may be classified into four types: 1) sensory, with hair cell loss; 2) neural, with degeneration of CN VIII nerve primary afferents; 3) metabolic, with atrophy of the stria vascularis; 4) mechanical, with a decline in basilar membrane properties and function.

Similar to presbycusis, presbyvertigo, or age-related vestibular dysfunction, has been reported; although data are sparse (Walther & Westhofen, 2007). Presbystasis, or age related balance dysfunction, has been more commonly studied. Presbyvertigo is a multifaceted condition which may occur due to damage within the vestibular system and central relays. Degeneration of the vestibular nuclei and vestibular portion of CN VIII, as well as direct damage to the vestibular end organs has been reported with age (Johnson, 1971; Lopez, Honrubia, & Baloh, 1997). It is estimated that 40 to 50% of reported dizziness can be attributed to disorders of the vestibular system (Marchetti & Whitney, 2005). Apart from direct vestibular declines, other factors unrelated to the vestibular system which may cause dizziness among the elderly

include medications, as well as muscle strength, joint flexibility, and coordination (Means, et al., 2005). In addition, decreases in visual acuity, cross sensitivity, and depth perception have been reported among the elderly (Lord & Dayhew, 2001; Ivers, Cumming, Mitchell, & Attebo, 1998). Psychological factors relatively common among older individuals such as anxiety, depression, and stress may cause dizziness. Medical conditions can also increase the risk of dizziness and falls. Specific diseases prevalent to the elderly population include osteoporosis, heart disease, diabetes, cerebrovascular disease, and hypotension. The incidence of neurodegenerative diseases such as Parkinson's disease, Alzheimer's disease, and dementia also increases with age (Kerber et al., 2006). In addition, peripheral sensitivity (i.e., feet, hands, etc.) and reaction time may affect balance among the elderly (Jacobson & McCaslin, 2008). Despite multimodal losses of sensory function over time, age-related vestibular dysfunction cannot be fully attributed to sensory declines; rather, structural degeneration within the vestibular system may be responsible.

Vestibular Functional Aging

Vestibular functional declines have been reported in both humans and animal models. Reports of vestibular function have generally relied upon measures such as vestibuloocular reflex (VOR), optokinetic nystagmus (OKN), vestibular-evoked myogenic potentials (VEMPs), and posturography testing. Indirect inferences can be made with these measures, as they rely upon the functioning of other systems in addition to the vestibular system. Declines in gain (ratio of eye-velocity to head velocity) for VOR, OKN, and visual-VOR (VVOR) have been reported in humans (Baloh et al., 1993; Kerber et al., 2006; Paige, 1992, 1994). Baloh and colleagues (1993) measured VOR, OKN, and visual-VOR on individuals over the age of 75. The authors observed decreasing VOR gains among the elderly compared to young individuals as amplitude increased. In addition, OKN and visual-VOR revealed decreases in gain of slow-phase velocity

and an increased phase lead of eye velocity for higher amplitude stimuli, respectively. Alternatively, Peterka, Black, and Schoenhoff (1990) found no age-related declines in VOR gain. Age related changes on vestibular evoked myogenic potential (VEMP) testing have been documented. Individuals over the age of 60 tend to have smaller VEMP amplitudes than their younger counterparts (Basta, Todt, & Ernst, 2005; Su, Huang, Young, & Cheng, 2004). In addition, increased thresholds and longer latencies have been reported with VEMP testing (Ochi & Ohashi, 2003; Su et al., 2004). No consistent declining trend was observed during caloric testing on individuals across the lifespan (Peterka, Black, & Schoenhoff, 1990). Sensory organization testing among older individuals suggested a decline in the ability to maintain balance with age among asymptomatic individuals, beginning at the fourth decade onward. This finding suggests that even older individuals who report no vestibular symptoms may still exhibit a decline in the ability to maintain balance with age (Cohen, Heaton, Congdon, & Jenkins, 1996; Borah et al., 2007). Alternatively, increases in magnitude of sway were observed in altered somatosensory, and visual conditions during posturography (Peterka, Black, & Schoenhoff, 1990).

Among animal strains, only a few studies have measured vestibular function, with the majority of vestibular aging data from mouse models. Shiga and colleagues (2005) measured VOR in C57BL/6 mice between the ages of 3 weeks and 60 weeks. The authors showed limited decreases in VOR gain in older mice compared to younger mice, suggesting that vestibular function is largely maintained until at least 60 weeks of age. It was concluded that central compensation may have maintained the VOR since peripheral morphology declined. Jones et al. (2006) measured vestibular function in 19 inbred mouse strains, including CE/J mice, ranging in age from 35 to 389 days old. They found significantly elevated VsEP thresholds in the CE/J

strain with age, suggesting a decrease in vestibular function. In a separate study, Jones et al. (2005) measured VsEPs for CBA/CaJ and C57BL/6J mice. It was determined that both strains maintain vestibular function until at least 190 days old. Mock (2008) measured auditory and vestibular function for CE/J, C57BL/6J and CBA/CaJ mice over the lifespan. In this study, ABR and DPOAE results were obtained as a measurement of auditory function and VsEPs were obtained to directly measure vestibular function from CBA/CaJ mice between the ages of 1.7 and 23.8 months, C57BL/6J mice between 1.01 and 23.8 months and CE/J mice between 1.0 and 20.6 months. Results showed that macular function decreased at a faster rate in the CE/J and CBA/CaJ strains than in the C57BL/6J strain and that auditory function declined at a significantly faster rate than gravity receptor function (most pronounced in the C57BL/6J strain).

Auditory brainstem response measures indicate that both CE/J and C57BL/6J strains exhibit similar forms of progressive sensorineural hearing loss, demonstrating a profound loss beyond 12 months of age (Johnson, Erway, Cook, Willot, & Zheng, 1997; Keithley, Canto, Zheng, Fischel-Ghodsian, & Johnson, 2004; Mock, 2008; Ouagazzal, Reiss, & Romand, 2006; White, Burgess, Hall, & Nadol, 2000; Zheng, Johnson, & Erway, 1999). VsEPs show that gravity receptor function declines in CBA/CaJ and CE/J mice with age; however, C57BL/6NNia mice maintain vestibular function until late in life (Mock, 2008). Gravity receptor functional aging does not correspond with the decline of hearing for these strains and little is known about the structural changes that correlate with and may influence gravity receptor dysfunction.

Structural Declines with Age

Degradation of structures in the vestibular system has been reported with age. Qualitative and quantitative changes have been observed in structures such as otoconia,

stereocilia, hair cells, synaptic ribbons, and neural components. The following is a review of reported aging effects on structures in the vestibular system.

Otoconia

Otoconia are tiny crystallite substances made of organic and inorganic material that are embedded in the outer layer of the otoconial membrane of the utricle and saccule. Otoconia vary in shape, depending upon species (Jang et al., 2006). Typically, otoconia in humans are cylindrical in shape (Ross, Peacor, Johnson, & Allard, 1976) while normal otoconia in rats are circular with sharp tips (Jang et al., 2006). The central core of otoconia is mostly composed of organic material, usually a form of glycoprotein, while the periphery is mostly inorganic, and is primarily composed of calcium carbonate (Lundberg, Zhao, & Yamoah, 2006). Otoconia remain attached to the surface of the otoconial membrane by both surface adhesion and an interconnecting network of filaments (Lins et al., 2000) likely made of the collagen-like protein otolin (Murayama et al., 2002). The size of otoconia varies, depending on the animal. For example, otoconia in guinea pigs can vary greatly from anywhere between 0.1 μm-25 μm, while otoconia in humans average up to 30 μm (Jang et al., 2006). Otoconia add mass to the otoconial membrane, and shift in response to gravity and linear accelerations of the head, thereby causing the underlying otoconial membrane to move and displace the stereocilia.

The quantity of otoconia in humans is reported to be severely compromised with age (Walther & Westhofen, 2007). Johnsson (1971) and Ross et al. (1976) observed the otoconial membranes of the utricle and saccule in postmortem temporal bones of individuals across the lifespan for gross changes. A decline in the number of otoconia in the aged utricle, and especially the saccule, was observed; however, the data was not quantified. Igarashi, Saito, Mizukoshi, and Alford (1993) calculated the ratio of the number of otoconia in each macular

organ between young and older human temporal bones and the ratio of the number of otoconia between the utricle and saccule of both age groups. The ratio of otoconia (young:old) in the utricle of young and older human temporal bones was 100:42 while the otoconia ratio in the saccule was 100:21. These results suggest that the number of otoconia decreases with age in both macular organs, with the saccule demonstrating a larger decline in otoconia than the utricle.

Animals also demonstrate a reduced ability to regenerate otoconia with increased age. Some mammals such as mice and guinea pigs maintain the ability to regenerate otoconia in both the utricle and the saccule with the help of globular substances, which are secreted from the sensory epithelium throughout the lifespan and eventually mature into otoconia (Suzuki, Ikeda, & Takasaka, 1997). Evidence has shown that otoconia regeneration ability decreases with age. Suzuki and colleagues conducted a study in which the amount of globular substances was measured in the utricle of young (2 months) and older (6 months) C57BL/6J mice. The data suggested that older mice have a reduced ability to regenerate otoconia compared to the younger mice.

Qualitative changes in otoconia have also been found with age. Fragmented, pitted, and fissured otoconia as well as some giant otoconia along the outer edges of the utricle have been reported in rats (Jang et al., 2006). Similarly, reports of fragmented otoconia have been observed in human otoconia (Walther & Westhofen, 2007). Degenerated otoconia also show a roughened surface, often with fractures through the midsection of the otoconia body (Igarashi et al., 1993; Walther & Westhofen, 2007). The extent to which these changes alter function is unknown.

Conversely, other studies have found no changes in gross morphology or structure of otoconia in aging animals. For example, Mock (2008) examined the otoconia from the utricular maculae of CBA/CaJ, CE/J and C57BL/6J mice across the lifespan. Using scanning electron

microscopy, no observed differences were found in the appearance or number of otoconia of older mice compared to younger mice. It was conceived that otoconia could not account for the decline in gravity receptor function in the CBA/CaJ and CE/J strains with age. Similarly, Takumida and Zhang (1997) found no noticeable morphological differences in otoconia from the utricle of aging guinea pigs. One limitation from both studies was that decreases in otoconia were only qualitatively observed; these data were not quantified.

Stereocilia

In the macular organs, stereocilia are embedded into the otoconial membrane. Stereocilia are critical to the sensory transduction of vestibular information as movement of the otoconial membrane in the otoconial organs or cupula in the cristae from acceleration forces shears the stereociliary bundles, opening mechanotransduction channels at their tips. Stereocilia are connected to one another by tip-links and side-links. Each hair cell has one hair bundle that contains 30-300 stereocilia depending on species (Colclasure & Holt, 2003). Cadherin 23 encodes for cadherin, a protein that is vital to the normal development of inner ear structures as well as maintenance of the stereociliary tip links and lateral links (Di Palma et al., 2001; Lagziel et al., 2005; Rzadzinska, Derr, Kachar, & Noben-Trauth, 2005).

Studies have reported evidence of aging in stereocilia for both human and animal models, including decreased stereocilia organization, increased fragility, and stereocilia that are larger than normal. Some stereocilia are clustered together and in a few instances, complete fusion of stereocilia was observed (Bloom & Hultcrantz, 1994; Rosenhall & Rubin, 1975).

Hair Cells

Hair cells are critical to the sensory transduction of vestibular information. The number of hair cells in the utricle varies, depending upon species. Desai, Zeh, and Lysakowski (2004)

estimated a total of almost 3250 hair cells in the sensory epithelium of the adult CBA mouse utricle, while Severinsen et al. (2008) counted 12,000 hair cells in the utricle of guinea pigs. In humans, the total number of hair cells in the young utricular macula (16 gestational week to 15 years) is estimated to be 36,000 (Severinsen, Sorensen, Kirkegaard, & Nyengaard, 2010). In older human postmortem temporal bones (mean age: 82 years), the average number of hair cells in the utricle was 27,508 (Gopen, Lopez, Ishiyama, Baloh, & Ishiyama, 2003).

Previous data have shown both quantitative and qualitative degeneration of hair cells with age. Severinsen et al. (2008) described an age-related decline in the number of type I hair cells in guinea pigs, in which the number of type I hair cells decreased by 20%. Similar declines have been found in humans. Richter (1980) determined that the number of sensory hair cells in humans begins to diminish beginning around age 30. Hair cell density also degenerates with age. Park, Hubel, and Woods (1987) compared the vestibular organs of young and old C57BL/6NNia mice using light and electron microscopy. The authors discovered that hair cell density decreased in all five vestibular organs and was more pronounced in the cristae and the saccule than in the utricle. The percentage of hair cell decrease was 14% in the utricle, 19% in the saccule and posterior crista, 23% in the horizontal crista, and 24% in the anterior crista. A decrease in hair cell density with aging has also been reported in human tissue. Merchant et al. (2000) found that type I and type II hair cell densities in all five vestibular organs declined with age. Similarly, Rauch et al. (2001) estimated that, on average, total hair cell density at birth in humans is 76-79 hair cells/0.01mm^2 in the cristae, 68 cells/0.01mm^2 in the utricle, and 61 cells/0.01mm^2 in the saccule. In the elderly temporal bones studied, the cristae lost type I hair cells at a significantly faster rate than the macular organs while type II hair cell losses occurred at an equal rate for all 5 vestibular organs.

Qualitative differences with age have been seen in both animal and human models. In a study of human temporal bones, Rosenhall and Rubin (1975) found an increase in lipofuscin, an age-related pigment, inclusions in type I and II hair cells as well as in supporting cells; however, these inclusions were more pronounced in type I hair cells. Similarly, Gleeson and Felix (1987) found increased severity of lipofuscin in the oldest temporal bone of three human temporal bones studied. In a study of young, middle-aged, and old C57BL/6NNia mice, Park et al. (1987) found that large, dense, inclusions formed on the hair cells and supporting cells of the old mice.

Synaptic Ribbons

Synaptic ribbons are electron-dense organelles located near the base of inner ear auditory and vestibular hair cells as well as photoreceptors and bipolar cells in the retina which are believed to act as a conveyor belt, transferring a readily releasable pool of vesicles to fuse to the plasma membrane to provide temporally precise, graded information to the primary afferents of the vestibulocochlear nerve. They are positioned in close proximity to neurotransmitter release sites, or active zones. Synaptic ribbons release vesicles immediately following the opening of calcium channels. In addition, they supply a re-releasable pool of vesicles so that vesicle release continues during sustained depolarization (Matthews & Fuchs, 2010). Synaptic ribbons are mainly spherical in shape, although barrel or plate-shaped synaptic ribbons have also been reported (LoGuidice & Matthews, 2009; Lysakowski & Goldberg, 1997). In the mammalian hair cell, synaptic ribbons are typically less than 200 nm in length (Matthews & Fuchs, 2010). Synaptic ribbons typically occur singly or in groups of two or three; however, as many as five or six synaptic ribbons occurring together have been observed (Park, Hubel, & Woods, 1987). Due to variations in size, synaptic ribbons can tether between 20 and 400 vesicles (Moser, Brandt, & Lysakowski, 2006). In the cochlea, synaptic ribbons range in size depending upon the location

along the basilar membrane. For example, synaptic ribbons located along the base of the cochlea are larger in size and have a greater vesicle tethering capacity compared to those located at the apical end (Martinez-Dunst, Michaels, & Fuchs, 1997; Schmitz, 2009). Ten to 20 synaptic ribbons are estimated to be present per inner hair cell in the cochlea (Liu, Li, & Jiang, 2009; Sterling & Matthews, 2005). In the crista ampullaris, estimates of synaptic ribbon counts range from five to 20 synaptic ribbons per type I hair cell, depending upon species (Lysakowski & Goldberg, 1997; 2008). The structural components of synaptic ribbons in auditory and vestibular hair cells are only beginning to be understood. Because of the large number of photoreceptor cells in the retina and the accessibility of the retina, more is known about the molecular structure of synaptic ribbons in the visual system (Nouvian, Beutner, Parsons, & Moser, 2006). Knowledge of the composition of visual-related synaptic ribbons can help us understand more about synaptic ribbons in the auditory and vestibular systems. One protein unique to the synaptic ribbon is RIBEYE (LoGuidice & Matthews, 2009; Zenisek, Horst, Merrifield, Sterling, & Matthews, 2004), which provides structural support to the synaptic ribbon (Nouvian et al., 2006). Other proteins found in the architecture of the synaptic ribbon include C-terminal binding protein 1 (CtBP1), C-terminal binding protein 2 (CtBP2), Rab3 interacting molecule 1 (RIM1), Rab3 interacting molecule 2 (RIM2), Bassoon, and Piccolo. Bassoon is necessary to anchor the synaptic ribbon to the plasma membrane (Khimich et al., 2005). Currently, very little is known regarding the effect of age on synaptic ribbons. A few studies have shown that abnormalities in synaptic ribbon structure can affect auditory function. Khimich and colleagues discovered that mice lacking the protein Bassoon had reduced auditory function compared to their normal counterparts. Similar results were found in homozygous *Bsn* mutant mice, which lack Bassoon in photoreceptor synaptic ribbons (Dick et al., 2003). These results suggest that a decreased

number of properly functioning synaptic ribbons can negatively impact function. Whether synaptic ribbons in the vestibular system decrease with age in a similar manner across all strains remains unclear. In a comparative study of young and old C57BL/6NNia mice, Park and colleagues reported that synaptic ribbons in the vestibular organs appeared to be well preserved with age; however, the data were not quantified.

Neural Components

Most type I and type II hair cells in the vestibular organs are innervated by dimorphic nerve afferents. These nerve terminals pick up the neurotransmitter glutamate released into the synapse during exocytosis and are critical for the transduction of vestibular input from chemical to electrical energy necessary for transfer via the vestibulocochlear nerve to the brain.

Evidence has shown that neural degeneration occurs in both the auditory and vestibular systems. Stamataki et al. (2006) compared the number of afferent contacts with the inner hair cells in C57 mice of different ages (2-3 months and 8-12 months) by assessing the number of synapses formed between afferent nerve fibers and the inner hair cell. They found a mean of 16.8 ± 2.4 synapses for the younger group and 9.2 ± 3.1 synapses for the older group showing that, on average, the number of primary afferents in the auditory system decreased with age. Leonard and Kevetter (2007) assessed the structural integrity of calyx nerve endings in the cristae ampullaris for young (3-11 months) and old (35 months and older) gerbils by injecting a calyx-identifying tracer. They found that younger gerbils exhibited well-pronounced calyces, while calyces for the older gerbils were missing from the epithelium. The effect of age on glutamate receptors within the vestibular system is currently unknown.

Statement of the Problem

Although our ability to maintain balance often declines with age, the structural changes related to this functional decline are not completely understood. Published studies have reported structural declines in gravity receptor function in human temporal bones and animal models, including a reduction in the quantity and quality of otoconia (Jang et al., 2006), stereocilia integrity (Bloom & Hultcrantz, 1994; Rosenhall & Rubin, 1975), hair cell number and density (Park et al., 1987; Rauch et al., 2001; Richter, 1980; Rosenhall & Rubin, 1975), and neural components (Leonard and Kevetter, 2007; Stamataki et al., 2006), however, data are sporadic at best. The overall goal of this research was to characterize structural correlates of gravity receptor functional aging. Structures were quantified within and surrounding the hair cell (hair cells, synaptic ribbons, post-synaptic receptor sites) in the utricle and correlated with vestibular functional data at various ages across the lifespan. It was hypothesized that aging in the utricle would correlate with gravity receptor functional aging as measured by VsEPs. Specifically, it was anticipated that quantitative changes in the number of hair cells, synaptic ribbons, and post-synaptic receptor sites would coincide with and be predicted by functional changes in VsEPs. Specific aim 1 examined structures in two mouse strains (CBA/CaJ and CE/J) which demonstrated different rates of decline in gravity receptor function with age. Structures were predicted to be most affected for CE/J mice, which demonstrate the greatest loss of vestibular function, followed by CBA/CaJ mice. Specific aim 2 sought to quantify structures in one mouse strain (C57BL/6J) which maintains gravity receptor function even into advanced age. A limited loss of structure in the C57BL/6J mouse strain was expected, as gravity receptor function is well preserved, even at advanced ages. Specific aim 3 sought to correlate structural data with age-

matched gravity receptor functional data for each strain as measured by VsEPs (reported previously by Mock, 2008).

Research Questions

1. What is the effect of age on structure in the utricle of the vestibular system?
2. How well do structural changes in the utricle with age correlate with functional declines observed with age?

CHAPTER II: METHODS

Overview of the Experiment

Gravity receptor function ages at different rates for CBA/CaJ, CE/J, and C57BL/6J strains and little is known about the structural changes that correlate with and may influence gravity receptor dysfunction. Structures were quantified in the utricle using confocal microscopy at age points representing young (6 months), middle (12 months) and old ages (18 months; 22 months). Structures of interest were hair cells, synaptic ribbons, and post-synaptic receptor sites. The current research was the first study to correlate structure with direct functional assessments in the vestibular system. Greater understanding of the effects of structural changes on functional aging of the vestibular system will improve knowledge regarding vestibular aging and provide better treatment strategies for balance-related concerns. The proposed research examined following hypothesis: structural aging in the utricle will correlate with gravity receptor function as measured by VsEPs.

Animals

Mice were purchased from The Jackson Laboratory and housed using standard husbandry until the appropriate ages for use. The animals were kept at room temperature with a light/dark cycle of 12 hours and given unlimited access to food and water. Animal care was supervised by the Department of Comparative Medicine at East Carolina University and all experimental protocols were approved by the East Carolina University Animal Care and Use Committee.

Mice are ideal for this research because 1) they have a relatively short lifespan (about two years), which is appropriate as well as feasible for aging research; 2) the mouse inner ear is structurally similar to humans, possessing similar genes that develop the inner ear; 3) data concerning function of the vestibular system are available in many mouse strains; and 4) several

mouse strains have been identified as models for human diseases and disorders, including inner ear disorders. The specific strains used in the current research are CBA/CaJ, C57BL6/J, and CE/J. These mouse strains were chosen because they are commonly used for inner ear research, particularly C57BL/6J and CBA/CaJ, and gravity receptor functional data are available for ages ranging from 2 to 24 months (Mock, 2008; Mock, Jones, & Jones, 2011).

Several genetic mutations have been discovered which result in early-onset, age-related hearing loss. *Ahl, or* $Cdh23^{753A}$, is a genetic mutation located on chromosome 10 which affects cadherin, a protein that is vital to the normal development of inner ear structures as well as maintenance of stereociliary tip links and lateral links (Di Palma et al., 2001; Lagziel et al., 2005; Rzadzinska et al. 2005). $Cdh23^{753A}$ was the first gene identified which causes late-onset, non syndromic hearing loss in mice (Johnson, Erway, Cook, Willot, & Zheng, 1997). *Ahl3* is located on chromosome 17 (Nemoto et al., 2004). The effect of $Cdh23^{753A}$ on gravity receptor function cannot be easily predicted. Previous studies measuring structural changes alone have provided some evidence that normal aging does indeed affect the number and integrity of structures within and surrounding the macular hair cells (i.e., otoconia, stereocilia, hair cells, neural components, etc.). What is unknown is if the presence of *Ahl* will affect normal degeneration of these structures with age.

C57BL/6J and CE/J carry $Cdh23^{753A}$, which results in early-onset age-related hearing loss. In addition, C57BL6/J mice carry another genetic mutation, *Ahl3*. The C57BL/6J and CE/J strains develop profound hearing loss with age; however, gravity receptor function declines at a significantly faster rate in the CE/J strain than in the C57BL/6J strain. In contrast, CBA/CaJ mice have no known genetic mutation that affects inner ear structures, exhibiting mild auditory and vestibular functional decline due to age alone.

A total of 50 temporal bone samples were obtained from CBA/CaJ (n = 14 temporal bones), C57BL/6J (21 temporal bones), and CE/J (15 temporal bones) mice at young (6 months), middle (12 months), and old ages (18-19 months; 20-22 months) for use in immunohistochemistry and confocal imaging.

Immunohistochemistry

Each animal was given a lethal injection of Sodium Pentobarbital (390 mg/ml) intraperitoneally and the temporal bones were dissected. Once separated from the skull, each temporal bone was post-fixed overnight in 4% Paraformaldehyde in 0.1 M Phosphate Buffer at room temperature. Specimens were rotated during post-fixation. Following fixation, the utricle was removed from the temporal bone and the otoconia and otoconial membrane were gently scraped off while in 0.01 M Phosphate Buffered Saline with 3% Triton (PBST; 0.3 M Sodium Chloride, 0.3% Triton-X 100, 0.01 M Phosphate Buffer, pH 7.4). Each specimen was washed with PBST three times for 15 minutes each at room temperature with rotation. Blocking solution (10% Normal Goat Serum in PBST) was applied overnight at 4˚C with rotation. The specimens were incubated in a primary antibody cocktail (Mouse anti-CtBP2: C-terminal binding protein 2; BD Transduction Laboratories; 1:300; Rabbit anti-Shank1a: Neuromics; 1:300) for 48 hours at 4°C with rotation. Following incubation, the specimens were washed in PBST three times for 50 minutes each at room temperature with rotation. Secondary antibodies were applied in a cocktail (CtBP2: Alexa 488 goat-anti-mouse RED-Invitrogen; 1:200; Shank1a: Alexa 633 goat-anti-rabbit GREEN-Invitrogen; 1:200) overnight at 4°C with rotation (once secondary antibodies are applied, the specimens were shielded from light). Each sample was washed with PBST three times for 20 minutes each at room temperature with rotation. The specimens underwent three final washes (15 minutes each) in 0.01 M Phosphate Buffered Saline at room temperature while

shaking. Following the washes, the specimens were mounted on a slide with ProLong® Gold antifade reagent (Invitrogen) and cover slipped.

Antibodies against transcriptional repressor carboxy-terminal binding protein (CtBP2) are similar to antibodies used against RIBEYE and stain both synaptic ribbons and hair cell nuclei (Khimich et al., 2005). Shank1a is an antibody used to stain Shank1 proteins located within the post-synaptic receptor site (Sheng & Kim, 2000; Naisbitt et al., 1999). Antibody specificity was confirmed by blocking CtBP2 and Shank1a staining with blocking peptides.

Confocal Microscopy

Specimens were viewed with an inverted Zeiss LSM 510 Confocal microscope (Figure 2.1) and images captured with Zen LSM 510 Version 4.2 SP1 software (Carl Zeiss MicroImaging GmbH, Jena, Germany). The 488 (25% intensity) and 633 (30% intensity) laser lines were used to view fluorescence. A complete description of confocal properties is located in Table 2.1.

Each utricle was divided into four quadrants: two areas medial to the striola (quadrants 1 and 2) and two areas lateral to the striola (quadrants 3 and 4). One area was chosen within each quadrant to be viewed more closely (Figure 2.2). Areas were chosen based upon their quality (no fissures, tears, gaps, etc. in the imaged area of the epithelium). Laser light was passed through the confocal microscope, exciting the fluorescent sample. The fluorescent light was reflected off the sample and through the microscope.

Confocal microscopy is beneficial because, unlike light and electron microscopy techniques, confocal imaging allows one to view structures deep inside the tissue and reconstruct separate images to create one composite image. Unlike conventional microscopes, the confocal microscope is ideal for thick specimens such as a utricular whole mount, as the microscope can

focus on a thin optical slice within the specimen. Other forms of microscopy will only focus thick specimens if the z-dimension does not exceed the optical wave depth of focus allowed by the objective in use. Should the optical wave depth not meet this criterion, focused light from the image will be combined with out-of-focus light from planes outside the plane of focus (LSM 510 user manual, 2009). In addition, confocal microscopy allows a 3-dimensional image or z-stack to be created by capturing thin optical slices at controlled increments along the z axis.

Filters

Four types of filters are typically used with a confocal microscope: 1) short-pass filters permit wavelengths shorter than a specified wavelength, 2) long-pass filters cut-off wavelengths shorter than a specified wavelength, 3) band-pass filters permit light within a specified wavelength range, and 4) dichroic mirrors separate excitation light from emitted light.

The 633 and 488 fluorophores will be filtered to permit only those wavelengths of interest to pass through. Filters of a slightly higher wavelength pattern will be applied to each channel to alleviate problems associated with the Stokes shift, which refers to the wavelength difference that occurs between the excitation spectra and the emission spectra. The Stokes shift usually causes the emission spectrum peak to occur at a wavelength that is 20 to 100 nm longer than that of the absorption peak spectrum (Pawley, 2006). Therefore, a longpass 650 lightpath will be used to filter the 633 fluorophore and a bandpass 505 lightpath will be applied to 488 fluorophore.

Objectives

Images were captured at a low magnification using a Plan-Neofluar 10x/0.3 NA objective with a scan speed of 5. To view images at a higher magnification, a C-Apochromat 63x/1.2 NA water-immersion objective was used with 3x scan zoom.

Nyquist Frequency

To prevent aliasing, in which an image is oversampled or undersampled, of image characteristics, the Nyquist theorem was applied when determining the image sampling rate in the z axis. Oversampling would promote more sampling than is necessary in which no additional information is obtained, decreasing the signal-to-noise ratio. With undersampling, insufficient sampling would occur such that information regarding the sample is lost. Undersampling would result in a loss of fine structural detail (LSM 510 user manual, 2009). Application of the appropriate sampling in the z axis ensured that fine image characteristics were preserved. Therefore, all images were scanned at 512 x 512 pixels at optimal z interval corresponding to the Nyquist frequency (0.16 μm).

Pinhole

Light was passed through a confocal aperture, or pinhole. The pinhole is situated in front of the image plane. The pinhole was used to permit only light within the focal plane to be measured by the photomultiplier tube, thus rejecting all light which is out of focus. Optimal pinhole properties were used for each specimen according to the objective lens numerical aperture and magnification to match the diameter of an Airy disk (one Airy unit). This allows for satisfactory z-resolution without reducing the number of photons that pass through the pinhole. Opening the pinhole beyond that of one Airy unit increases the number of photons detected but reduces the resolution of the image as a larger pinhole detects photons from other planes beyond the focal plane (Pawley, 2006). In contrast, a less than optimal pinhole will decrease the number of photons detected by the photomultiplier tube, thereby requiring more laser exposure which has the potential to cause photobleaching of the specimen.

The illuminated point from the image and the point observed were focused onto one another to create a confocal beam path (LSM 510 user manual, 2009). Once the fluoresced light has been measured, each point in the sample was transferred to a computer, which constructed a 2D image of the sample. A 3D sample was constructed by combining 2D slices of the sample at different depths, beginning toward the apical (superficial) portion of the hair cell when synaptic ribbons and post-synaptic receptor sites were first observed and coursing deeper through the hair cell until synaptic ribbons and post-synaptic receptor sites were no longer observed.

Each Z-stack was analyzed using 3-D reconstruction under blinded conditions with Volocity 3D imaging software (PerkinElmer/Improvision, Waltham, MA). The number of hair cells, synaptic ribbons, and post-synaptic receptor sites was quantified in a 47.6 µm x 47.6 µm (2265.76 μm^2) area. Data was compared among different age groups within each strain and correlated with functional results using statistical analyses. Following quantification, structural data was correlated with age-matched VsEP thresholds as reported by Mock (2008) and Mock, Jones, and Jones (2011).

Data Analysis

Once the three dimensional z-stack was captured by computer, the image was saved on a USB drive. Each image was transferred to Volocity 3D imaging software for data analysis. To quantify hair cells and synaptic ribbons, each z-stack was opened and the Alexa 633 (green) channel was disabled, allowing only the Alexa 488 (red) channel to be visualized. Hair cells were then manually quantified in the imaged area by visualizing those cell nuclei which were oval in shape (to distinguish hair cell nuclei from supporting cell nuclei, which are hexagonal in shape) and placing a marker on each identified hair cell to prevent the hair cell from being counted twice.

To quantify synaptic ribbons, the series of 2D images which compose the 3D z-stack was examined sequentially. Each image was 0.16 µm thick. Those CtBP2 points which were observed in two or more consecutive images and no larger than one micron in diameter were counted as a synaptic ribbon. A marker was placed at each identified synaptic ribbon in order to prevent the synaptic ribbon from being counted twice.

Due to the increased level of background staining for the Alexa 633 antibody, post-synaptic receptor sites were quantified using a specialized protocol created with Volocity software. The Alexa 488 (red) channel was disabled, allowing only the Alexa 633 channel to be visualized. Under the Measurements tab, the Find Objects Using Intensity feature was implemented to identify illuminated points in the image. Then, a thresholding procedure was used to identify those points which represented post-synaptic receptor sites. All illuminated points were placed in order by the software according to size. The largest point that reliably appeared to represent a post-synaptic receptor site was identified (of average size compared to all points identified by the software, distinct specific staining, no bright clusters, etc.), and the volume was recorded as the upper limit for filtering (points bigger than the cutoff will be filtered out of the points identified by the software). Then the smallest measured point that reliably appeared to represent a post-synaptic receptor site was identified (of average size, not characteristic of image noise), and the volume was recorded as the lower limit for filtering (points smaller than the cutoff will be filtered out). Using the Exclude Objects by Size feature in the Volocity software, the lower limit and upper limit values were entered into the software, which then prompted the software to exclude all those points which were larger or smaller than the upper and lower limit volumes, leaving only those points which appeared to represent a post-

synaptic receptor site. The remaining identified points quantified by the software were then recorded as the number of post-synaptic receptor sites for that particular image.

Function Studies

After quantitative analysis of hair cell, synaptic ribbon, and post-synaptic receptor sites for these strains, structural data was compared to age-matched gravity receptor functional data measured with VsEPs as reported previously by Mock (2008) and Mock, Jones, and Jones (2011) to determine what structures of interest, if any, significantly correlated with gravity receptor functional aging. The use of VsEP data to characterize gravity receptor function was preferred to other measures used to evaluate vestibular function because other indicators such as OKN and VOR depend upon systems outside of the inner ear, and do not directly assess the macular end organs. Although these measurements are useful in assessing the integrity of entire reflex arcs, they are not direct measures of inner ear function. In contrast, VsEP measurements use subcutaneous far-field electrode recording strategies to detect evoked potentials from the vestibulocochlear nerve and central relays.

VsEP data gathered by Mock (2008) and Mock, Jones, and Jones (2011) was used for correlation with structural data performed in this research. Protocols for VsEPs are thoroughly described elsewhere (reviewed by Jones, 2008; Jones & Jones, 2007; Mock, 2008); therefore, a brief overview of the procedure performed by Mock (2008) and Mock, Jones, and Jones (2011) is described.

Prior to function testing, each mouse was deeply anesthetized and placed supine on a heating pad and core body temperature to maintain core body temperature at 37° ± 0.2°C using a homeothermic heating system (FHC, Inc.). Recording electrodes were placed subcutaneously at the nuchal crest (noninverting electrode), posterior to the right pinna (inverting electrode), and at

the right hip (ground electrode). The head was oriented such that the naso-occipital axis was in the vertical direction (nose up) and the head was coupled to a mechanical shaker for delivery of linear acceleration stimuli.

Stimuli were presented at a rate of 17 pulses per second. A trace of positive polarity and a trace of negative polarity were averaged together to produce one waveform (Figure 2.3). Two waveforms were produced for every presentation level measured (+6 to -18 dB re: 1.0 g/ms), with the exception of +6 dB, in which two waveforms were recorded in quiet and two waveforms were recorded in the presence of a forward masker. The masker was used to ensure that the auditory system was not contributing to the VsEP. The first three positive peaks and the first three negative troughs were labeled and threshold, P1-N1 amplitude, and P1 latency was recorded from the intensity series. Threshold was recorded as the level midway between the lowest observed response and the first waveform where no response occurred. P1-N1 amplitude was measured by determining the difference between the amplitude (in microvolts) of the first positive and first negative response for the +6 dB masked waveform pair (see figure 3). Latency was recorded as the amount of time occurring between the onset of the stimulus and the first measured response peak.

Statistical Analysis

Comparisons between age groups were made using a univariate analysis of variance (ANOVA). Linear regression was performed to correlate structural data with VsEP threshold data with age.

Preliminary Data

A study examining the effects of aging on structure (hair cells, synaptic ribbons, post-synaptic receptor sites) in the CBA/CaJ strain (at six, 12, and 18 months only) provided some

interesting data. Table 2.2 describes the mean, standard deviation, minimum, and maximum counts of number of hair cells, CtBP2 per hair cell, and Shank1a per hair cell for the CBA/CaJ strain. Values for average number of hair cells per 2265.76 μm^2 ranged from 49.50-55.50 for the six month age group, 40.00-55.50 for the 12 month age group, and 41.00-53.00 for the 18 month age group. Figure 4 represents an example of an image from six month old CBA/CaJ mouse. Analysis of variance testing demonstrated no significant difference among age groups in terms of hair cell number (six months: 52.56 ± 3.13; 12 months: 48.15 ± 5.73; 18 months: 48.17 ± 5.00; Table 2.3, 2.4). Similar to the hair cell counts, the number of CtBP2 per hair cell was similar across ages; six months (7.36 ± 0.36), 12 months (6.96 ± 0.84), and 18 months (7.18 ± 0.81; Table 5). Analysis of variance testing for Shank1a per hair cell showed that there was a difference with age (six months: 9.97 ± 2.41; 12 months: 7.58 ± 1.27; 18 months: 6.62 ±1.61). Post hoc Tukey analysis demonstrated that the number of Shank1a per hair cell for the 18 month age group was significantly lower than the number of Shank1a per hair cell for the six month age group (Figure 2.5; Table 2.6). Structural data was analyzed using univariate ANOVA once all data were collected.

VsEP Data

VsEP function decreased with age for CBA/CaJ mice (from database generated by Mock, 2008). Six month old CBA mice (-11.0 dB ± 1.22) exhibited better vestibular function compared to 12 month old CBA mice (-7.5 dB ± 3.29). VsEP threshold varied greatly among the 12 month age group (ranges from -10.5 dB to -1.5 dB). The 18 month age group exhibited the poorest vestibular function in terms of VsEP threshold compared to the younger age groups (-3.50 ± 2.45).

Comparison of Structural Data with Functional Data

Structural data was plotted against VsEP functional threshold data (Figure 2.6). A declining trend with age was observed among all structures in that structural decline with age was associated with increased VsEP thresholds as age increases. Structural data was correlated with functional thresholds using linear regression once data from all four age groups was obtained.

Assumptions

Assumptions for normality and constant variance were tested for each dependent variable to determine if the analyses were valid (Table 2.7). The Levene's test statistic for the hair cell response variable revealed a p-value of 0.58. The test of normality revealed a p-value of 0.16. For the CtBP2 per hair cell response variable, the Levene's test revealed a p-value 0.38 while the test for normality revealed a p-value of 0.94. The Shank1a per hair cell variable revealed a Levene's p-value of 0.36 and a Shapiro-Wilk p-value of 0.66. Therefore, the assumptions of normality and constant variance were upheld for the response variables.

Discussion

The results provide new evidence which may help explain the morphological mechanisms responsible for gravity receptor dysfunction with age. Specifically, the results suggest that the quantity of hair cells as well as synaptic ribbons per hair cell remain relatively stable until at least 18 months of age. Conversely, the number of post-synaptic receptor sites per hair cell did appear to decline between six months and 18 months of age. The similar rates of decline for hair cells and synaptic ribbon counts per hair cell suggest that these structures may not be involved in age-related declines in balance with age. These results suggest that post-synaptic receptor sites play a substantial role in gravity receptor functional declines with age.

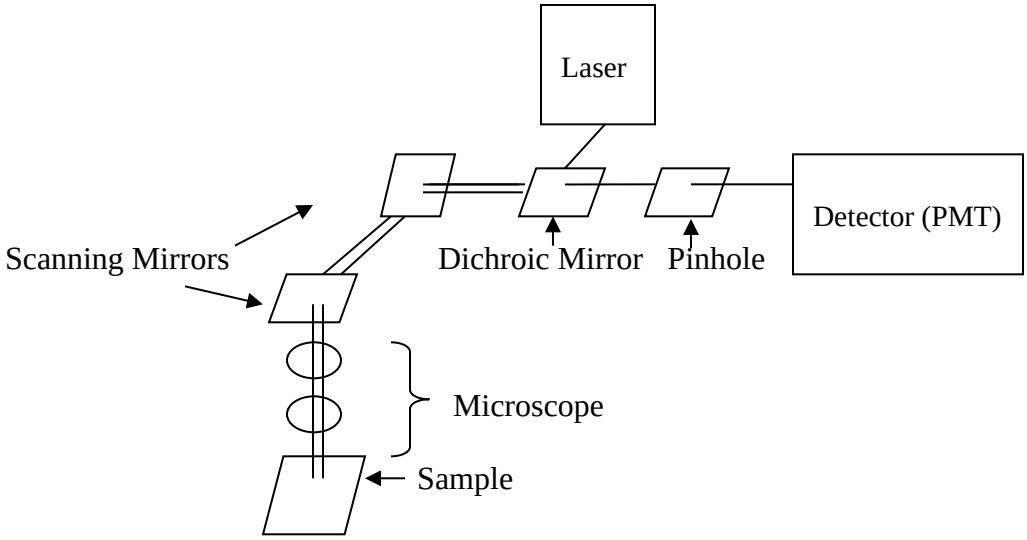

Figure 2.1: Schematic of a laser scanning confocal microscope. Laser light is emitted through a dichroic mirror and directed toward x and y scanning mirrors. The light passes through the mirrors and into the microscope, which emits the light and excites the fluorescent sample. The fluorescent light is then reflected back through the microscope and to the scanning mirrors, where the light is descanned. The light then passes through the dichroic mirror and pinhole, which rejects all out-of-focus light. Finally the light arrives and is measured by a photomultiplier tube (Prasad, Semwogerere, Weeks, 2007).

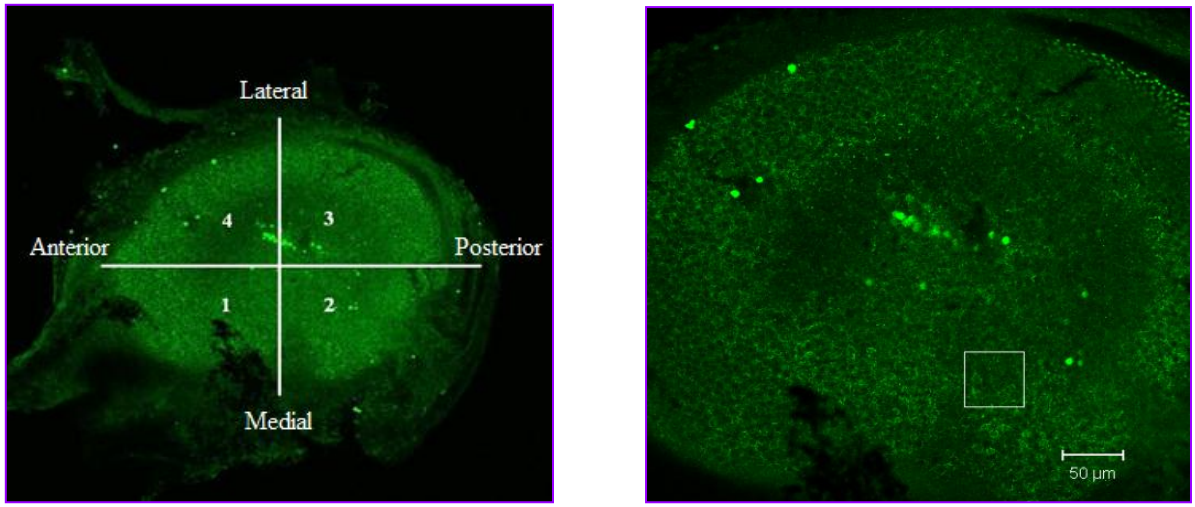

Figure 2.2: Confocal utricular single images from a young B6.129 mouse, imaged using a Plan-Neofluar 20x/0.5 Na objective (left) and and a C-Apochromat 63x/1.2 NA water-immersion objective (right) stained with Shank1a (green). Each utricle will be divided into four quadrants. One area in each quandrant will be viewed more closely with a 3x scan zoom.

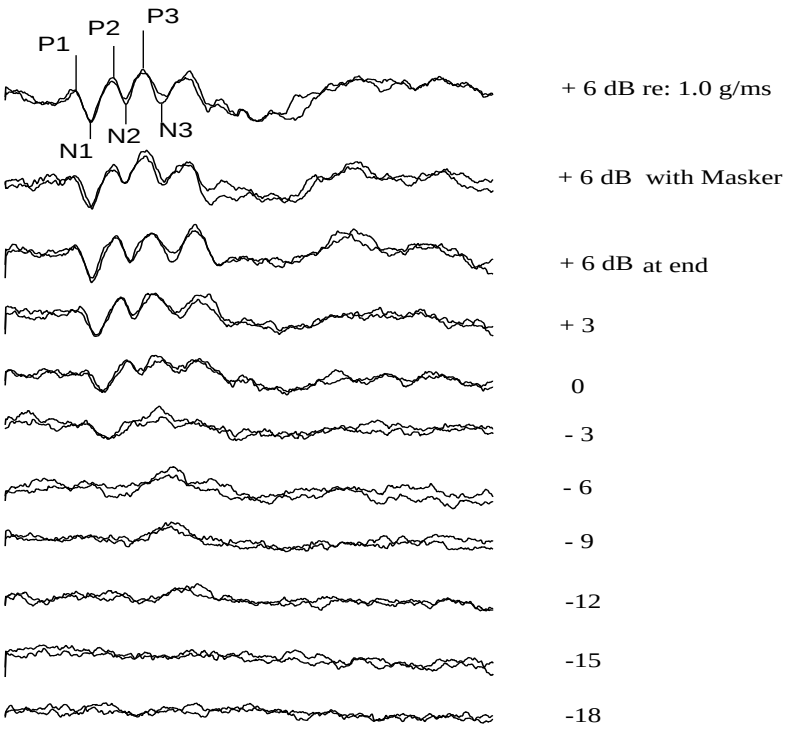

Figure 2.3: Intensity series +6 to -18 dB re: 1.0 g/ms VsEP waveform. The total time depicted is ten milliseconds. VsEPs are compound action potentials that are generated by the vestibular portion of the VIII cranial nerve (vestibulocochlear nerve) and central relays (Nazareth and Jones, 1998). They are a direct measure of vestibular function, relying on the functional integrity of both the utricle and saccule. P1 represents activation of the peripheral portion of the vestibulocochlear nerve while waves following P1 and N1 are generated by central relays (Nazareth & Jones, 1998). From Mock et al. (2008). Used with permission.

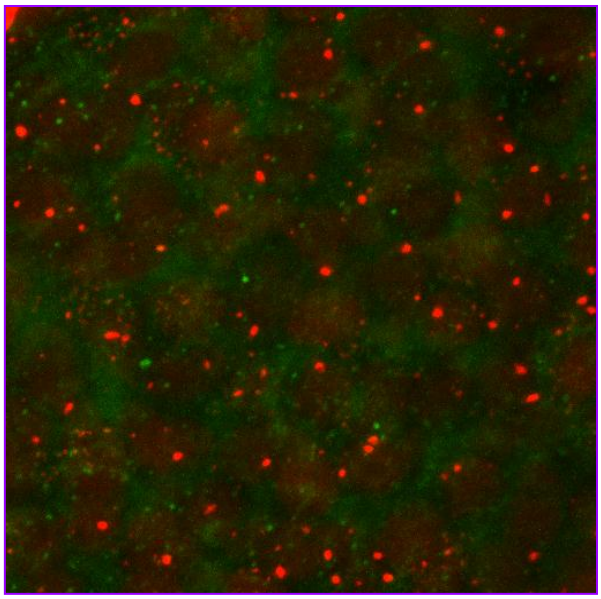

Figure 2.4: Maximum intensity projection from a z-stack of a 6 month CBA mouse, imaged using a C-Apochromat 63x/1.2 NA water-immersion objective and zoomed 3x. The utricle was stained with CtBP2 (red) and Shank1a (green). The synaptic ribbons (red) and post-synaptic receptor sites (green) are represented as bright, punctuate points throughout the image while the hair cell nuclei (red) are distinguished in the background from synaptic ribbons by their significantly larger, oval appearance. For this image, the number of hair cells was 53, CtBP2 per hair cell was 7.28, and Shank1a per hair cell was 8.17.

Figure 2.5: Bar graph of mean number of hair cells, synaptic ribbons, and post-synaptic receptor sites for CBA/CaJ mouse strain. The number of hair cells and synaptic ribbons remain relatively stable among all age groups. The mean number of post-synaptic receptor sites declines between the 6 and 18 month age groups.

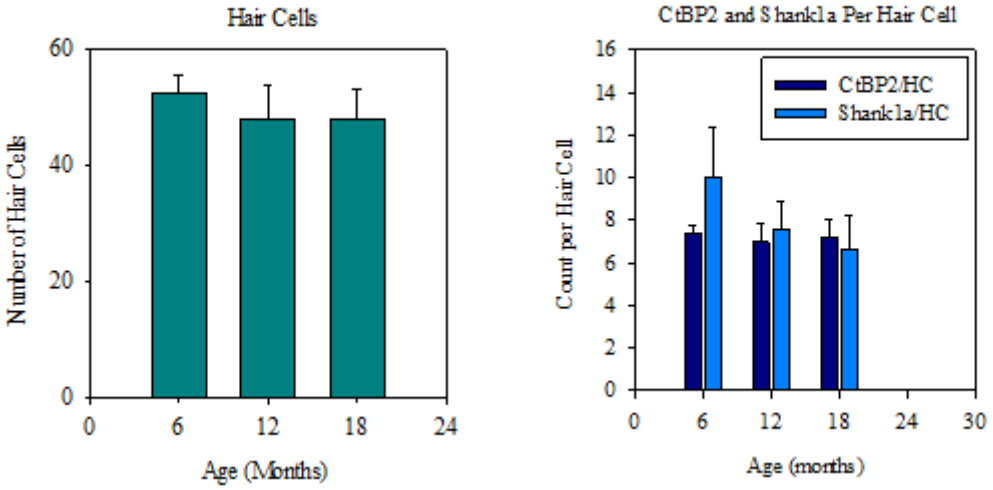

Figure 2.6: Scatter plot of mean VsEP threshold as a function of mean hair cell density (left), synaptic ribbons per hair cell (middle), and post-synaptic receptor sites per hair cell (right) for 6, 12, and 18 month CBA age groups.

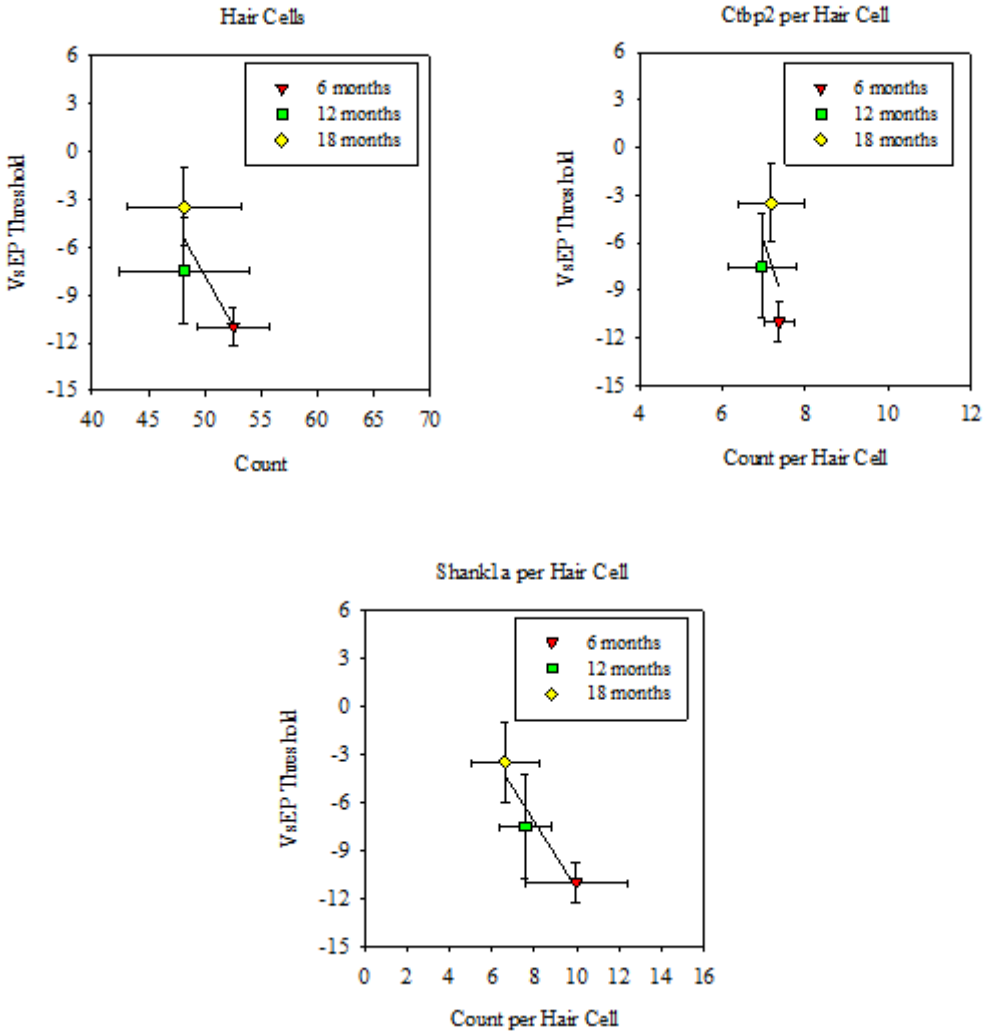

Table 2.1:

Confocal laser scanning properties

Property	Confocal Setting
Lasers	Argon 488; HeNe2 633
Laser Properties	Argon output: 30%; HeNe2 output: 25%
Imaging Setup	Mode: Channel mode
	Switch track every: Frame
	Alexa Fluor 633: Ch1; Alexa Fluor 488: Ch2
Light Path	LP 650-Ch1; BP 505-Ch2
Objectives	Plan-Neofluar 10x/0.3 NA; C-Apochromat 63x/1.2 NA water-immersion
Pinhole	Optimal
Scan Mode	Frame
	x : 512; y: 512; z: 0.16 (optimal z)
Scan Speed	5
Averages	Number: 1
	Mode: line
	Method: mean
	Depth: 8 bit
	Direction: right
Scan Area (Zoom)	Plan-Neofluar 10x/0.3 NA: 1; C-Apochromat 63x/1.2 NA water-immersion: 3
Channels	Argon 488: Detector gain 600-800; HeNe2 633: Detector gain 600-800

Table 2.2:

CBA descriptive statistics for hair cell number, CtBP2 per hair cell, Shank1a per hair cell, and VsEP threshold

Structure	Age	Mean	Standard Deviation	Minimum	Maximum
Hair Cell Number	6 months	52.56	3.13	49.5	55.5
	12 months	48.15	5.73	40.0	55.5
	18 months	48.17	5.00	41.0	53.0
CtBP2 per Hair Cell	6 months	7.36	0.36	6.86	7.64
	12 months	6.96	0.84	6.00	8.20
	18 months	7.18	0.81	6.30	8.60
Shank1a per Hair Cell	6 months	9.97	2.41	6.65	12.08
	12 months	7.58	1.27	5.70	9.10
	18 months	6.62	1.61	4.70	8.40
VsEP Threshold	6 months	-11.00	1.22	-13.5	-10.5
	12 months	-7.50	3.29	-10.5	-1.5
	18 months	-3.50	2.45	-4.5	1.5

Table 2.3:

CBA ANOVA table for hair cell count, CtBP2 per hair cell, and Shank1a per hair cell

Structure	Sum of Squares	df	Mean Square	F	P-Value
Hair Cell Number	56.88	2	28.44	1.20	0.34
	285.46	12	23.79		
CtBP2 per Hair Cell	0.37	2	0.18	0.34	0.72
	6.50	12	0.54		
Shank1a per Hair	27.38	2	13.69	4.46	0.04*
Cell	36.84	12	3.07		

* Less than $\alpha = 0.05$

Table 2.4:

CBA multiple comparisons Tukey post hoc table for hair cell number and age group

Structure	Age Group (I)	Age Group (J)	P-Value	95% Confidence Interval	
Hair Cell	6	12	0.40	-4.32	12.14
Number		18	0.37	-4.00	12.80
	12	6	0.40	-12.14	4.32
		18	1.00	-7.90	7.86
	18	6	0.37	-12.80	4.00
		12	1.00	-7.86	7.90

Table 2.5:

CBA multiple comparisons Tukey post hoc table for CtBP2 per hair cell and age group

Structure	Age Group (I)	Age Group (J)	P-Value	95% Confidence Interval	
CtBP2 per	6	12	0.70	-0.91	1.72
Hair Cell		18	0.93	-1.09	1.45
	12	6	0.70	-1.72	0.91
		18	0.87	-1.41	0.97
	18	6	0.93	-1.45	1.09
		12	0.87	-0.97	1.41

Table 2.6:

CBA multiple comparisons Tukey post hoc table for shank1a per hair cell and age group

Structure	Age Group (I)	Age Group (J)	P-Value	95% Confidence Interval	
Shank1a	6	12	0.15	-0.75	5.52
per Hair		18	0.03	0.33	6.37
Cell	12	6	0.15	-5.52	0.75
		18	0.65	-1.87	3.79
	18	6	0.03	-6.37	-0.33
		12	0.65	-3.79	1.87

Table 2.7:

CBA table of assumptions of constant variance and normality for hair cell count, CtBP2 per hair cell and Shank1a per hair cell

Structure	Levene's test P-Value	Shapiro-Wilk test P-Value
Hair cell count	0.58	0.16
CtBP2 per hair cell	0.38	0.94
Shank1a per hair cell	0.36	0.66

CHAPTER III: STRUCTURAL CORRELATES FOR VESTIBULAR FUNCTIONAL AGING IN CBA/CaJ MICE

Abstract

CBA/CaJ is a mouse strain that has no known genetic mutations affecting the inner ear, thereby serving as a control model for auditory and vestibular aging. The purpose of this study was to characterize the effect of age on three structures within the utricle of the inner ear; hair cells, synaptic ribbons, and post-synaptic receptor sites-all of which are critical to sensory transduction. Utricles were dissected, stained with CtBP2 (marker for hair cell nuclei and synaptic ribbons) and Shank1a (marker for post-synaptic receptor sites), and imaged using confocal microscopy. Structures were quantified and averaged over four distinct areas of the utricle at several age points across the lifespan. The number of hair cells and CtBP2 per hair cell was similar from early to middle age groups, but significantly declined by 22 months. Shank1a and synaptic colocalization counts per hair cell remained relatively stable with age. When compared with gravity receptor functional data, hair cells and CtBP2 per hair cell exhibited a significant relationship with observed macular functional declines with age. Results suggest that presynaptic elements may play a role in age-related gravity receptor dysfunction. In addition to hair cells and synaptic ribbons, further structures in the periphery or central vestibular systems may be responsible for functional declines in balance with age.

Introduction

Imbalance and risk of falls are significant concerns among the elderly. According to the National Institute on Deafness and Other Communication Disorders (2002), approximately one-third of individuals over the age of 65 are reported to fall each year, which can have significant implications on an individual's safety and quality of life. Balance is influenced by the vestibular system in the inner ear, which detects and encodes movement of the head. In addition to the vestibular system, postural stability is also impacted by the proprioceptive and visual systems. With age, degeneration of these modalities occurs. Physiological changes with age include a decline in visual acuity, cross sensitivity, and depth perception among the elderly (Ivers, Cumming, Mitchell, Attebo, 1998; Lord & Dayhew, 2001). Peripheral neuropathy and prolongations in reaction time may also affect balance with age (Jacobson & McCaslin, 2008). Additional factors that may cause dizziness among the elderly include medications, as well as altered muscle strength, joint flexibility, and coordination (Means et al., 2005). Although our ability to maintain balance declines with age, the structural changes responsible for these functional declines are not completely understood.

Functional changes in the vestibular system have been reported in both humans and animal models. Reports of vestibular function have generally relied upon measures such as vestibuloocular reflex (VOR), visual-vestibuloocular reflex (VVOR), vestibular-evoked myogenic potentials (VEMPs), optokinetic nystagmus (OKN), and posturography testing. Indirect inferences may be made with these measures, as they rely upon the functioning of additional systems beyond the vestibular system. Declines in gain (ratio of eye-velocity to head velocity) for VOR, VVOR, and OKN have been reported among elderly individuals (Baloh et al., 1993; Enrietto, Jacobson, Baloh, 1999; Kerber et al., 2006; Paige, 1992, 1994). For example,

Baloh and colleagues (1993) measured VOR, OKN, and visual-VOR on individuals over the age of 75. Declines in VOR gain were observed among the elderly when compared to young individuals. VOR gain grew poorer as stimulus amplitude increased. In addition, OKN and visual-VOR revealed decreases in gain of slow-phase velocity and an increased phase lead of eye velocity for higher amplitude stimuli. Alternatively, Peterka, Black, and Schoenhoff (1991) found no age-related declines in VOR gain. Age-related changes on vestibular evoked myogenic potential (VEMP) testing have also been documented. Individuals over the age of 60 tend to have smaller VEMP amplitudes than younger adults (Basta, Todt, & Ernst, 2005; Su, Huang, Young, & Cheng, 2004). In addition, increased thresholds and longer latencies with age have been reported with VEMP testing (Ochi & Ohashi, 2003; Su et al., 2004). There is no consistent declining trend observed during caloric testing for individuals across the lifespan (Peterka, Black, & Schoenhoff, 1991). During posturography testing, increases in sway magnitude were observed in altered somatosensory and visual conditions in individuals over the age of 75 (Peterka, Black, & Schoenhoff, 1991). In addition, sensory organization testing among older individuals suggested a decline in the ability to maintain balance with age among asymptomatic individuals, beginning at the fourth decade onward. This finding implies that even older individuals who report no vestibular symptoms may still exhibit a decline in balance with age (Borah et al., 2007; Cohen, Heaton, Congdon, & Jenkins, 1996).

Among animal strains, few studies have measured vestibular function, with the majority of vestibular aging data from mouse models. Jones et al. (2006) measured gravity receptor function directly with vestibular sensory evoked potentials (VsEPs) in 19 inbred mouse strains ranging in age from 35 to 389 days old. A heterogenous rate of vestibular decline with age between mouse strains was observed across the lifespan, with some strains exhibiting little to no

decline in gravity receptor function with age while other strains showed severe age-related vestibular dysfunction. Jones and colleagues hypothesized that genes responsible for early-onset age-related hearing loss may also impact gravity receptor function to varying degrees. In a separate study, Jones et al. (2005) measured gravity receptor function for CBA/CaJ and C57BL/6J mice, which are two mouse strains commonly used in inner ear research. Both mouse strains were reported to maintain macular function until at least 190 days old. In a separate study, Mock (2008) measured gravity receptor function for CBA/CaJ, CE/J, and C57BL/6J mice across the lifespan. Results indicated a significant age-related decline in gravity receptor function for the CBA/CaJ mouse strain (0.39 dB re: 1 g/ms increase in VsEP threshold per month), although not to the extent of the CE/J mouse strain (0.47 dB re: 1 g/ms increase in VsEP threshold per month). C57BL/6J mice maintained the best gravity receptor function with age, exhibiting only slight declines at the oldest ages (0.12 dB re: 1 g/ms per month decline of macular function with age).

In the vestibular system, both qualitative and quantitative changes in structures at the hair cell level have been observed in human temporal bones and animal models. Previously reported age-related structural declines include a reduction in the quantity and quality of otoconia (Igarashi et al., 1993; Jang et al., 2006; Johnsson, 1971; Ross et al., 1976; Suzuki et al., 1997; Walther & Westhofen, 2007), stereocilia integrity (Bloom & Hultcrantz, 1994; Rosenhall & Rubin, 1974), and hair cell number and density (Gleeson & Felix, 1987; Merchant et al., 2000; Park et al., 1987; Rauch et al., 2001; Richter, 1980; Rosenhall & Rubin, 1975; Severinsen et al., 2007; Shiga et al., 2005). Although structural changes have been observed in the vestibular system with age, the extent to which structural declines explain age-related vestibular dysfunction is unknown.

Only one study to our knowledge has examined the relationship between function and structure in the vestibular system. Shiga et al. (2005) measured VOR gain in C57BL/6 mice between the ages of 3 weeks and 60 weeks. Limited declines in VOR gain were observed in older mice compared to younger mice, suggesting that vestibular function is largely maintained until at least 60 weeks of age; however, a decline in hair cell density was measured in the cristae of the lateral semicircular canal to the extent that hair cell density recorded at the oldest age group (60 weeks) decreased to 70% of that measured at three weeks of age. Shiga and colleagues concluded that age-related structural changes in the vestibular system are a poor indicator for vestibular functional changes with age and suggested that central compensation may have helped maintain VOR function. Structural correlates for age-related vestibular dysfunction remain unclear because few have examined both entities together. Improving literature in two areas by examining structures known to be critical to sensory transduction across the lifespan and comparing structural changes to age-related vestibular functional data will help improve our knowledge regarding the effect of age on the vestibular system.

The purposes of the present study was to quantitatively examine three structures at the hair cell level of the utricle of the inner ear which are critical to sensory transduction; hair cells, synaptic ribbons, and post-synaptic receptor sites, as well as synaptic ribbon/post-synaptic receptor site colocalizations. Structural data were compared with age-matched gravity receptor functional data as measured by vestibular sensory evoked potentials (VsEPs; Mock et al., 2011). The present study sought to answer two questions: 1) what is the effect of age on structural elements in the utricle of the vestibular system in the CBA/CaJ strain, a mouse strain which represents normal aging, and 2) how well do age-related structural changes in the utricle explain aging gravity receptor function as measured by VsEPs? It was hypothesized that structures

would decline at a similar rate corresponding to gravity receptor function across the lifespan. Better understanding of the effects of age on the vestibular system may provide better insight into the underlying factors that may be responsible for gravity receptor functional declines with age.

Methods

Animals and Animal Preparation

CBA/CaJ mice were obtained from The Jackson Laboratory (Bar Harbor, ME). This mouse strain is commonly used in aging research, as it carries no known genetic mutations affecting the inner ear. Animals were housed at East Carolina University using standard husbandry procedures until the appropriate age for examining tissues. A total of 10 mice yielding 14 utricles (six months: n = three temporal bones; 12 months: n = four temporal bones; 19 months: n = four temporal bones; 22 months: n = three temporal bones) were used. Males and females were combined into one group as gravity receptor functional aging exhibits similar changes between genders for the CBA/CaJ mouse strain (Mock, 2011). The protocol was consistent with the recommendations of the American Veterinary Medical Association (AVMA) Guidelines on Euthanasia and approved by the Animal Care and Use Committee at East Carolina University.

Each mouse was injected with a lethal dose of Sodium Pentobarbital (3900 mg/kg) injected intraperitoneally. The temporal bones were dissected and fixed overnight in 4% Paraformaldehyde in 0.1 M Phosphate Buffer at room temperature. Following fixation, the utricle was dissected from the temporal bone and the otoconia and otoconial membrane was gently scraped off while bathed in 0.01 M Phosphate Buffered Saline with 3% Triton (PBST; 0.3

M Sodium Chloride, 0.3% Triton-X 100, 0.01 M Phosphate Buffer, pH 7.4). Each specimen was washed with PBST three times for 15 minutes each at room temperature. Blocking solution (10% Normal Goat Serum in PBST) was applied overnight at 4˚C. Following blocking, specimens were incubated in a primary antibody cocktail (Mouse anti-CtBP2: C-terminal binding protein 2; BD Transduction Laboratories; 1:300; Rabbit anti-Shank1a: Neuromics; 1:300; 5% Normal Goat Serum in PBST) for 48 hours at 4 °C. Specimens were then washed in PBST three times for 50 minutes each at room temperature. Secondary antibodies were applied in a cocktail (for CtBP2: Alexa 488 goat-anti-mouse RED-Invitrogen; 1:200; for Shank1a: Alexa 633 goat-anti-rabbit GREEN-Invitrogen; 1:200) overnight at 4°C (once secondary antibodies were applied, the specimens were shielded from light). Samples underwent three final washes (15 minutes each) in 0.01 M Phosphate Buffered Saline at room temperature. Following the washes, each specimen was mounted on a slide with ProLong® Gold antifade reagent (Invitrogen) and cover slipped.

Samples were viewed with an inverted Zeiss LSM 510 Confocal microscope and images captured using Zeiss LSM 510 Version 4.2 SP1 software. The 488 (20% intensity) and 633 (25% intensity) laser lines were used to view fluorescence. Laser light was passed through a bandpass filter of 505-530 nm for the red channel and a longpass filter of 650 nm for the green channel (Figure 1). Images were captured at a low magnification using a Plan-Neofluar 10x/0.3 NA objective. To view images at a higher magnification, a C-Apochromat 63x/1.2 NA water-immersion objective was used with 3x scan zoom.

Each utricle was divided into four quadrants: two medial areas (quadrants 1 and 2) and two lateral areas (quadrants 3 and 4) based upon the utricle's natural curvature (Figure 3.2a). One area within each quadrant was imaged for further analysis (Figure 3.2b). Each area was

selected based upon quality (no fissures, tears, gaps, etc. in the imaged area of the epithelium) and uniformity of fluorescence. The areas were scanned at 512 x 512 pixels at optimal z interval (0.16 µm; according to Nyquist Frequency), yielding 30-50 image slices per area. All specimens yielded four complete images (one image per quadrant). In a comparison of structural counts in medial versus lateral areas, no significant differences were observed; therefore, the data were combined to evaluate response variables as a function of age.

Data Analysis

Once the three-dimensional z stack was captured by the computer, the image was transferred to Volocity 3D imaging software for data analysis. To quantify hair cells and synaptic ribbons, each z stack was opened and the Alexa 633 (green) channel was disabled, allowing only the Alexa 488 (red) channel to be visualized. Hair cells were then manually quantified in the imaged area by visualizing those cell nuclei which were oval in shape (to distinguish hair cell nuclei from supporting cell nuclei, which are hexagonal in shape) and a marker was placed on each identified hair cell to prevent the hair cell from being counted twice.

To quantify CtBP2 labeling, the series of 2D images that composed the 3D z stack were examined sequentially. Those CtBP2 points that were observed in two or more consecutive images and no larger than one micron in diameter were counted as a synaptic ribbon. A marker was placed at each identified synaptic ribbon in order to prevent the synaptic ribbon from being counted twice.

Due to the increased level of background staining for the Alexa 633 antibody, post-synaptic receptor sites were quantified using a specialized protocol created with Volocity software. The Alexa 488 (red) channel was disabled, allowing only the Alexa 633 channel to be

visualized. An intensity and size thresholding procedure was implemented to identify those points that represented post-synaptic receptor sites. Colocalizations between CtBP2 and Shank1a were also quantified manually. Each CtBP2 and Shank1a point that was observed in two or more consecutive images, no larger than one micron in diameter, and appeared to touch or overlap was counted as one colocalization. A marker was placed at each identified synaptic colocalization in order to prevent it from being counted twice.

Age-matched VsEP threshold data from Mock et al. (2011) were correlated with the structural data. VsEP measures were detailed in Mock et al. and followed well established procedures developed by Jones and colleagues (reviewed by Jones, 2009; Jones & Jones, 2008).

The number of hair cells, CtBP2, and Shanka were quantified in a 47.6 µm x 47.6 µm (2265.76 μm^2) area. Counts from each area in the utricle were averaged together to obtain a mean hair cell, synaptic ribbon, post-synaptic receptor site, and synaptic colocalization count per hair cell. Results were then compared among different age groups, and compared with direct functional threshold results, as measured by VsEP threshold, obtained previously by Mock et al. (2011). Comparisons between age groups were made using univariate analysis of variance (ANOVA). Linear regression was performed to correlate structural data with VsEP thresholds across the lifespan. A p-value of less than 0.05 was determined to be statistically significant.

Results

Quantitative Data for the CBA/CaJ Mouse Strain

Table 3.1 shows the means, standard deviations, minimum, and maximum counts for the number of hair cells, CtBP2 per hair cell, Shank1a per hair cell, and synaptic colocalizations per hair cell. A total count across the utricle was estimated for each structure by multiplying each

structural count per imaged area (2265.76 nm^2) by the total area of the utricular maculae epithelium (0.198 $mm^{2)}$ as measured by Desai, Zeh, and Lysakowski (2005). Values for average number of hair cells per 2265.76 μm^2 ranged from 50.00 to 55.00 for the six month age group, 46.00 to 50.00 for the 12 month age group, 43.00 to 52.00 for the 19 month age group, and 36.00 to 39.00 for the 22 month age group. Analysis of variance testing for hair cell number demonstrated a significant difference among age groups (six months: 51.58 ± 2.98; 12 months: 48.81 ± 2.05; 19 months: 47.19 ± 3.98; 22 months: 38.00 ± 1.56; Table 3.2). Post hoc Tukey analysis demonstrated that the number of hair cells was similar at young and mid ages (six, 12, 19 months) but declined significantly by 22 months (Figure 3.3; Table 3.3). When multiplied by the total area of the utricular maculae epithelium, values were 4507.47 at six months, 4265.40 at 12 months, 4123.83 at 19 months, and 3320.74 at 22 months. Values for the number of CtBP2 per hair cell ranged from 7.36 to 7.64 at six months, 6.41 to 8.49 at 12 months, 6.34 to 7.59 at 19 months, and 4.15 to 5.71 at 22 months. Similar to hair cell counts, analysis of variance testing for CtBP2 per hair cell demonstrated a significant difference among age groups (six months: 7.53 ± 0.15; 12 months: 7.67 ± 0.89; 19 months: 6.95 ± 0.54; 22 months: 4.93 ± 0.78; Table 3.2). Post hoc Tukey analysis indicated that the number of CtBP2 per hair cell for the 22 month age group was significantly lower than that for the six, 12, and 19 month age groups (Figure 3.3; Table 3.4). The number of Shank1a per hair cell varied from 9.77 to 12.08 at six months, 7.28 to 12.10 at 12 months, 8.24 to 9.40 at 19 months, and 6.02 to 12.18 at 22 months. Total CtBP2 counts across the utricular epithelium were 33941.23 at six months, 32715.64 at 12 months, 28660.65 at 19 months, and 16371.25 at 22 months. No significant differences in Shank1a per hair cell was observed between age groups (six months: 11.07 ± 1.18; 12 months: 10.15 ± 2.36; 19 months: 8.83 ± 0.61; 22 months: 8.52 ± 3.24; Total Shank1a counts: six months: 49897.67; 12

months: 43293.84; 19 months: 36413.46; 22 months: 28292.71; Figure 3.3, Table 3.2). Values for synaptic colocalizations were smaller than CtBP2 and Shank1a counts alone. The number of synaptic colocalizations per hair cell ranged from 3.49 to 4.33 at six months, 3.15 to 5.23 at 12 months, 3.43 to 3.87 at 19 months, and 2.86 to 3.49 at 22 months. Similar to Shank1a, analysis of variance testing for synaptic colocalizations demonstrated no significant difference among age groups (six months: 3.78 ± 0.47; 12 months: 4.03 ± 0.93; 19 months: 3.69 ± 0.20; 22 months: 3.21 ± 0.32; Total synaptic colocalization counts: six months: 17038.23, 12 months: 17189.57; 19 months: 15216.95; 10659.58; Figure 3.3, Table 3.2).

CBA/CaJ Gravity Receptor Function

Table 3.1 illustrates average VsEP threshold per age group. Values for VsEP thresholds averaged -10.5 dB re: 1.0 g/ms at six months (all age-matched animals yielded a VsEP threshold of -10.5 dB), -10.5 to -1.5 dB re: 1 g/ms at 12 months, -4.5 to -1.5 dB re: 1 g/ms at 19 months, and -4.5 to 1.5 dB re: 1 g/ms at 22 months. VsEP thresholds grew consistently poorer with age (six months: -10.5 dB ± 0.00; 12 months: -6.75 dB ± 3.77; 19 months: -3.75 dB ± 1.50). The 22 month age group exhibited the poorest gravity receptor function (-1.50 dB ± 3.00).

Comparisons of Structural Data with Functional Data

Tests of assumptions for normality and constant variance were examined for each response variable to determine if our models were valid. Results indicated that the assumption of normality and constant variance were upheld for each response variable.

All measured structures exhibited a poorer relationship with gravity receptor function (as VsEP thresholds became more elevated, a general decline in all structural elements was observed; Figure 3.4). Hair cell and CtBP2 per hair cell counts exhibited significant linear

relationships with VsEP threshold. Linear regression indicated that VsEP threshold increased by 0.42 dB re: 1.0 g/ms for every decline in hair cell number (intercept: 14.14; r^2: 0.34; p-value: 0.03). VsEP threshold increased by 2.22 dB re: 1.0 g/ms for every decline in CtBP2 per hair cell (intercept: 9.63; r^2: 0.46; p-value: 0.01). Data points for each age group appeared to cluster together along our line of best fit, especially for hair cell and CtBP2 per hair cell counts, with specimens for the six month age group exhibiting the highest structural counts and the most sensitive gravity receptor function compared to the 22 month age group, which tended to exhibit the lowest structural counts and poorest VsEP thresholds. Shank1a and synaptic colocalization counts per hair cell were not correlated. For every decline in Shank1a per hair cell, VsEP threshold increased by 0.91 dB re: 1.0 g/ms (intercept: 3.18; r^2: 0.22; p-value: 0.09). VsEP threshold increased by 2.64 dB re: 1.0 g/ms for every decline in synaptic colocalization per hair cell (intercept: 4.22; r^2: 0.15; p-value: 0.17). Shank1a counts per hair cell varied more widely across animals and were not clustered as well among age groups based upon Shank1a per hair cell. Therefore, Shank1a did not show a relationship with VsEP threshold (synaptic colocalizations also showed no significant linear relationship with VsEP threshold).

Discussion

Overall, the present study showed age-related structural declines for hair cell and synaptic ribbon counts, exhibiting a significant relationship with gravity receptor functional changes across the lifespan. The number of post-synaptic receptor sites and synaptic colocalizations remained stable with age. These findings provide new insight concerning: 1) age-related structural changes in the CBA/CaJ mouse, a strain that represents normal aging; and 2) the relationship between structural changes in the vestibular system and gravity receptor

function with age. Our results provide evidence that may help explain the structural mechanisms responsible for age-related gravity receptor dysfunction. Hair cell and CtBP2 per hair cell counts exhibited a significant decline at the oldest age group (22 months). Conversely, the number of post-synaptic receptor sites and synaptic colocalizations per hair cell exhibited no significant age-related changes. The significant relationship between VsEP threshold and hair cell and synaptic ribbon counts per hair cell suggest that pre-synaptic structures may be involved in observed age-related gravity receptor functional declines. Post-synaptic elements do not appear to decline with age.

Observed hair cell decline was consistent with previous data suggesting age-related quantitative changes in hair cells, including changes in hair cell number and density (Dimitri, & Merchant, 2001; Gleeson & Felix, 1987; Merchant et al., 2000; Park, Hubel, & Woods, 1987; Rauch, Velazquez-Villasenor, Richter, 1980; Rosenhall & Rubin, 1975, Severinsen et al., 2007; Shiga et al., 2005). Total hair cell counts (Table 3.1) were on average higher than previous reports of hair cell number of the utricular maculae, which averaged 3613 hair cells in adult ICR mice (Li, Xue, & Peterson, 2008); however, to date, this is the first study to quantify hair cell totals in the CBA/CaJ mouse utricle across the lifespan. Synaptic ribbon decline with age is a unique finding. Only one known study has examined synaptic ribbons within the vestibular system across the lifespan. Park and colleagues (1987) grossly identified the prevalence of synaptic ribbons in the vestibular organs of aging C57BL/6NNia mice. No substantial loss of synaptic ribbons was observed with age, although the data were not quantified. To date, the current study is the only known quantitative measurement of synaptic ribbons in the vestibular organs across the lifespan. Our finding of age-related hair cell and CtBP2 declines is consistent with observed aging gravity receptor dysfunction for this strain and do imply that these pre-

synaptic structures play a role in age-related gravity receptor dysfunction. No significant age-related decline in post-synaptic receptor sites per hair cell was observed. This finding is in contrast to a previous examination of neural components in which researchers qualitatively observed that calyces in the cristae of the aging gerbil were missing from the epithelium (Leonard & Kevetter, 2007); however, there are several notable differences between the current study, which examined post-synaptic receptor sites in the aging mouse utricle, and Leonard and Kevetter's study. In addition to the disparate vestibular organ and mammalian species examined by Leonard and Kevetter, those synapses that were innervated by bouton or dimorphic afferents were not taken into account. To our knowledge, this is the first study to quantitatively examine post-synaptic receptor sites in the mouse utricle across the lifespan. Additional structural changes in the peripheral vestibular system have been reported, including a reduction in the quantity of otoconia and otoconia precursors (Johnsson, 1971; Mock 2008, Mock, Jones, & Jones, 2011; Suzuki, Ikeda, Takasaka, 1997); although Mock et al. (2011) reported no gross changes in otoconia for the CBA/CaJ strain, suggesting that otoconia density could not account for gravity receptor functional declines with age.

Although structural elements were quantitatively examined, qualitative changes in the pre-synaptic and post-synaptic structures cannot be ruled out. Previous reports of age-related qualitative declines in structure include increases in hair cell lipofuscin (age-related pigment) and inclusions (Park, Hubel, & Woods, 1987; Richter, 1980; Rosenhall & Rubin, 1975, Severinsen et al., 2007), fragmented and pitted otoconia (Igarashi et al., 1993; Jang et al., 2006; Ross et al., 1976; Walther & Westhofen, 2007), and increased fragility, disorganization, and formation of giant stereocilia (Bloom & Hultcrantz, 1994; Rosenhall & Rubin, 1974). In addition, the extent of contribution of hair cell apoptosis on gravity receptor functional declines is currently unknown.

It is interesting to note that the numbers of synaptic colocalizations were relatively maintained with age. One would expect a decline among these structural colocalizations, as the co-occurance of a synaptic ribbon with a post-synaptic receptor site is vital to sensory transduction: neither structure may function appropriately without the other. Instead, three to five synaptic colocalizations per hair cell were observed across the lifespan. Synaptic ribbon counts per hair cell declined from a mean of 7.53 synaptic ribbons per hair cell at six months to 4.93 synaptic ribbons per hair cell at 22 months. Post-synaptic receptor site counts per hair cell were always greater than synaptic ribbon counts, ranging from a mean of 11.07 at six months to 8.52 at 22 months. Each synaptic colocalization consisted of one synaptic ribbon and one post-synaptic receptor site. Therefore, synaptic colocalization counts were driven by our synaptic ribbon counts (the number of synaptic colocalizations by default could not be greater than our synaptic ribbon counts). This sanctions an important question: although the numbers of synaptic colocalizations remain stable across the lifespan, why does gravity receptor function decline in this mouse strain with age? One possibility which may account for observed functional declines in the vestibular system is that some synaptic colocalizations may lose function over time.

Gomez-Casati et al. (2010) examined synaptic colocalizations using antibodies for RIBEYE/CtBP2 and GluR2/3 in the utricle of a young transgenic mouse strain that exhibits severe vestibular dysfunction (elimination of erb8 signaling in supporting cells resulting in a defect of synapse formation). Frequent misalignment of presynaptic and postsynaptic components as well as declines in previously formed synaptic structures was observed. Gomez-Casati and colleagues concluded that this transgenic mouse strain demonstrated an initial defect in synaptic formation as well as a maintenance error for synaptic structures. Their findings provided evidence that vestibular dysfunction observed for this mouse strain was a consequence

of synaptic defects in the utricular maculae epithelium. Although age was not examined in their study, results show that structural maintenance of presynaptic and postsynaptic elements, both quantitatively and functionally, are critical to a normal functioning vestibular system. Although we observed no decline in synaptic colocalizations with age for the CBA/CaJ mouse strain, functional impairment of presynaptic and postsynaptic structures which may be responsible for age-related gravity receptor dysfunction cannot be ruled out.

Other potential contributors outside of the peripheral vestibular system may be involved in aging vestibular dysfunction. For example, decreased metabolic activity and vascular supply to the vestibular system have been reported with age (Felipe et al., 2008; Ishiyama, 2009; Lyon & King, 1997; Lyon & Davis, 2002; Lyon & Wanamaker, 1993). Changes in central relays of the vestibular system have also been reported, including degeneration of the vestibular nuclei and vestibular portion of CN VIII (Alvarez et al., 2000; Johnson, 1971; Lopez, Honrubia, & Baloh, 1997).

These findings have a substantial impact on aging research for the elderly. It is estimated that 40 to 50% of reported dizziness can be attributed to disorders of the vestibular system (Marchetti & Whitney, 2005). In addition to direct structural declines in the vestibular system with age, other factors unrelated to the vestibular system which may cause dizziness among the elderly include medications, as well as muscle strength, joint flexibility, and coordination (Means, et al., 2005). Visual changes such as loss of visual acuity, cross sensitivity, and depth perception have been reported among older individuals (Ivers, Cumming, Mitchell, & Attebo, 1998; Lord & Dayhew, 2001). Medical conditions can also increase the risk of dizziness and falls. Specific diseases prevalent to the elderly population include osteoporosis, heart disease, diabetes, cerebrovascular disease, and hypotension. In addition, peripheral sensitivity (i.e. feet,

hands, etc.) and reaction time may affect balance among the elderly (Jacobson & McCaslin, 2008). In addition to structural changes in the vestibular system, balance dysfunction may also be influenced by these other modalities.

In summary, the current study found that, in CBA/CaJ mice 1) the number of hair cells and synaptic ribbons exhibited a decrease, significantly declining at advanced ages; 2) the number of post-synaptic receptor sites and synaptic colocalizations remained relatively stable over time; and 3) age-related declines in balance correlate relatively well with age-related declines in hair cell and synaptic morphology. The observed decline in hair cell quantity supports other reports of hair cell declines with age. The decline in the number of synaptic ribbons is a new finding and may help steer future evidence for structural correlates of gravity receptor functional declines with age.

Figure 3.1: Maximum intensity projection from a z-stack of a 6 month CBA/CaJ mouse imaged using a C-Apochromat 63x/1.2 NA water-immersion objective and zoomed 3x. The utricle was stained with CtBP2 (red) and Shank1a (green). The synaptic ribbons (red) and post-synaptic receptor sites (green) are represented as bright areas of fluorescence throughout the image while the hair cell nuclei (red) are distinguished in the background from synaptic ribbons by their significantly larger, oval appearance. All red areas of fluorescence larger than one micron in diameter was excluded from our synaptic ribbon count. For this image, the number of hair cells was 53, CtBP2 per hair cell was 7.28, and Shank1a per hair cell was 8.17.

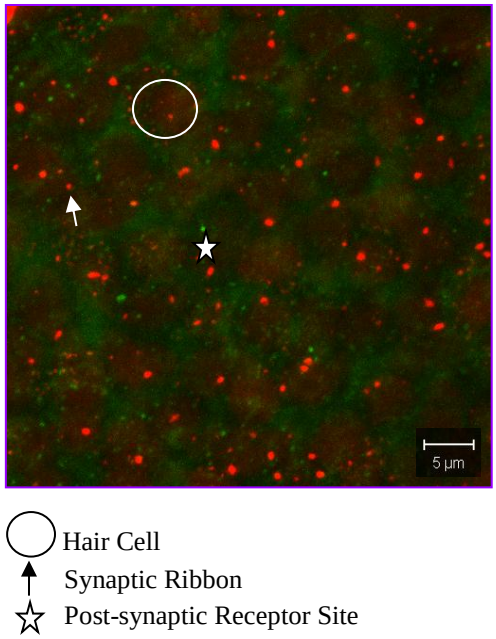

Figure 3.2: Confocal utricular single images from a young B6.129 mouse, imaged using a Plan-Neofluar 20x/0.5 Na objective (*Figure 3.2a*) and and a C-Apochromat 63x/1.2 NA water-immersion objective (*Figure 3.2b*) stained with Shank1a (green). Each utricle was divided into four quadrants. One area in each quandrant was viewed more closely with a 3x scan zoom.

Figure 3.2a.

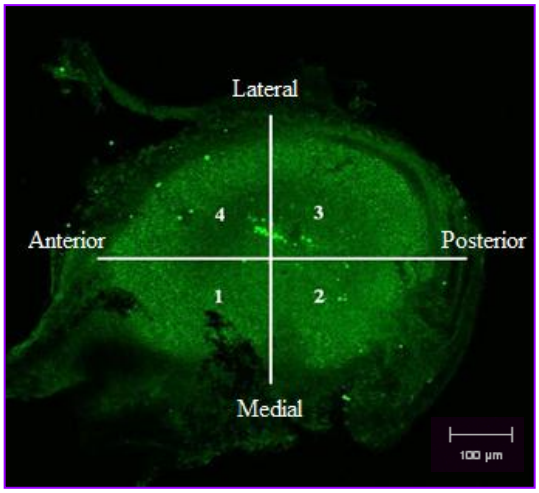

Figure 3.2b.

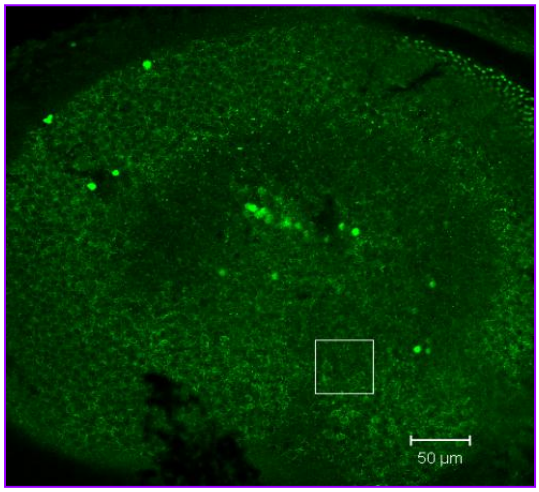

Figure 3.3: Bar graphs representing mean number of hair cells (*Figure 3.3a*), synaptic ribbons and post-synaptic receptor sites (*Figure 3.3b*), and synaptic colocalizations (*Figure 3.3c*). Hair cell and synaptic ribbon counts exhibited a significant decline by 22 months (denoted by an asterisk). The mean number of post-synaptic receptor sites and synaptic colocalizations remained relatively stable among all age groups.

Figure 3.3a.

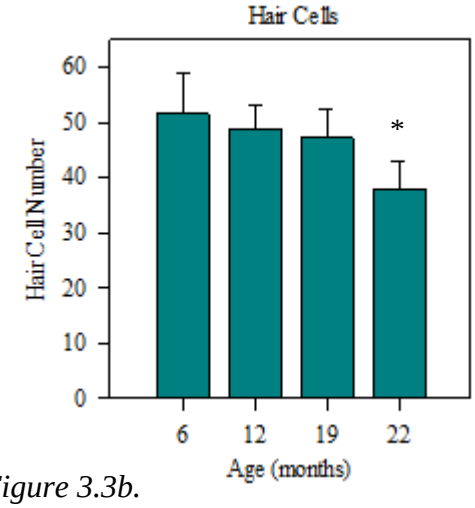

Figure 3.3b.

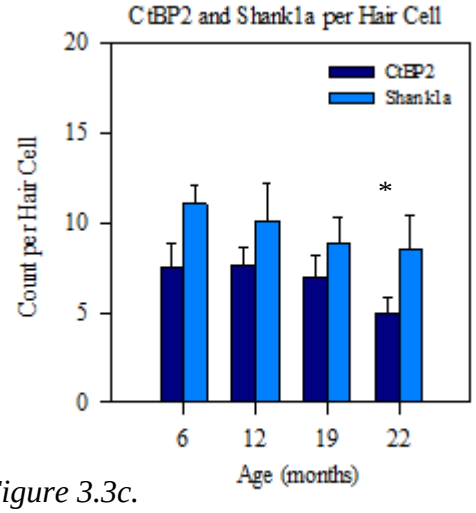

Figure 3.3c.

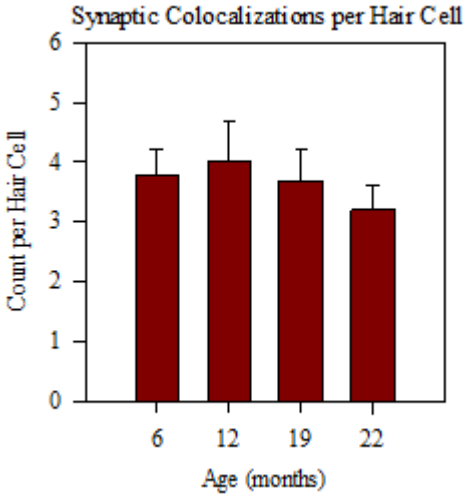

Figure 3.4: Scatter plot of mean VsEP threshold as a function of mean hair cell density (*Figure 3.4a*), synaptic ribbons per hair cell (HC; *Figure 3.4b*), post-synaptic receptor sites per hair cell (*Figure 3.4c*) and synaptic colocalizations (*Figure 3.4d*) for 6, 12, 19, and 22 month CBA/CaJ age groups.

Figure 3.4a.

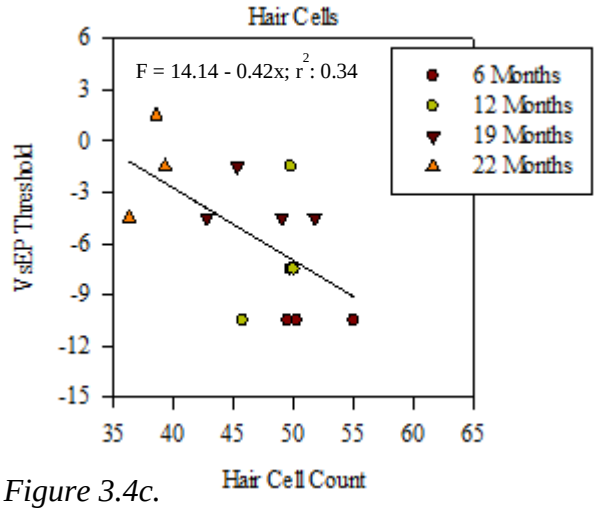

Figure 3.4b.

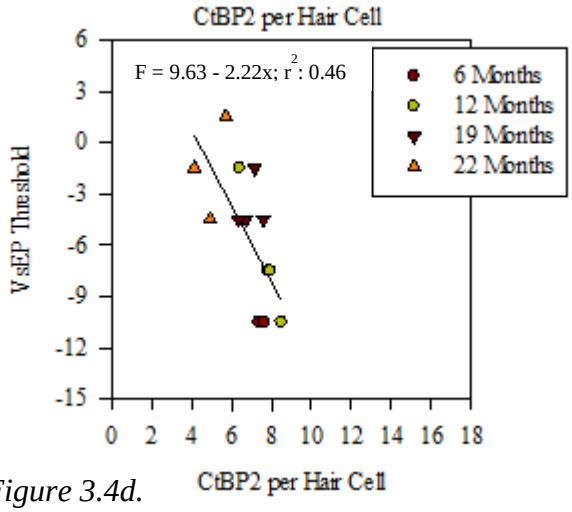

Figure 3.4c.

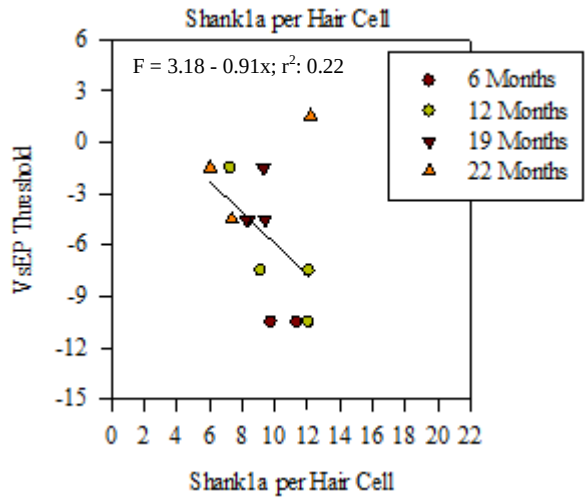

Figure 3.4d.

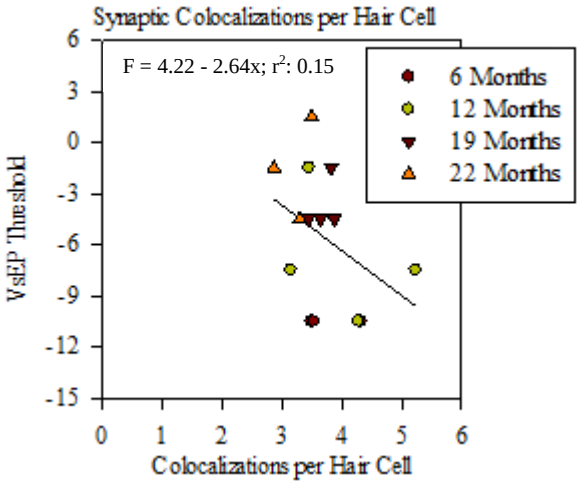

Table 3.1:

CBA/CaJ descriptive statistics for hair cell number, CtBP2 per hair cell, Shank1a per hair cell, synaptic colocalizatons per hair cell, and VsEP threshold. Structure totals were calculated based upon the mean area (0.198 mm^2) of the mouse utricular maculae epithelium (Desai, Zeh, & Lysakowski, 2005).

Structure	Age	N	Mean	Std. Dev.	Min.	Max.	Total
Hair Cell Number	6 months	3	51.58	2.98	50	55	4507.47
	12 months	4	48.81	2.05	46	50	4265.40
	19 months	4	47.19	3.98	43	52	4123.83
	22 months	3	38.00	1.56	36	39	3320.74
CtBP2 per Hair Cell	6 months	3	7.53	0.15	7.36	7.64	33941.23
	12 months	4	7.67	0.89	6.41	8.49	32715.64
	19 months	4	6.95	0.54	6.34	7.59	28660.65
	22 months	3	4.93	0.78	4.15	5.71	16371.25
Shank1a per Hair	6 months	3	11.07	1.18	9.77	12.08	49897.67
Cell	12 months	4	10.15	2.36	7.28	12.10	43293.84
	19 months	4	8.83	0.61	8.24	9.40	36413.46
	22 months	3	8.52	3.24	6.02	12.18	28292.71
Colocalizations	6 months	3	3.78	0.47	3.49	4.33	17038.23
(CtBP2 and Shank1a	12 months	4	4.03	0.93	3.15	5.23	17189.57
per Hair Cell	19 months	4	3.69	0.20	3.43	3.87	15216.95
	22 months	3	3.21	0.32	2.86	3.49	10659.58
VsEP Threshold	6 months	3	-10.50	0.00	-10.50	-10.50	-
	12 months	4	-6.75	1.89	-10.50	-1.50	-
	19 months	4	-3.75	0.75	-4.50	-1.50	-
	20 months	3	-1.50	1.73	-4.50	1.50	-

Table 3.2:

CBA/CaJ ANOVA table for hair cell count, CtBP2 per hair cell, Shank1a per hair cell and synaptic colocalizations per hair cell.

Structure	Sum of Squares	df	Mean Square	F	P-Value
Hair Cell Number	317.33	3	105.78	12.78	0.00*
	82.76	10	8.28		
CtBP2 per Hair Cell	15.16	3	5.05	11.23	0.00*
	4.50	10	0.45		
Shank1a per Hair	13.52	3	4.51	1.08	0.40
Cell	41.60	10	4.16		
Colocalizations per	1.16	3	0.39	1.14	0.38
Hair Cell	3.39	10	0.34		

* Less than $\alpha = 0.05$

Table 3.3:

CBA/CaJ multiple comparisons Tukey post hoc table for hair cell number and age group.

Structure	Age Group (I)	Age Group (J)	P-Value	95% Confidence Interval	
Hair Cell Number	6	12	0.61	-3.95	9.49
		19	0.25	-2.33	11.12
		22	0.00*	6.40	20.77
	12	6	0.61	-9.49	3.95
		19	0.85	-4.60	7.85
		22	0.00*	4.09	17.53
	19	6	0.25	-11.12	2.33
		12	0.85	-7.85	4.60
		22	0.01*	2.47	15.91
	22	6	0.00*	-20.77	-6.40
		12	0.00*	-17.53	-4.09
		19	0.01*	-15.91	-2.47

* Less than $\alpha = 0.05$

Table 3.4:

CBA/CaJ multiple comparisons Tukey post hoc table CtBP2 per hair cell and age group.

Structure	Age Group (I)	Age Group (J)	P-Value	95% Confidence Interval	
CtBP2 per Hair Cell	6	12	0.99	-1.71	1.43
		19	0.68	-0.99	2.15
		22	0.00*	0.92	4.28
	12	6	0.99	-1.43	1.71
		19	0.47	-0.74	2.17
		22	0.00*	1.17	4.31
	19	6	0.68	-2.15	0.99
		12	0.47	-2.17	0.74
		22	0.01*	0.45	3.59
	22	6	0.00*	-4.28	-0.92
		12	0.00*	-4.31	-1.17
		19	0.01*	-3.59	-0.45

* Less than $\alpha = 0.05$

Table 3.5:

CBA/CaJ multiple comparisons Tukey post hoc table Shank1a per hair cell and age group.

Structure	Age Group (I)	Age Group (J)	P-Value	95% Confidence Interval	
Shank1a per Hair Cell	6	12	0.93	-3.84	5.69
		19	0.51	-2.53	7.00
		22	0.46	-2.54	7.64
	12	6	0.93	-5.69	3.84
		19	0.80	-3.10	5.72
		22	0.73	-3.14	6.39
	19	6	0.51	-7.00	2.53
		12	0.80	-5.72	3.10
		22	1.00	-4.45	5.08
	22	6	0.46	-7.64	2.54
		12	0.73	-6.39	3.14
		19	1.00	-5.08	4.45

Table 3.6:

CBA/CaJ multiple comparisons Tukey post hoc table CtBP2 and Shank1a colocalizations per hair cell and age group.

Structure	Age Group (I)	Age Group (J)	P-Value	95% Confidence Interval	
Colocalizations per Hair Cell	6	12	0.95	-1.60	1.12
		19	1.00	-1.27	1.45
		22	0.64	-0.88	2.02
	12	6	0.95	-1.12	1.60
		19	0.84	-0.92	1.60
		22	0.32	-0.55	2.17
	19	6	1.00	-1.45	1.27
		12	0.84	-1.60	0.92
		22	0.71	-0.88	1.84
	22	6	0.64	-2.02	0.88
		12	0.32	-2.17	0.55
		19	0.71	-1.84	0.88

Table 3.7:

CBA/CaJ linear regression table for hair cells, CtBP2 per hair cell, Shank1a per hair cell, and colocalizations per hair cell.

Structure	Intercept (b_0)	Slope (b_1)	P-Value	Goodness of Fit (r^2)
Hair Cells	14.14	-0.42	0.03*	0.34
CtBP2 per Hair Cell	9.63	-2.22	0.01*	0.46
Shank1a per Hair Cell	3.18	-0.91	0.09	0.22
Colocalizations per Hair Cell	4.22	-2.64	0.17	0.15

* Less than $\alpha = 0.05$

CHAPTER IV: STRUCTURAL CORRELATES FOR VESTIBULAR FUNCTIONAL AGING IN TWO MOUSE STRAINS CARRYING *Ahl*

Abstract

C57BL/6J and CE/J mouse strains carry the genetic mutation *Cdh23*^{753A} (*Ahl)*, which results in early-onset, age-related hearing loss; however, gravity receptor function declines at a significantly faster rate in the CE/J strain compared to the C57BL/6J strain (Mock, 2008). The purpose of the present study was to characterize the effect of age on three structures within the utricle of the inner ear: hair cells, synaptic ribbons, and post-synaptic receptor sites. Utricles were dissected, stained with CtBP2 and Shank1a, and imaged using confocal microscopy. Structures were quantified and averaged over three to four distinct areas (~2300 μm^2) of the utricle at several ages across the lifespan. For C57BL/6J mice, no decline in these structural elements was observed across age. This finding is consistent with minimal observed declines in gravity receptor function (0.12 dB re: 1.0 g/ms per month; Mock, 2008). All structures measured for the CE/J strain were maintained with age. Structural maintenance with age for CE/J mice is in stark contrast to functional aging wherein CE/J mice exhibited substantial declines in gravity receptor function (0.47 dB re: 1.0 g/ms per month; Mock, 2008). Age-related structural changes could not fully explain the extent of gravity receptor dysfunction observed with age for the CE/J strain. Overall, results suggest that the presence of *Ahl* does not result in significant loss of vestibular structures with age. Additional factors must be responsible for age-related declines in gravity receptor function seen in CE/J mice.

Introduction

Our ability to maintain balance is influenced, in part, by sensory input from the inner ear vestibular system, which detects and encodes movement of the head. In addition to the vestibular system, balance is also impacted by other systems such as the proprioceptive and visual systems. Together, these modalities influence our overall ability to maintain proper balance. With age, these sensory systems may degenerate, which significantly impacts our ability to maintain postural control. Twenty-five to thirty-nine percent of individuals 65 years or older are estimated to fall each year (Keskin et al. 2008). Approximately 24% of individuals who fall will sustain some form of severe injury that requires medical attention or results in a fracture or restriction of activity. Over 1.6 million older individuals are estimated to visit emergency departments for fall-related injuries each year (National Institute on Aging, 2006). For the elderly, falling may lead to extended stays in hospital settings, or even nursing homes (Means et al., 2005). This can have significant implications on quality of life as balance dysfunction with age can be detrimental to an individual's sense of control and independence. Although numerous studies have shown that our ability to maintain balance declines with age, the structural changes related to this functional decline are not completely known.

Both qualitative and quantitative changes in vestibular structural elements have been observed in human temporal bones and animal models. Previously reported age-related structural declines include a reduction in the quantity and quality of otoconia and globular substances (Igarashi, Saito, Mizukoshi, & Alford, 1993; Jang, Hwang, Shin, Bae, & Kim., 2006; Johnsson, 1971; Ross, Peacor, Johnsson, & Allard, 1976; Suzuki, Ikeda, & Takasaka, 1997; Walther & Westhofen, 2007), stereocilia integrity (Bloom & Hultcrantz, 1994; Rosenhall & Rubin, 1974), and hair cell number and density (Gleeson & Felix, 1987; Merchant et al., 2000;

Park, Hubel, & Woods, 1987; Rauch, Velazquez-Villasenor, Dimitri, & Merchant, 2001; Richter, 1980; Rosenhall & Rubin, 1975, Severinsen et al., 2007; Shiga et al., 2005). Yet, to date, structural aging has not been correlated with vestibular functional declines observed with age.

Recent studies have identified a rapidly expanding number of genetic mutations resulting in disparate rates of early-onset age related hearing loss. Currently, eight genetic mutations have been identified which result in early-onset age related hearing loss. *Cdh23*^{Ahl}, or *Ahl*, is a single nucleotide substitution in the cadherin23 (*Cdh23)* gene located on chromosome 10. *Cdh23* is a protein that is vital to the normal development of inner ear structures as well as maintenance of stereociliary tip links and lateral links (Di Palma et al., 2001; Lagziel et al., 2005; Rzadzinska et al. 2005). *Ahl* was the first genetic mutation identified which causes late-onset, non syndromic hearing loss in mice (Johnson et al., 1997). *Ahl2* is located on chromosome 5. The hearing loss produced by this genetic mutation is dependent upon a predisposing *Ahl* genotype (Johnson & Zheng, 2002). *Ahl3* is located on chromosome 17 (Nemoto et al., 2004). *Ahl4* is located on chromosome 10. This genetic mutation results in an onset of hearing loss earlier than that of *Ahl*. *Ahl5 and Ahl6* have been mapped on chromosome 10 and on chromosome 18, respectively (Drayton & Noben-Trauth, 2005). *Ahl8* is located on the distal portion of chromosome 11 (Johnson et al., 2008). The nomenclature *Ahl7* has been reserved for future identification (The Jackson Laboratory, 2011). While the role of *Ahl* on the auditory system is well known, the effect of *Ahl* on the vestibular system is less understood.

C57BL/6J and CE/J mouse strains both carry *Ahl* mutations. In addition, C57BL/6J mice harbor another genetic locus for age-related hearing loss, known as *Ahl3*. Both C57BL/6J and CE/J mice exhibit similar patterns of auditory decline with age; however, gravity receptor function in the CE/J mouse strain declines at a significantly faster rate than in the C57BL/6J

mouse strain (Mock, 2008). Indeed, gravity receptor function in C57BL/6J mice is remarkably preserved into advanced age. The structural correlates any functional declines are unknown.

Two recent studies are of importance to this research. In a study by Shiga et al. (2005), hair cell density in the cristae of the horizontal semicircular canal was examined and compared with vestibulo-ocular reflex (VOR) function in the C57BL/6 mouse strain from three weeks to 15 months of age. VOR is an indirect measure of gravity receptor function, although it typically reflects integrity of the horizontal semicircular canal. VOR gain was maintained until at least 15 months of age (oldest age group measured) in the C57BL/6 mouse strain. In contrast, a decline in hair cell density was observed early in life to the extent that hair cell density declined to 80% of that measured at three weeks by six months of age. Hair cell density declined a further 70% by 15 months of age. Shiga and colleagues concluded that structural declines in the peripheral vestibular system do not correlate well with aging vestibular function.

Macular function was measured across the lifespan for C57BL/6J and CE/J mice (Mock et al., 2008). 148 C57BL/6J mice ranging in age from one to 24 months and 96 CE/J mice ranging in age from one to 21 months were measured using vestibular sensory evoked potentials (VsEPs), which are compound action potentials that are generated by the vestibular portion of the VIII cranial nerve (vestibulocochlear nerve) and central relays (Nazareth & Jones, 1998). VsEPs are a direct measure of vestibular function, relying on the functional integrity of both the utricle and saccule. In addition, otoconia density was qualitatively examined for both mouse strains. C57BL/6J mice demonstrated an average decline of 0.12 dB re: 1.0 g/ms per month while CE/J mice exhibited a 0.47 dB re: 1.0 g/ms decrease per month in gravity receptor function. CE/J mice demonstrated over twice as much VsEP dynamic range loss at the oldest age groups when compared to the C57BL/6J strain (CE/J: 56% loss of dynamic range at 20-21

months; C57BL/6J: 21% loss of dynamic range at 22-23 months); however, no loss of otoconia in the utricle or saccule was observed in either mouse strain, suggesting that otoconia density could not account gravity receptor functional declines with age.

The effect of *Ahl* on gravity receptor function cannot be easily predicted. Previous studies measuring structural changes alone have provided some evidence that normal aging does indeed affect the number and integrity of structures within and surrounding the macular hair cells (i.e., otoconia, stereocilia, hair cells, neural components, etc.). What is unknown is if the presence of *Ahl* will affect degeneration of these structures with age.

Three structures at the hair cell level of the utricle of the inner ear which are critical to sensory transduction were characterized across the lifespan; hair cells, synaptic ribbons, and post-synaptic receptor sites, as well as the prevalence of synaptic ribbon/post-synaptic receptor site colocalizations for the C57BL/6J and CE/J mouse strains. Structural data for each strain was then compared with age-matched gravity receptor functional data as measured by VsEP threshold. The present study sought to answer two questions: 1) what is the effect of age on morphological structures in the utricle of the vestibular system in two strains carrying *Ahl* and 2) how well do structural changes in the utricle explain aging gravity receptor function as measured by VsEPs? It was hypothesized that structures would decline at a similar rate corresponding to gravity receptor function across the lifespan, with CE/J mice exhibiting a faster rate of structural decline with age compared to the C57BL/6J strain. A better understanding of the effect of *Ahl* on the vestibular system may provide insight into the underlying factors which may be responsible for gravity receptor functional declines with age.

Methods

Animals and Animal Preparation

C57BL/6J and CE/J mice were obtained from The Jackson Laboratory (Bar Harbor, ME). Animals were housed using standard husbandry procedures at East Carolina University until the appropriate age for testing. A total of 14 C57BL/6J mice yielding 21 utricles (six months: n = three temporal bones; 12 months: n = 10 temporal bones; 18 months: n = three temporal bones; 22 months: n = five temporal bones) were used. For the CE/J strain, a total of 9 mice yielded 15 utricles (six months: n = four temporal bones; 12 months: n = two temporal bones; 18 months: six temporal bones; 22 months: three temporal bones). Males and females were combined into one group as gravity receptor functional aging exhibits similar changes between genders for both mouse strains (Mock, 2008). C57BL/6J and CE/J mouse strains are commonly used in inner ear research. Both strains carry *Ahl*, which affects the gene $Cdh23^{ahl}$ located on chromosome 10. $Cdh23^{ahl}$ encodes for cadherin 23, a protein that is found in sensory cells and stereociliary bundles of the inner ear (Lagziel et al., 2005). Although the effects of *Ahl* on auditory and gravity receptor function with age has been documented (Johnson et al., 1997; Keithley et al., 2004; Mock, 2008; Mock, Jones, & Jones, 2011; Ouagazzal et al., 2006; White et al., 2000; Zheng et al., 1999), the role *Ahl* plays in aging structural changes within the vestibular system is largely unknown. The protocol was consistent with the recommendations of the American Veterinary Medical Association (AVMA) Guidelines on Euthanasia and approved by the Animal Care and Use Committee at East Carolina University:

Each mouse was injected with a lethal dose of Sodium Pentobarbital (3900 mg/kg) injected intraperitoneally. The temporal bones were dissected and fixed overnight in 4% Paraformaldehyde in 0.1 M Phosphate Buffer at room temperature. Following fixation, the

utricle was dissected from the temporal bone and the otoconia and otoconial membrane were gently scraped off while bathed in 0.01 M Phosphate Buffered Saline with 3% Triton (PBST; 0.3 M Sodium Chloride, 0.3% Triton-X 100, 0.01 M Phosphate Buffer, pH 7.4). Each specimen was washed with PBST three times for 15 minutes each at room temperature. Blocking solution (10% Normal Goat Serum in PBST) was applied overnight at 4˚C. Following blocking, specimens were incubated in a primary antibody cocktail (Mouse anti-CtBP2: C-terminal binding protein 2; BD Transduction Laboratories; 1:300; Rabbit anti-Shank1a: Neuromics; 1:300; 5% Normal Goat Serum in PBST) for 48 hours at 4 °C. The utricles were then washed in PBST three times for 50 minutes each at room temperature. Secondary antibodies were applied in a cocktail (for CtBP2: Alexa 488 goat-anti-mouse RED-Invitrogen; 1:200; for Shank1a: Alexa 633 goat-anti-rabbit GREEN-Invitrogen; 1:200) overnight at 4°C (once secondary antibodies were applied, the specimens were shielded from light). Specimens underwent three final washes (15 minutes each) in 0.01 M Phosphate Buffered Saline at room temperature. Following the washes, each specimen was mounted on a slide with ProLong® Gold antifade reagent (Invitrogen) and cover slipped.

The utricles were viewed with an inverted Zeiss LSM 510 Confocal microscope and images captured using Zeiss LSM 510 Version 4.2 SP1 software. The 488 (20% intensity) and 633 (25% intensity) laser lines were used to view fluorescence. Laser light was passed through a bandpass filter of 505-530 nm for the red channel and a longpass filter of 650 nm for the green channel (Figure 4.1). Images were captured at a low magnification using a Plan-Neofluar 10x/0.3 NA objective. To view images at a higher magnification, a C-Apochromat 63x/1.2 NA water-immersion objective was used with 3x scan zoom.

Each utricle was divided into four quadrants: two medial areas (quadrants 1 and 2) and two lateral areas (quadrants 3 and 4) based upon the utricle's natural curvature (Figure 2a). One area was chosen within each quadrant to be imaged for further analysis (Figure 2b). Each area was selected based upon quality (no fissures, tears, gaps, etc. in the imaged area of the epithelium) and uniformity of fluorescence. The areas were scanned at 512 x 512 pixels at optimal z interval (0.16 µm; according to Nyquist Frequency), yielding 30-50 image slices per area. 17 out of 21 C57BL/6J specimens yielded four complete images (one image per quadrant); four specimens yielded three images (at least one image representing the medial and lateral areas). For the CE/J strain, 13 out of 15 specimens yielded four complete images (one image per quadrant); two specimens yielded three images (at least one image representing the medial and lateral areas). In a comparison of structural counts in medial versus lateral areas, no significant differences were observed; therefore, the data were combined to evaluate response variables as a function of age.

Data Analysis

Once the three-dimensional z stack was captured by the computer, the image was transferred to Volocity 3D imaging software for data analysis. To quantify hair cells and synaptic ribbons, each z stack was opened and the Alexa 633 (green) channel was disabled, allowing only the Alexa 488 (red) channel to be visualized. Hair cells were then manually quantified in the imaged area by visualizing those cell nuclei which were oval in shape (to distinguish hair cell nuclei from supporting cell nuclei, which are hexagonal in shape) and a marker was placed on each identified hair cell to prevent the hair cell from being counted twice. To quantify synaptic ribbons (i.e. CtBP2), the series of 2D images that composed the 3D z stack

were examined sequentially. Those CtBP2 points that was observed in two or more consecutive images and no larger than one micron in diameter was counted as a synaptic ribbon. A marker was placed at each identified synaptic ribbon in order to prevent it from being counted twice.

Due to the increased level of background staining for the Alexa 633 antibody, post-synaptic receptor sites were quantified using a specialized protocol created with Volocity software. The Alexa 488 (red) channel was disabled, allowing only the Alexa 633 channel to be visualized. An intensity and size thresholding procedure was implemented to identify those points that represented post-synaptic receptor sites. Colocalizations between CtBP2 and Shank1a were also quantified manually. Each CtBP2 and Shank1a point that was observed in two or more consecutive images, no larger than one micron in diameter, and appeared to touch or overlap was counted as one colocalization. A marker was placed at each identified synaptic colocalization in order to prevent it from being counted twice.

Age-matched VsEP threshold data from Mock (2008) were correlated with the structural data. VsEP measures were detailed in Mock's study and followed well established procedures developed by Jones and colleagues (reviewed by Jones, 2009; Jones & Jones, 2008).

The number of hair cells, synaptic ribbons, and post-synaptic receptor sites were quantified in a 47.6 µm x 47.6 µm (2265.76 μm^2) area. Counts from each quadrant in the utricle were averaged together to obtain a mean hair cell, synaptic ribbon, post-synaptic receptor site, and synaptic colocalization count per hair cell for each mouse strain. Results were then compared among different age groups, and correlated with direct functional threshold results, as measured by VsEP threshold, obtained previously by Mock (2008). Comparisons between age groups were made using univariate analysis of variance (ANOVA). Linear regression was

performed to correlate structural data with VsEP thresholds across the lifespan. A p-value of less than 0.05 was determined to be statistically significant.

Results

Quantitative Data for C57BL/6J Mouse Strain

Table 4.1 describes the descriptive statistics for the structural data measured for the C57BL/6J mouse strain. A total count across the utricle was calculated for each structure by multiplying each structural count per imaged area (2265.76 nm^2) by the total area of the utricular maculae epithelium (0.198 $mm^{2)}$ as measured by Desai, Zeh, and Lysakowski (2005). C57BL/6J values for average number of hair cells per 2265.76 μm^2 per specimen ranged from 54.67 to 57.25 for the six month age group, 47.75 to 58.25 for the 12 month age group, 47.50 to 56.00 for the 18 month age group, and 46.00 to 57.75 for the 22 month age group. Analysis of variance testing for hair cell number demonstrated no significant difference between age groups (six months: 56.31 ± 1.42; 12 months: 51.37 ± 3.88; 18 months: 52.92 ± 4.71; 22 months: 52.35 ± 4.47; Table 4.2; Total hair cell count: six months: 4920.81; 12 months: 4489.12; 18 months: 4624.57; 22 months: 4574.76; Table 4.2). Values for the number of CtBP2 per hair cell ranged from 5.90 to 7.99 for the six month age group, 7.57 to 13.73 for the 12 month age group, 8.05 to 11.08 for the 18 month age group, and 10.61 to 13.32 for the 22 month age group. A significant difference in CtBP2 per hair cell was observed among age groups (six months: 6.86 ± 1.06; 12 months: 11.32 ± 1.91; 18 months: 9.27 ± 1.60; 22 months: 11.99 ± 1.34; Total CtBP2 count: six months: 33756.77; 12 months: 50816.80; 18 months: 42869.74; 22 months: 54851.33; Table 4.2). Post hoc Tukey analysis demonstrated that the number of CtBP2 per hair cell for the 12 and 22 month age groups were significantly higher than the youngest age group (six months;

Figure 3a; Table 4). The number of Shank1a per varied widely among specimens, especially for the younger age groups (six and 12 months). Shank1a per hair cell ranged from 9.40 to 16.98 at six months, 7.03 to 20.40 at 12 months, 8.50 to 10.90 at 18 months, and 7.99 to 10.99 at 22 months. No significant difference in shank1a per hair cell was observed among age groups (six months: 12.73 ± 3.87; 12 months: 14.01 ± 4.76; 18 months: 9.35 ± 1.35; 22 months: 9.32 ± 1.28; Total Shank1a count: six months: 62641.94; 12 months: 64790.19; 18 months: 43239.71; 22 months: 42636.73; Figure 4.3, Table 4.2). Values for synaptic colocalizations were considerably smaller than single counts of CtBP2 and Shank1a per hair cell alone, given that many synaptic ribbons occurred singly without a corresponding post-synaptic receptor site. Synaptic colocalizations per hair cell ranged from 1.87 to 2.88 for the six month age group, 1.74 to 5.12 for the 12 month age group, 3.29 to 3.87 for the 18 month age group, and 2.88 to 3.39 for the 22 month age group. Similar to hair cell and Shank1a per hair cell counts, no significant change in the number in synaptic colocalizations per hair cell (six months: 2.47 ± 0.53; 12 months: 3.91 ± 1.00; 18 months: 3.51 ± 0.32; 22 months: 3.10 ± 0.24; Total synaptic colocalization count: six months: 12154.41; 12 months: 17552.44; 18 months: 16232.23; 22 months: 14181.74; Table 4.2; Figure 4.3c) was observed.

C57BL/6J Gravity Receptor Function

Table 4.1 illustrates average VsEP threshold per age group for the C57BL/6J mouse strain. Values for VsEP threshold in C57BL/6J mice ranged from -13.5 to -10.5 dB re: 1.0 g/ms for the six month age group, -10.5 to -7.5 dB re: 1.0 g/ms for the 12 month age group, -10.5 dB re: 1.0 g/ms for the 18 month age group (all age-matched animals yielded a VsEP threshold of -10.5), and -10.5 to -4.5 dB re: 1.0 g/ms for the 22 age group. Six month old C57BL/6J mice (-

12.90 dB ± 1.34) exhibited better vestibular function compared to 12 month old C57BL/6J mice (-8.50 dB ± 1.55); however, these results were not significantly different. VsEP threshold improved slightly for the 18 month age group with all mice tested at that age exhibiting the same threshold (-10.50 dB ± 0.00). The 22 month age group was similar to the 12 month age group in terms of VsEP threshold (-8.10 dB ± 2.51).

Comparisons between C57BL/6J Structural Data and Gravity Receptor Function

The rate of decline between gravity receptor function and structural data exhibited an inverse relationship (Figure 4.4). Although slight declines in VsEP threshold were observed with age for the C57BL/6J strain, the majority of our structural data remained stable, even into advanced ages. In fact, CtBP2 counts per hair cell significantly increased at the younger age groups measured (six months versus 12 months). Therefore, structural changes in the vestibular system of C57BL/6J mice do not appear to explain gravity receptor functional declines observed for this strain.

Quantitative Data for CE/J Mouse Strain

Table 4.8 describes the descriptive statistics for the structural data measured in the CE/J mouse strain. A total count across the utricle was calculated for each structure by multiplying each structural count per imaged area (2265.76 nm^2) by the total area of the utricular maculae epithelium (0.198 $mm^{2)}$ as measured by Desai, Zeh, and Lysakowski (2005). CE/J values for average number of hair cells per 2265.76 μm^2 ranged from 46.50 to 56.50 for the six month age group, 50.25 to 50.75 for the 12 month age group, 39.75 to 52.00 for the 18 month age group, and 41.00 to 48.00 for the 20 month age group. Hair cell counts remained stable for the younger age groups (6 months: 49.88 ± 4.66; 12 months: 50.50 ± 0.35; Table 4.8). A slight decline in the

number of hair cells was observed for age groups beyond 12 months (18 months: 46.81 ± 4.65; 20 months: 45.42 ± 3.84; Table 4.8; Figure 4.5); however, this decline was insignificant. Total estimated hair cell counts across the epithelium were 4358.91 at six months, 4413.09 at 12 months, 4090.63 at 18 months, and 3969.16 at 20 months. The number of CtBP2 per hair cell ranged from 7.40 to 9.67 for the 6 month age group, 7.28 to 8.08 for the 12 month age group, 5.50 to 9.47 for the 18 month age group, and 7.51 to 8.09 for the 20 month age group. CtBP2 per hair cell remained relatively stable among all age groups measured (6 months: 8.37 ± 1.05; 12 months: 7.68 ± 0.57; 18 months: 7.40 ± 1.60; 20 months: 7.85 ± 0.30; Total CtBP2 count: six months: 36484.06; 12 months: 33892.52; 18 months: 30270.64; 20 months: 31157.89; Table 4.8; Figure 4.5). Shank1a per hair cell varied from 6.13 to 11.58 at 6 months, 7.83 to 10.50 at 12 months, 5.65 to 13.58 at 18 months, and 7.26 to 10.73 at 20 months. No significant decline with age was observed across age groups (6 months: 9.24 ± 2.27; 12 months: 9.17 ± 1.89; 18 months: 8.42 ± 3.25; 20 months: 9.15 ± 1.76; Total Shank1a count: six months: 40276.31; 12 months: 40468.02; 18 months: 34443.08; 20 months: 36317.80; Table 4.8, Figure 4.5). The number of synaptic colocalizations per hair cell varied from 2.48 to 3.28 at 6 months, 2.86 to 3.21 at 12 months, 1.65 to 3.55 and 18 months, and 2.43 to 2.85 at 20 months. Similar to the other structures measured in the CE/J strain, no significant difference was observed for synaptic colocalization counts per hair cell (6 months: 2.99 ± 0.35; 12 months: 3.04 ± 0.25; 18 months: 2.57 ± 0.66; 2.70 ± 0.23; Total synaptic colocalization count: six months: 13033.14; 12 months: 13415.79; 18 months: 10512.91; 20 months: 10716.73; Table 4.8; Figure 4.5).

CE/J Gravity Receptor Function

Table 4.8 illustrates average VsEP threshold per age group. Values for VsEP threshold in the CE/J strain ranged from -13.5 to -4.5 dB re: 1.0 g/ms at six months, -7.5 to 1.5 dB re: 1.0 g/ms at 12 months, -7.5 to 1.5 dB re: 1.0 g/ms at 18 months, and -4.5 to 1.5 dB re: 1.0 g/ms at 20 months. 6 month old CE/J mice (-9.30 dB ± 3.42) exhibited better vestibular function compared to 12 month old CE/J mice (-3.75 dB ± 3.77). VsEP threshold remained relatively stable from 12 to 18 months (-3.00 dB ± 3.87). The 20 month age group exhibited the poorest gravity receptor function (-0.90 ± 2.51).

Comparisons between CE/J Structure and Gravity Receptor Function

A similar rate of decline was observed between all measured structures and gravity receptor function (Figure 4.6). VsEP thresholds declined an average of 0.18 dB re: 1.0 g/ms for every decline in hair cell (intercept: 4.84; r^2: 0.02; p-value: 0.57). CtBP2 counts per hair exhibited an even greater effect on gravity receptor function, as VsEP thresholds diminished an average of 1.95 dB re: 1.0 g/ms for every decline in CtBP2 per hair cell (intercept: 11.28; r^2: 0.21; p-value: 0.09). VsEP thresholds declined an average of 0.24 dB re: 1.0 g/ms for every decline in Shank1a per hair cell (intercept: -1.76; r^2: -0.01; p-value: 0.68). Synaptic colocalization counts per hair cell exhibited the largest relationship with gravity receptor function, as VsEP thresholds declined an average of 3.04 dB re: 1.0 g/ms for every decline in colocalization counts per hair cel (intercept: 4.52; r^2: 0.09; p-value: 0.28); however, these data were not significant.

Discussion

Overall, structural data measured for C57BL/6J and CE/J mice were maintained across the lifespan. Structural aging is for the C57BL/6J strain is consistent with minimal observed declines in gravity receptor function across the lifespan. Maintenance of structural elements as observed in the CE/J mouse strain is in contrast to vestibular functional aging, in that CE/J mice exhibit severe age-related gravity receptor dysfunction. The findings of this study provide new insight concerning 1) age-related structural changes in the C57BL/6J and CE/J mouse strain, which both harbor *Ahl* mutations, and 2) the relationship between structural changes in the vestibular system and gravity receptor function with age. Our results suggest that, although structural data corresponds with aging gravity receptor function for one mouse strain which harbors *Ahl* (C57BL/6J), structural aging for the CE/J mouse strain is disparate to aging vestibular functional declines and suggests that other structures in the periphery or central vestibular system may be responsible. Whether similar maintenance of structural elements holds true for other mouse strains carrying *Ahl* remains to be seen.

Interestingly, some age-related structural declines were observed for the CBA/CaJ mouse strain (chapter 3), which serves as a model for normal aging. Examination of structural elements in the CBA/CaJ mouse strain revealed quantitative declines in pre-synaptic elements at the oldest age group (hair cells and CtBP2 per hair cell; 22 months; p value < 0.05). Declines in these structures correspond to normal age-related vestibular dysfunction. C57BL/6J mice demonstrate a minimal loss of gravity receptor dysfunction with age. It was hypothesized that the C57BL/6J strain would exhibit a limited decline in structure. Indeed, results showed that both pre-synaptic as well as post-synaptic elements were largely maintained across the lifespan. CE/J mice exhibit substantial declines in gravity receptor function with age. It was hypothesized that structures

would decline at a rate corresponding to function. However, the CE/J strain exhibited no loss in structure with age. CBA/CaJ gravity receptor function as measured by age-matched VsEP thresholds indicated significant age-related declines in function (0.39 dB re: 1 g/ms increase in VsEP threshold per month), although not to the extent of the CE/J mouse strain (0.47 dB re: 1 g/ms increase in VsEP threshold per month). C57BL/6J mice exhibited the best gravity receptor function, demonstrating only slight declines at the oldest ages (0.12 dB re: 1 g/ms per month decline of macular function with age). Structural declines observed for the CBA/CaJ mouse strain which were not seen in the C57BL/6J and CE/J mouse strains is a unique finding, and suggests that the presence of *Ahl* may result in a limited loss of structure over the lifespan.

Observed hair cell maintenance for the C57BL/6J and CE/J mouse strains is in contrast to previous reports of age-related quantitative and qualitative changes in hair cells, including changes in hair cell number and density, as well as increases in lipofuscin (age-related pigment) and inclusions (Gleeson & Felix, 1987; Merchant et al., 2000; Park, Hubel, & Woods, 1987; Rauch, Velazquez-Villasenor, Dimitri, & Merchant, 2001; Richter, 1980; Rosenhall & Rubin, 1975, Severinsen et al., 2007; Shiga et al., 2005). Total hair cell counts over the entire utricular maculae for the C57BL/6J and CE/J strains (C57BL6J: 4652.32 total hair cells; CE/J: 4207.95 total hair cells) were on average higher than previous reports of hair cell number of the utricular maculae, which averaged 3613 hair cells in adult ICR mice (Li, Xue, & Peterson, 2008); however, to date, this is the first study to quantify hair cell totals in the utricles of C57BL/6J and CE/J mice across the lifespan. Synaptic ribbon maintenance across the lifespan is a unique finding. Only one known study has examined synaptic ribbons within the vestibular system across the lifespan. Park and colleagues (1987) grossly identified the prevalence of synaptic ribbons in the vestibular organs of aging C57BL/6NNia mice. No substantial loss of synaptic

ribbons was observed with age, although the data were not quantified. To date, the current research is the only known quantitative measurement of synaptic ribbons in the vestibular organs across the lifespan. No significant age-related decline in post-synaptic receptor sites per hair cell was observed. This finding is in contrast to a previous examination of neural components (Leonard & Kevetter, 2007), in which degeneration of primary afferents in the vestibular system with age was observed; however, there are several notable differences between our study, which examined post-synaptic receptor sites in the aging mouse utricle, and Leonard and Kevetter's study, which qualitatively examined calyces in the cristae of the aging gerbil. In addition to the disparate vestibular organ and mammalian species examined by Leonard and Kevetter, those synapses that were innervated by bouton or dimorphic afferents were not taken into account. To our knowledge, this is the first study to quantitatively examine post-synaptic receptor sites in the mouse utricle across the lifespan.

It is interesting to note that the numbers of synaptic colocalizations were maintained with age for both mouse strains. One would expect a decline among these structural colocalizations, as the co-occurrence of a synaptic ribbon with a post-synaptic receptor site is vital to sensory transduction: neither structure may function appropriately without the other. Instead, two to four synaptic colocalizations per hair cell were observed across the lifespan for both mouse strains. Synaptic ribbon counts per hair cell were smaller on average for both mouse strains when compared to post-synaptic receptor sites (Table 4.1; Table 4.8). Each synaptic colocalization consists of one synaptic ribbon and one post-synaptic receptor site. Therefore, synaptic colocalization counts were driven by synaptic ribbon counts (the number of synaptic colocalizations by default could be no greater than synaptic ribbon counts). An important question arises: although the numbers of synaptic colocalizations remain stable across the

lifespan, why do the C57BL/6J and CE/J mouse strains exhibit age-related gravity receptor dysfunction? One possibility which may account for observed functional declines in the vestibular system is that some synaptic colocalizations may lose function over time.

Gomez-Casati et al. (2010) examined synaptic colocalizations using antibodies for RIBEYE/CtBP2 and GluR2/3 in the utricle of a young transgenic mouse strain that exhibits severe vestibular dysfunction (elimination of erb8 signaling in supporting cells resulting in a defect of synapse formation). Frequent misalignment of presynaptic and postsynaptic components as well as declines in previously formed synaptic structures was observed. Gomez-Casati and colleagues concluded that this transgenic mouse strain demonstrated an initial defect in synaptic formation as well as a maintenance error for synaptic structures. Their findings provided evidence that vestibular dysfunction observed for this mouse strain was a consequence of synaptic defects in the utricular maculae epithelium. Although age was not examined in their study, results show that structural maintenance of presynaptic and postsynaptic elements, both quantitatively and functionally, are critical to a normal functioning vestibular system. Although we observed no decline in synaptic colocalizations with age for either mouse strain, functional impairment of presynaptic and postsynaptic structures which may be responsible for age-related gravity receptor dysfunction cannot be ruled out.

Although structural elements were quantitatively examined, qualitative changes in the pre-synaptic and post-synaptic structures cannot be ruled out. A number of structural changes in the peripheral vestibular system have been reported, including a reduction in the quality of otoconia (Igarashi, Saito, Mizukoshi, & Alford, 1993; Jang, Hwang, Shin, Bae, & Kim, 2006; Ross, Peacor, Johnsson, & Allard, 1976; Walther & Westhofen, 2007), stereocilia integrity (Bloom & Hultcrantz, 1994; Rosenhall & Rubin, 1974), and hair cell structure (Park, Hubel, &

Woods, 1987; Richter, 1980; Rosenhall & Rubin, 1975, Severinsen et al., 2007). Other possible indicators of aging vestibular dysfunction may include physiological changes such as decreased metabolic activity and vascular supply (Ishiyama, 2009; Lyon & Davis, 2002; Lyon & King, 1997; Lyon & Wanamaker, 1993). In addition, changes in central relays of the vestibular system have been reported, including degeneration of the vestibular nuclei and vestibular portion of CN VIII (Alvarez et al., 2000; Johnson, 1971; Lopez, Honrubia, & Baloh, 1997). Although no structural declines were observed in the present study, qualitative changes of the measured structures with age cannot be ruled out.

These findings have significant implications for elderly humans. Balance is a major concern among the elderly as falls can lead to a loss of independence, which may significantly impact one's sense of well-being and safety. The need for care and treatment for the problems elderly individuals face will become even more relevant as the number of elderly individuals continues to rise in the United States. Given the prevalence of imbalance and falls among the elderly, determining the structural and physiological culprits responsible for aging vestibular dysfunction is imperative. It is estimated that 40 to 50% of reported dizziness can be attributed to disorders of the vestibular system (Marchetti & Whitney, 2005). In addition to direct structural declines in the vestibular system with age, other factors unrelated to the vestibular system which may cause dizziness among the elderly include medications, as well as muscle strength, joint flexibility, and coordination (Means et al., 2005). Visual changes such as loss of visual acuity, cross sensitivity, and depth perception have been reported among the elderly (Ivers, Cumming, Mitchell, & Attebo, 1998; Lord & Dayhew, 2001). Medical conditions can also increase the risk of dizziness and falls. Specific diseases prevalent to the elderly population include osteoporosis, heart disease, diabetes, cerebrovascular disease, and hypotension. In

addition, peripheral sensitivity (i.e., feet, hands, etc.) and reaction time may affect balance among the elderly (Jacobson & McCaslin, 2008). Despite multimodal losses of sensory function over time, age-related vestibular dysfunction cannot be fully attributed to sensory declines. Therefore, additional factors must be responsible for aging vestibular dysfunction.

In summary, structural maintenance observed within the utricle of the vestibular system with age was an unexpected finding given the extent of age-related gravity receptor dysfunction, especially for the CE/J mouse strain. C57BL/6J and CE/J mice exhibited better maintenance of structural elements across the lifespan when compared to structural data for the CBA/CaJ mouse strain, which exhibit quantitative structural declines in the number of hair cells and synaptic ribbon with age. One would expect that mice carrying *Ahl* would experience structural declines at least to the extent of those of the CBA/CaJ strain, given that CBA/CaJ mice represent a normal aging model; however, this was not the case. Structural stability in the presence of gravity receptor functional decline with age in two mouse strains carrying *Ahl* is an unexpected finding. Other structural and physiological changes in the vestibular periphery and central areas which may influence vestibular dysfunction with age remain to be seen.

Figure 4.1: Maximum intensity projection from a z-stack of a 6 month CBA/CaJ mouse imaged using a C-Apochromat 63x/1.2 NA water-immersion objective and zoomed 3x. The utricle was stained with CtBP2 (red) and Shank1a (green). The synaptic ribbons (red) and post-synaptic receptor sites (green) are represented as bright areas of fluorescence throughout the image while the hair cell nuclei (red) are distinguished in the background from synaptic ribbons by their significantly larger, oval appearance. All red areas of fluorescence larger than one micron in diameter was excluded from our synaptic ribbon count. For this image, the number of hair cells was 53, CtBP2 per hair cell was 7.28, and Shank1a per hair cell was 8.17.

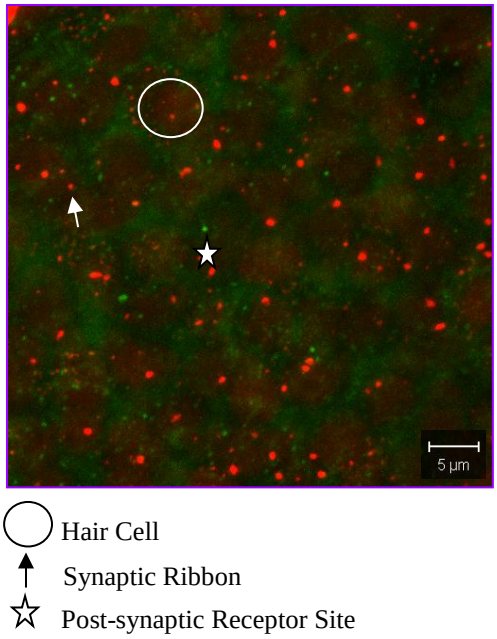

Figure 4.2: Confocal utricular single images from a young B6.129 mouse, imaged using a Plan-Neofluar 20x/0.5 Na objective (*Figure 4.2a*) and and a C-Apochromat 63x/1.2 NA water-immersion objective (*Figure 4.2b*) stained with Shank1a (green). Each utricle was divided into four quadrants. One area in each quandrant was viewed more closely with a 3x scan zoom.

Figure 4.2a.

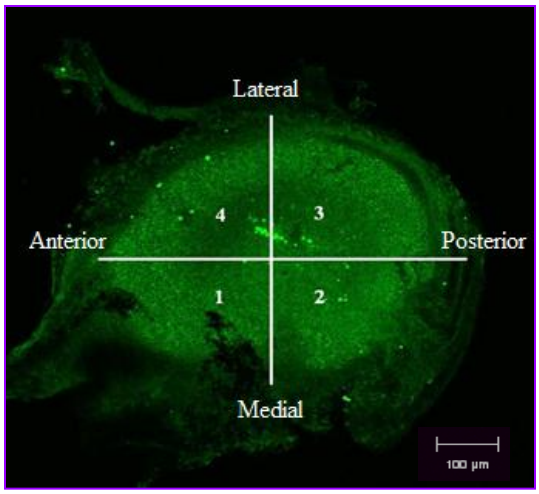

Figure 4.2b.

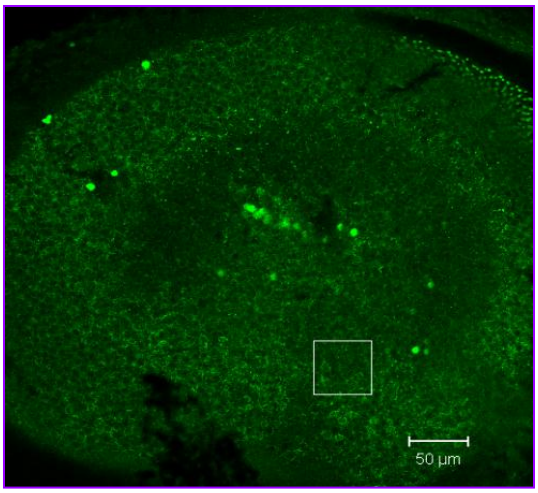

Figure 4.3: Bar graph of mean number of hair cells (*Figure 4.3a*), synaptic ribbons, post-synaptic receptor sites (*Figure 4.3b*), and synaptic colocalizations (*Figure 4.3c*) for the C57BL/6J strain. The mean number synaptic ribbons per hair cell exhibited a significant increase from six to 12 months and from six to 22 months (denoted by an asterisk). All other structures remained stable with age.

Figure 4.3a.

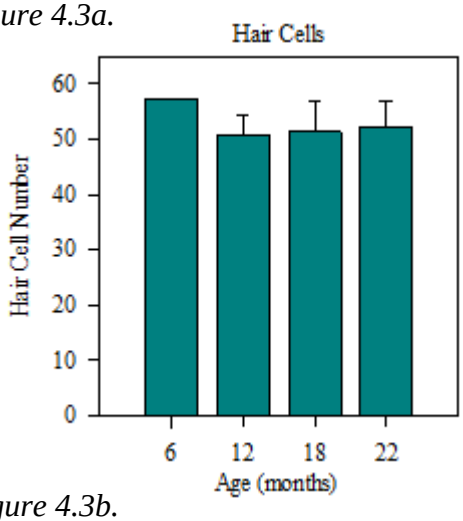

Figure 4.3b.

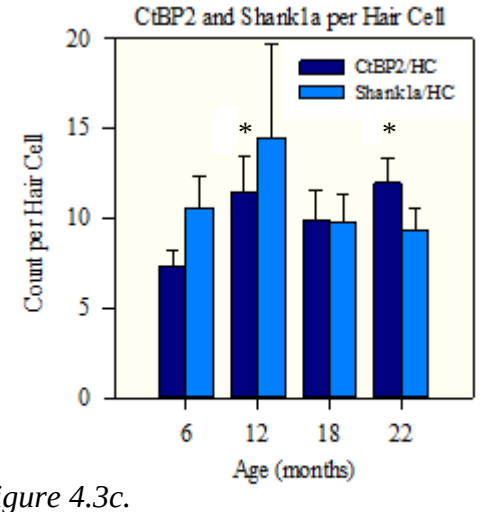

Figure 4.3c.

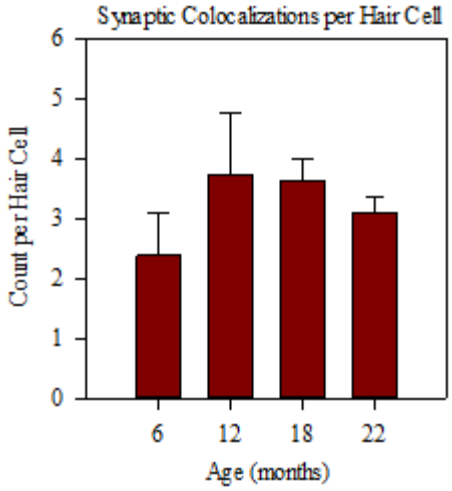

Figure 4.4: Scatter plot of VsEP threshold as a function of hair cells (*Figure 4a*), synaptic ribbons per hair cell (*Figure 4b*), post-synaptic receptor sites per hair cell (*Figure 4c*), and synaptic colocalizations per hair cell (*Figure 4d*) for six, 12, 18, and 22 month C57BL/6J age groups.

Figure 4.4a.

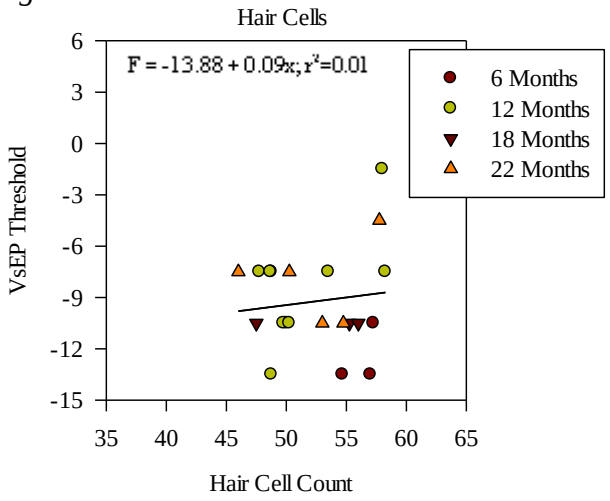

Figure 4.4b.

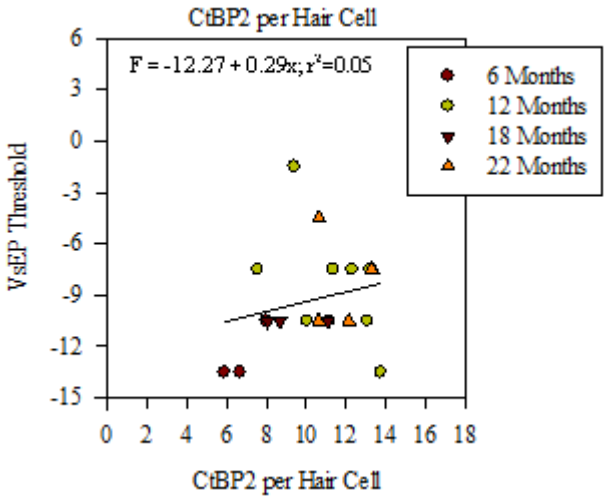

Figure 4.4c.

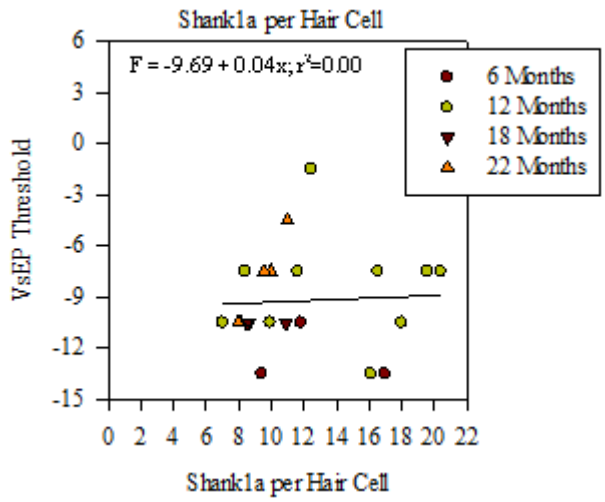

Figure 4.4d.

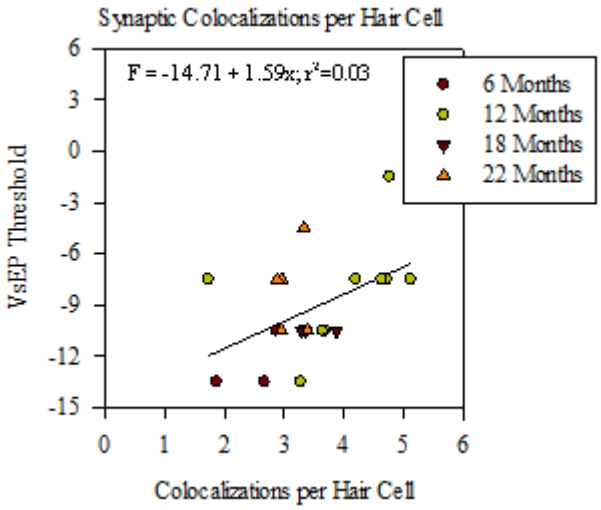

Figure 4.5: Bar graph of mean number of hair cells (*Figure 4.5a*), synaptic ribbons, post-synaptic receptor sites (*Figure 4.5b*), and synaptic colocalizations (*Figure 4.5c*) for the CE/J strain. All structures remained stable with age.

Figure 4.5a.

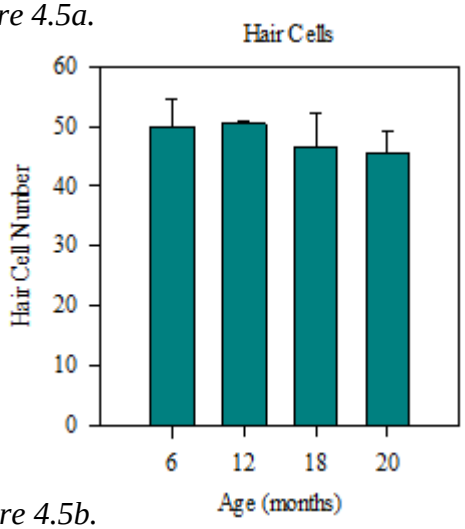

Figure 4.5b.

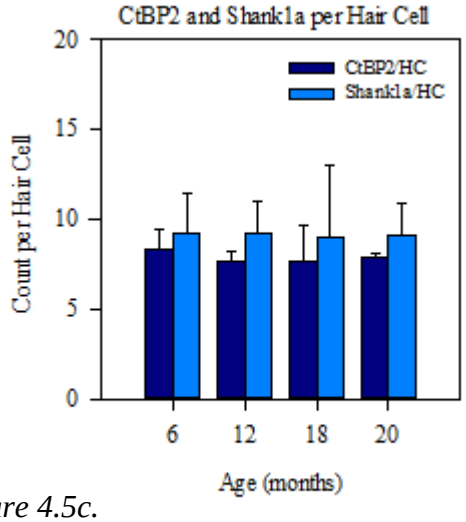

Figure 4.5c.

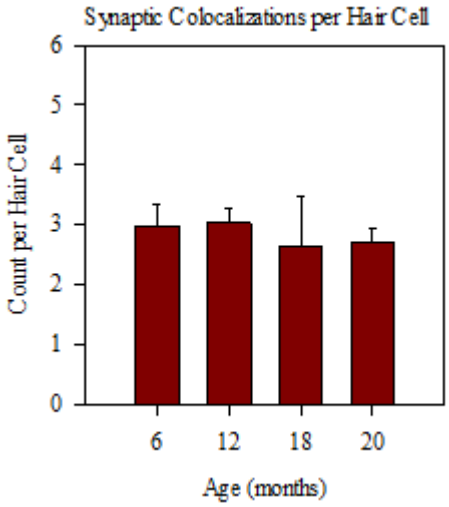

Figure 4.6: Scatter plot of VsEP threshold as a function of hair cells (*Figure 4.6a*), synaptic ribbons per hair cell (*Figure 4.6b*), post-synaptic receptor sites per hair cell (*Figure 4.6c*), and synaptic colocalizations per hair cell (*Figure 4.6d*) for six, 12, 18, and 20 month CE/J ages.

Figure 4.6a.

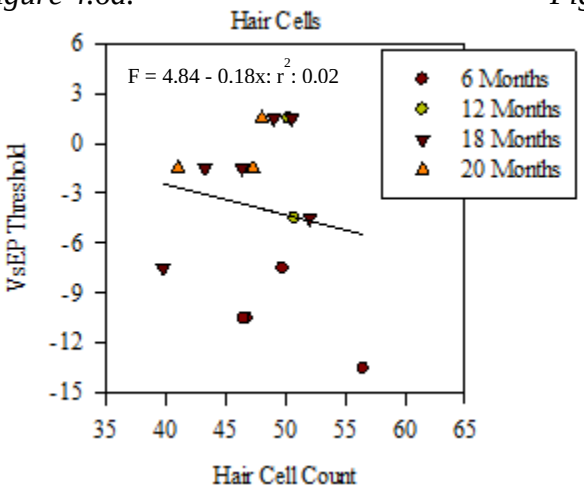

Figure 4.6b.

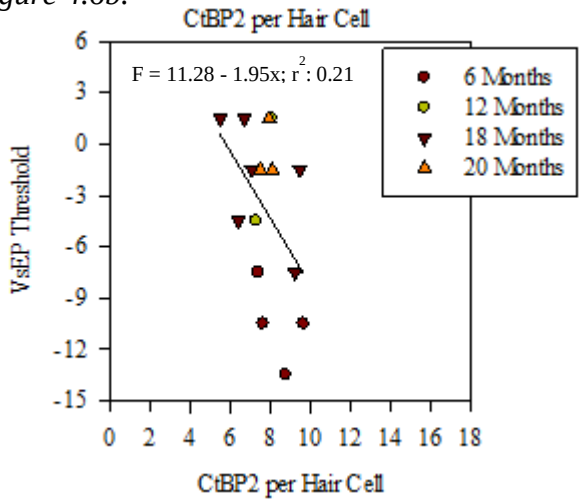

Figure 4.6c.

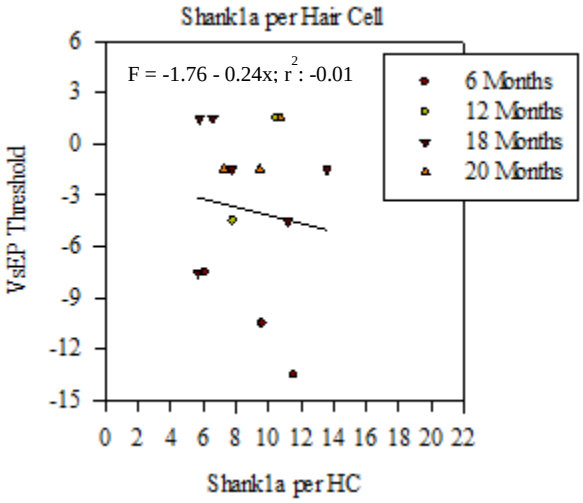

Figure 4.6d.

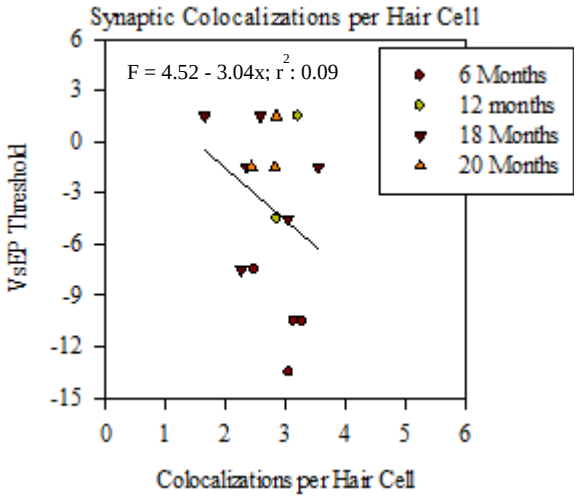

Table 4.1:

C57BL/6J descriptive statistics for hair cell number, CtBP2 per hair cell, Shank1a per hair cell, CtBP2 and Shank1a per hair cell colocalizatons per hair cell, and VsEP threshold. Structure totals were calculated based upon the mean area (0.198 mm^2) of the mouse utricular maculae epithelium (Desai, Zeh, & Lysakowski, 2005).

Structure	Age	N	Mean	Std. Dev.	Min.	Max.	Total
Hair Cell Number	6 months	3	56.31	1.42	54.67	57.25	4920.81
	12 months	10	51.37	3.88	47.75	58.25	4489.12
	18 months	3	52.92	4.71	47.50	56.00	4624.57
	22 months	5	52.35	4.47	46.00	57.75	4574.76
CtBP2 per Hair Cell	6 months	3	6.86	1.05	5.90	7.99	33756.77
	12 months	10	11.32	1.91	7.57	13.73	50816.80
	18 months	3	9.27	1.60	8.05	11.08	42869.74
	22 months	5	11.99	1.38	10.61	13.32	54851.33
Shank1a per Hair Cell	6 months	3	12.73	3.87	9.40	16.98	62641.94
	12 months	10	14.01	4.76	7.03	20.40	64790.19
	18 months	3	9.35	1.35	8.50	10.90	43239.71
	22 months	5	9.32	1.28	7.99	10.99	42636.73
Colocalizations (CtBP2 and Shank1a per Hair Cell	6 months	3	2.47	0.53	1.87	2.88	12154.41
	12 months	10	3.91	1.00	1.74	5.12	17552.44
	18 months	3	3.51	0.32	3.29	3.87	16232.23
	22 months	5	3.10	0.24	2.88	3.39	14181.74
VsEP Threshold	6 months	3	-12.90	1.34	-13.50	-10.50	-
	12 months	10	-8.50	1.55	-10.50	-7.50	-
	18 months	3	-10.50	0.00	-10.50	-10.50	-
	22 months	5	-8.10	2.51	-10.50	-4.50	-

Table 4.2:

C57BL/6J ANOVA table for hair cell count, CtBP2 per hair cell, Shank1a per hair cell and CtBP2 and Shank1a colocalizations per hair cell.

Structure	Sum of Squares	df	Mean Square	F	P-Value
Hair Cell Number	56.93	3	18.98	1.22	0.33
	264.12	17	15.54		
CtBP2 per Hair Cell	62.08	3	20.69	7.43	0.00*
	47.35	17	2.79		
Shank1a per Hair	99.15	3	33.05	2.31	0.11
Cell	243.74	17	14.34		
Colocalizations per	5.62	3	1.87	3.18	0.05*
Hair Cell	10.02	17	0.59		

* Less than or equal to $\alpha = 0.05$

Table 4.3:

C57BL/6J multiple comparisons Tukey post hoc table for hair cell number and age group.

Structure	Age Group (I)	Age Group (J)	P-Value	95% Confidence Interval	
Hair	6	12	0.26	-2.44	12.32
Cell		18	0.72	-5.76	12.54
Number		22	0.53	-4.23	12.14
	12	6	0.26	-12.32	2.44
		18	0.93	-8.93	5.83
		22	0.97	-7.12	5.15
	18	6	0.72	-12.54	5.76
		12	0.93	-5.83	8.93
		22	1.00	-7.62	8.75
	22	6	0.53	-12.14	4.23
		12	0.97	-5.15	7.12
		18	1.00	-8.75	7.62

Table 4.4:

C57BL/6J multiple comparisons Tukey post hoc table CtBP2 per hair cell and age group.

Structure	Age Group (I)	Age Group (J)	P-Value	95% Confidence Interval	
CtBP2 per Hair Cell	6	12	0.00*	-7.59	-1.34
		18	0.32	-6.28	1.46
		22	0.00*	-8.59	-1.66
	12	6	0.00*	1.34	7.59
		18	0.28	-1.07	5.18
		22	0.89	-3.26	1.93
	18	6	0.32	-1.46	6.28
		12	0.28	-5.18	1.07
		22	0.16	-6.18	0.75
	22	6	0.00*	1.66	8.59
		12	0.89	-1.93	3.26
		18	0.16	-0.75	6.18

* Less than $\alpha = 0.05$

Table 4.5:

C57BL/6J multiple comparisons Tukey post hoc table Shank1a per hair cell and age group.

Structure	Age Group (I)	Age Group (J)	P-Value	95% Confidence Interval	
Shank1a per Hair Cell	6	12	0.95	-8.37	5.80
		18	0.70	-5.40	12.17
		22	0.62	-4.45	11.27
	12	6	0.95	-5.80	8.37
		18	0.28	-2.42	11.75
		22	0.15	-1.20	10.59
	18	6	0.70	-12.17	5.40
		12	0.28	-11.75	2.42
		22	1.00	-7.83	7.89
	22	6	0.62	-11.27	4.45
		12	0.15	-10.59	1.20
		18	1.00	-7.89	7.83

Table 4.6:

C57BL/6J multiple comparisons Tukey post hoc table CtBP2 and Shank1a Colocalizations per hair cell and age group.

Structure	Age Group (I)	Age Group (J)	P-Value	95% Confidence Interval	
Colocalizations per Hair Cell	6	12	0.05*	-2.88	0.00
		18	0.38	-2.81	0.75
		22	0.68	-2.22	0.96
	12	6	0.05*	0.00	2.88
		18	0.85	-1.03	1.84
		22	0.25	-0.38	2.00
	18	6	0.38	-0.75	2.81
		12	0.85	-1.84	1.03
		22	0.89	-1.19	2.00
	22	6	0.68	-0.96	2.22
		12	0.25	-2.00	0.38
		18	0.89	-2.00	1.19

* Less than $\alpha = 0.05$

Table 4.7:

C57BL/6J linear regression table for hair cells, CtBP2 per hair cell, Shank1a per hair cell, and colocalizations per hair cell.

Structure	Intercept (b_0)	Slope (b_1)	P-Value	Goodness of Fit (r^2)
Hair Cells	-13.88	0.09	0.60	0.01
CtBP2 per Hair Cell	-12.27	0.29	0.31	0.05
Shank1a per Hair Cell	-9.69	0.04	0.81	0.00
Colocalizations per Hair Cell	-14.71	1.59	0.03*	0.03

* Less than $\alpha = 0.05$

Table 4.8:

CE/J descriptive statistics for hair cell number, CtBP2 per hair cell, Shank1a per hair cell, CtBP2 and Shank1a colocalizatons per hair cell, and VsEP threshold. Structure totals were calculated based upon the mean area (0.198 mm^2) of the mouse utricular maculae epithelium (Desai, Zeh, & Lysakowski, 2005).

Structure	Age	N	Mean	Std. Dev.	Min.	Max.	Total
Hair Cell Number	6 months	4	49.88	4.66	46.50	56.50	4358.91
	12 months	2	50.50	0.35	50.25	50.75	4413.09
	18 months	6	46.81	4.65	39.75	52.00	4090.63
	20 months	3	45.42	3.84	41.00	48.00	3969.16
CtBP2 per Hair Cell	6 months	4	8.37	1.05	7.40	9.67	36484.06
	12 months	2	7.68	0.57	7.28	8.08	33892.52
	18 months	6	7.40	1.60	5.50	9.47	30270.64
	20 months	3	7.85	0.30	7.51	8.09	31157.89
Shank1a per Hair Cell	6 months	4	9.24	2.27	6.13	11.58	40276.31
	12 months	2	9.17	1.89	7.83	10.50	40468.02
	18 months	6	8.42	3.25	5.65	13.58	34443.08
	20 months	3	9.15	1.76	7.26	10.73	36317.80
Colocalizations (CtBP2 and Shank1a per Hair Cell	6 months	4	2.99	0.35	2.48	3.28	13033.14
	12 months	2	3.04	0.25	2.86	3.21	13415.79
	18 months	6	2.57	0.66	1.65	3.55	10512.91
	20 months	3	2.70	0.23	2.43	2.85	10716.73
VsEP Threshold	6 months	4	-9.30	3.42	-13.5	-4.5	-
	12 months	2	-3.75	3.77	-7.5	1.5	-
	18 months	6	-3.00	3.87	-7.5	1.5	-
	20 months	3	-0.90	2.51	-4.5	1.5	-

Table 4.9:

CE/J ANOVA table for hair cell count, CtBP2 per hair cell, Shank1a per hair cell and CtBP2 and Shank1a colocalizations per hair cell.

Structure	Sum of Squares	df	Mean Square	F	P-Value
Hair Cell Number	54.76	3	18.25	0.99	0.43
	202.83	11	18.44		
CtBP2 per Hair Cell	2.32	3	0.77	0.51	0.68
	16.71	11	1.52		
Shank1a per Hair	2.16	3	0.72	0.10	0.96
Cell	77.93	11	7.08		
Colocalizations per	0.59	3	0.20	0.79	0.52
Hair Cell	2.72	11	0.25		

Table 4.10:

CE/J multiple comparisons Tukey post hoc table for hair cell number and age group.

Structure	Age Group (I)	Age Group (J)	P-Value	95% Confidence Interval	
Hair	6	12	1.00	-11.82	10.57
Cell		18	0.69	-5.27	11.41
Number		20	0.55	-5.41	14.33
	12	6	1.00	-10.57	11.82
		18	0.72	-6.86	14.25
		20	0.58	-6.71	16.88
	18	6	0.69	-11.41	5.27
		12	0.72	-14.25	6.86
		20	0.97	-7.75	10.53
	20	6	0.55	-14.33	5.41
		12	0.58	-16.88	6.71
		20	0.97	-10.53	7.75

Table 4.11:

CE/J multiple comparisons Tukey post hoc table for CtBP2 per hair cell and age group.

Structure	Age Group (I)	Age Group (J)	P-Value	95% Confidence Interval	
CtBP2 per Hair Cell	6	12	0.91	-2.52	3.91
		18	0.62	-1.42	3.37
		20	0.94	-2.31	3.36
	12	6	0.91	-3.91	2.52
		18	0.99	-2.75	3.31
		20	1.00	-3.55	3.22
	18	6	0.62	-3.37	1.42
		12	0.99	-3.31	2.75
		20	0.95	-3.07	2.17
	20	6	0.94	-3.36	2.31
		12	1.00	-3.22	3.55
		20	0.95	-2.17	3.07

Table 4.12:

CE/J multiple comparisons Tukey post hoc table for Shank1a per hair cell and age group.

Structure	Age Group (I)	Age Group (J)	P-Value	95% Confidence Interval	
Shank1a per Hair Cell	6	12	1.00	-6.86	7.01
		18	0.96	-4.35	5.99
		20	1.00	-6.03	6.21
	12	6	1.00	-7.01	6.86
		18	0.99	-5.80	7.29
		20	1.00	-7.30	7.33
	18	6	0.96	-5.99	4.35
		12	0.99	-7.29	5.80
		20	0.98	-6.39	4.93
	20	6	1.00	-6.21	6.03
		12	1.00	-7.33	7.30
		20	0.98	-4.93	6.39

Table 4.13:

CE/J multiple comparisons Tukey post hoc table for CtBP2 and Shank1a colocalizations per hair cell and age group.

Structure	Age Group (I)	Age Group (J)	P-Value	95% Confidence Interval	
Colocalizations per Hair Cell	6	12	1.00	-1.34	1.25
		18	0.58	-0.55	1.38
		20	0.87	-0.85	1.43
	12	6	1.00	-1.25	1.34
		18	0.46	-0.76	1.68
		20	0.34	-1.03	1.70
	18	6	0.58	-1.38	0.55
		12	0.67	-1.68	0.76
		20	0.98	-1.19	0.93
	20	6	0.87	-1.43	0.85
		12	0.88	-1.70	1.03
		20	0.98	-0.93	1.19

Table 4.14:

CE/J linear regression table for hair cells, CtBP2 per hair cell, Shank1a per hair cell, and colocalizations per hair cell.

Structure	Intercept (b_0)	Slope (b_1)	P-Value	Goodness of Fit (r^2)
Hair Cells	4.84	-0.18	0.57	0.02
CtBP2 per Hair Cell	11.28	-1.95	0.09	0.21
Shank1a per Hair Cell	-1.76	-0.24	0.68	-0.01
Colocalizations per Hair Cell	4.52	-3.04	0.28	0.09

CHAPTER V: DISCUSSION

In summary, quantitative declines in hair cells and synaptic ribbons were observed for one mouse strain (CBA/CaJ) that demonstrates normal aging, while structural elements were largely maintained for two mouse strains (C57BL/6J and CE/J) that harbor *Ahl*. Age-related vestibular dysfunction correlated relatively well with declines in pre-synaptic elements for the CBA/CaJ strain. Limited loss of structure with age for C57BL/6J mice is also consistent with observed minimal age-related declines in gravity receptor function for this strain (Mock, 2008). Maintenance of structural elements as observed for the CE/J strain is disparate from their corresponding macular function, in which CE/J mice exhibit severe gravity receptor dysfunction with age.

Structural Aging Varies Across Mouse Strains

From the present study, structural changes with age were not uniform across mouse strains. Of the three structural elements measured, age-related declines in hair cells and synaptic ribbons differed across strains, in that CBA/CaJ mice exhibited a decline in pre-synaptic structural elements while C57BL/6J and CE/J mice demonstrated no age-related declines in structure. With regard to age, Shank1a did not decline significantly across all strains, suggesting that this structure cannot explain age-related declines in gravity receptor function.

Several changes in structure within and surrounding the hair cell in the maculae of the vestibular system have been reported previously, including a reduction in the quantity and quality of otoconia and globular substances (Johnsson, 1971; Ross, Peacor, Johnsson, & Allard, 1976; Igarashi, Saito, Mizukoshi, Alford, 1993; Jang, Hwang, Shin, Bae, Kim., 2006; Walther & Westhofen, 2007; Suzuki, Ikeda, & Takasaka, 1997), stereocilia integrity (Rosenhall & Rubin, 1974; Bloom & Hultcrantz, 1994), and hair cell number and density (Shiga et al., 2005; Park,

Hubel, & Woods, 1987; Rauch, Velazquez-Villasenor, Dimitri, & Merchant, 2001; Richter, 1980; Rosenhall & Rubin, 1975, Severinsen et al., 2008; Gleeson & Felix, 1987; Merchant et al., 2000). However, quantitative declines in one structure cannot be fully attributed to vestibular functional declines with age. These published data provide varying levels of support for the current findings.

CBA/CaJ Strain

To our knowledge, only one structure has been examined specifically in the CBA/CaJ mouse strain; that is otoconia. In a study by Mock et al. (2011), no loss of otoconia was observed in the utricle or saccule of the CBA/CaJ strain, suggesting that otoconia density could not account for gravity receptor functional declines with age. However, the data were not quantified. To date, no other data regarding age-related structural changes have been examined in CBA/CaJ mice. Hair cell and synaptic ribbon declines with age in the CBA/CaJ strain is a novel finding, and suggests that these structures are involved in age-related gravity receptor declines.

C57BL/6J and CE/J Strains

For the C57BL/6J and CE/J strains, previous data have shown some age-related quantitative degeneration of structure, while other structures do not appear to be affected by age. In a study by Shiga et al. (2005), hair cell density in the cristae of the horizontal semicircular canal was examined and compared with VOR function in the vestibular system of the C57BL/6 mouse from three weeks to 15 months of age. Shiga and colleagues observed that VOR gain in C57BL/6 mice increased in an age-dependent manner from three weeks to three months. Limited declines in VOR gain were measured until at least 15 months (oldest age group measured). Conversely, a decline in hair cell density was observed early in life to the extent that

density decreased to 80% of that measured at three weeks by six months of age. Hair cell density declined a further 70% by 15 months of age. Shiga and colleagues suggested that quantitative structural declines in the peripheral vestibular system do not correlate well with aging vestibular function. In addition, Park et al. (1987) compared the vestibular organs of young (5-6 weeks) and old (29-31 months) C57BL/6NNia mice using light and electron microscopy. The authors discovered that hair cell density decreased in all five vestibular organs with the utricle exhibiting a 14% decline in old mice compared with younger mice. The results from these studies are disparate from our findings, in which we observed a structural maintenance of hair cells until at least 20 to 22 months of age; however, there are some notable differences. In Shiga's study, structural data was not measured in the utricle, but rather the horizontal semicircular canal. Inconsistencies with Park and colleagues' findings of hair cell decline at advanced ages may be accounted for by the fact that the oldest age group measured was 22 months; Park's aging study examined mice approaching 29-31 months of age. Therefore, the present study cannot rule out that C57BL/6J mice exhibit hair cell loss at more advanced ages. Only one known study has examined synaptic ribbons within the vestibular system of the mouse across the lifespan. Park and colleagues examined the prevalence of synaptic ribbons in the organs of the vestibular system of the C57BL/6NNia mouse strain. The number of synaptic ribbons appeared to remain stable with age; however, the data were not quantified (Park, Hubel, & Woods, 1987). These data support our findings of synaptic ribbon stability in both the C57BL/6J and CE/J mouse strains. In a study by Mock et al. (2008), otoconia density was qualitatively examined in the C57BL/6J and CE/J strains across the lifespan. No loss of otoconia in the utricle or saccule was observed in either mouse strain, suggesting that otoconia density could not account for observed gravity receptor functional declines with age; however, the data

were not quantified. Reported evidence regarding neural degeneration in the inner ear is sparse, although one account has been reported in the auditory system of the inner ear in C57BL/6J mice. Stamataki et al. (2006) compared the number of afferent contacts with the inner hair cells in C57BL/6J mice of different ages (2-3 months and 8-12 months) by assessing the number of synapses formed between afferent nerve fibers and the inner hair cell. Stamataki and colleagues measured a mean of 16.8 ± 2.4 synapses for the younger group and 9.2 ± 3.1 synapses for the older group showing that, on average, the number of primary afferents in the auditory system decreased with age. For the C57BL/6J and CE/J strains, no significant decline in post-synaptic receptor sites per hair cell with age was observed. This finding is in contrast to a previous examination of neural components in which calyces appeared to be missing from the epithelium in the cristae of the aging gerbil (Leonard and Kevetter, 2007); however, several differences are notable between the current study, which examined post-synaptic receptor sites in the aging mouse utricle, and Leonard and Kevetter's study. In addition to the disparate vestibular organ and mammalian species examined by Leonard and Kevetter, only calyces were measured-those synapses that were innervated by bouton or dimorphic afferents were not taken into account. Also, the calyces were only qualitatively examined, the data were not quantified. To our knowledge, the present study is the first to quantitatively examine post-synaptic receptor sites in the mouse utricle across the lifespan.

Observed Structural Declines do not Fully Explain Functional Aging

Both indirect and direct functional declines have been observed with age. Shiga et al., (2005) measured VOR in C57BL/6 mice between the ages of three weeks and 60 weeks. Limited declines in VOR gain were observed in older mice compared to younger mice, suggesting that vestibular function is largely maintained until at least 60 weeks of age. However,

Shiga and colleagues concluded that central compensation may have maintained the VOR since peripheral morphology declined. Jones et al. (2006) measured vestibular function in 19 inbred mouse strains, including CE/J mice, ranging in age from 35 to 389 days old. Significantly elevated VsEP thresholds in the CE/J strain with age were observed, suggesting a decrease in vestibular function. In a separate study, Jones et al. (2005) measured VsEPs for CBA/CaJ and C57BL/6J mice. Both strains maintained vestibular function until at least 190 days old. Mock (2008) measured auditory and vestibular function for CE/J, C57BL/6J and CBA/CaJ mice over the lifespan. VsEPs were obtained to directly measure vestibular function from CBA/CaJ mice between the ages of 1.7 and 23.8 months, C57BL/6J mice between 1.01 and 23.8 months and CE/J mice between 1.0 and 20.6 months. Results showed that macular function decreased at a faster rate in the CE/J and CBA/CaJ strains than in the C57BL/6J strain. C57BL/6J mice demonstrated an average decline of 0.12 dB re: 1.0 g/ms per month while CBA/CaJ mice exhibited a 0.39 dB re: 1.0 g/ms per month decline in gravity receptor function. CE/J mice demonstrated the largest decline in macular function, as VsEP thresholds increased by 0.47 dB re: 1.0 g/ms per month. CBA/CaJ and CE/J mice demonstrated over twice as much VsEP dynamic range loss at the oldest age groups when compared to the C57BL/6J strain (CBA/CaJ: 49% loss of dynamic range at 18-23 months; CE/J: 56% loss of dynamic range at 20-21 months; C57BL/6J: 21% loss of dynamic range at 22-23 months).

Overall, the current study did not define precise correlates of age-related gravity receptor dysfunction, suggesting that functional aging must be accounted for by additional structures not measured herein. The structures measured in the current study did not change significantly, especially for CE/J mice; this finding suggests that perhaps observed declines in pre-synaptic

structures in concert with additional structures not measured here may be responsible for age-related declines in macular function.

Other Possible Mechanisms

Several changes in structures within and surrounding the hair cell in the maculae of the vestibular system not measured herein have been reported previously, including a reduction in the quantity and quality of otoconia and globular substances (Igarashi, Saito, Mizukoshi, Alford, 1993; Jang, Hwang, Shin, Bae, Kim., 2006; Johnsson, 1971; Ross, Peacor, Johnsson, & Allard, 1976; Suzuki, Ikeda, & Takasaka, 1997; Walther & Westhofen, 2007;) and stereocilia integrity (Bloom & Hultcrantz, 1994; Rosenhall & Rubin, 1974). Other potential contributors outside of the peripheral vestibular system may be involved in aging vestibular dysfunction, such as decreased metabolic activity (Lyon & Davis, 2002; Lyon & King, 1997), vascular supply (Ishiyama, 2009; Lyon & Wanamaker, 1993), and changes in central vestibular relays, including degeneration of the vestibular nuclei and vestibular portion of CN VIII (Alvarez et al., 2000; Johnson, 1971; Lopez, Honrubia, & Baloh, 1997). To our knowledge, no other structure beyond those structures measured in the present study has been compared with direct gravity receptor functional data. Comparison of additional structural changes with functional aging warrants future consideration.

Complexity of Aging

There are many theories that are used to explain the complex nature of the aging process; however, no single theory explains the complex nature of the changes that occur with aging. Moody (2009) describes five theories of aging: 1) wear-and-tear theory (body wears out over time), 2) autoimmune theory (immune system weakens over time, allowing the body to be more susceptible to autoimmune diseases such as rheumatoid arthritis), 3) aging-clock theory, (body is

programmed like a clock, and a gland such as the hypothalamus, thalamus, or pituitary gland regulates age-related physiological changes), 4) cross-linkage theory (cell function is limited by cross-linking compounds accumulating in the collagen protein), and 5) cellular theory (cell's ability to undergo division becomes impaired, preventing cellular repair).

Beginning in the fourth decade of life, there is a decreased efficiency of organ and body function. As age increases, a decreased ability for cells to undergo mitosis, decline in nucleoprotein production, accumulation of insoluble compounds in the cytoplasm, and chemical changes in intracellular fluid is observed. Cellular changes with age are indistinguishable at times from cellular changes due to disease or injury. Cowdry (1952) differentiates between four types of cells: 1) vegetative intermitotics, in which cells function as reproductive mechanisms (i.e. basal cells of the epidermis), 2) differentiating intermitotics, in which cells exhibit increased specialization (i.e. cells which differentiate to become leukocytes), 3) reverting postmitotics, in which cells are capable of reversing the aging cellular process (i.e. liver cells, which are able to regenerate in the case of cell death), and 4) fixed postmitotics, which are specialized cells that age and die. These cells do not have the ability to regenerate or reverse the aging process (i.e. cardiac muscle cells, rod and cone cells, hair cells). According to Cowdry's theory of cellular aging, hair cells within the auditory and vestibular system of mammals are classified as fixed postmitotics – they establish specialized function and eventually age and die.

Aging effects on the auditory system have been widely documented. Reports of atrophic changes in the auditory system have been noted in pillar cells, stria vascularis, tectorial membrane, hair cells, and ganglion cells, sulcus cells, Henson's cells, and Reissner's membrane. Estimates of hearing loss range from 30 to 35% of individuals between the ages of 65 and 75. Almost 50% of those individuals over the age of 75 are estimated to have hearing loss (National

Institute on Deafness and Other Communication Disorders, 2010). Cochlear pathologies associated with age-related hearing loss include a decline in the number and integrity of hair cells and supporting cells (Li & Hultcrantz, 1994), spiral ganglion cell degeneration (Sha et al., 2008), endocochlear potential decline (Gratton, Smyth, Lam, Boettcher, & Schmiedt, 1997), accumulation of lipofuscin in the outer hair cells (Li & Hultcrantz, 1994), changes in vascular supply (Brown, Miller, & Nuttall, 1995; Gratton, & Schulte, 1995) and giant inner hair cell stereocilia (Li & Hultcrantz, 1994). According to Schuknecht (1964), morphological changes in the inner ear which are responsible for age-related hearing loss, or presbycusis, may be classified into four types: 1) sensory, with hair cell loss; 2) neural, with degeneration of CN VIII nerve primary afferents; 3) metabolic, with atrophy of the stria vascularis; 4) mechanical, with a decline in basilar membrane properties and function.

Study Limitations

One limitation to the current study is the relatively small sample size of specimens measured across strains. For each age group, our goal was to have a minimum of six specimens. Each mouse yielded two utricles: rather than using only one utricle from each mouse, both utricles were processed (to prevent tissues from being wasted). In some cases, one utricle was damaged or lost during processing, leaving a single utricle from a mouse salvageable for processing. To combat this small sample size, structures were quantified over four areas for each specimen and averaged together to obtain a mean structural count. Each utricle was considered to be an independent sample on the basis that genetic mutations can affect the ears independently. In the auditory system, age-related hearing loss is often similar between ears but is not always identical.

Specimens were collected at various times for different age groups. Although the staining protocol was consistent among all temporal bone and utricle processing sessions as well as confocal microscope settings, specimens were processed in groups as they reached the appropriate age; therefore, slight variations in staining were inherent among processing groups. As a result, some minor differences in fluorescence were observed between processing groups. Processing for age groups and mouse strains were randomized (a given group may have had both age and strain differences) so that similar groups were not processed at the same time. Alexa 633 goat-anti-rabbit (secondary antibody used to stain for Shank1a) in particular, resulted in some background staining. To combat these disparities in Shank1a fluorescence and prevent background fluorescence from being identified as a post-synaptic receptor site, an automated count was adapted using data imaging software and an intensity and size threshold was established manually for every z-stack. A young C57Bl/6J mouse was used as a control for several processing sessions to verity consistency of staining. To rule out additional technical errors, structural counts were repeated among all age groups for each strain and were consistent with previous counts.

Future Direction

The present study used confocal microscopy to quantitatively examine structures across the lifespan. Confocal microscopy limited the utility of evaluating structures qualitatively. Previous reports of qualitative changes in structural elements have been reported with age. Fragmented, pitted, and fissured otoconia as well as some giant otoconia along the outer edges of the utricle have been reported in rats (Jang et al., 2006). Similarly, reports of fragmented otoconia have been observed in human otoconia (Walther & Westhofen, 2007). Degenerated otoconia also show a roughened surface, often with fractures through the midsection of the

otoconia body (Igarashi et al., 1993; Walther & Westhofen, 2007). Studies have reported evidence of aging in stereocilia for both human and animal models, including decreased stereocilia organization, increased fragility, and stereocilia that are larger than normal. Some stereocilia are clustered together and in a few instances, complete fusion of stereocilia was observed (Bloom & Hultcrantz, 1994; Rosenhall & Rubin, 1975). In a study of young, middle-aged, and old C57 mice, Park et al. (1987) found that large, dense, inclusions formed on the hair cells and supporting cells of the old mice. There are reports that spheroid synaptic ribbons with electron-lucent or hollow-like centers may be in the process of degeneration (Park, Hubel, & Woods, 1987). In addition, lipofuscin, or age-related pigment has been reported in hair cells of aging mice. Qualitative differences with age have also been observed in humans. In a study of human temporal bones, Rosenhall and Rubin (1975) found an increase in lipofuscin, an age-related pigment, inclusions in type I and II hair cells as well as in supporting cells; however, these inclusions were more pronounced in type I hair cells. Similarly, Gleeson and Felix (1987) found increased severity of lipofuscin in the oldest temporal bone of three human temporal bones studied. The extent to which these qualitative structural changes alter function is not yet known and warrants future consideration.

In addition, other potential contributors outside of the peripheral vestibular system may be involved in aging vestibular dysfunction, such as decreased metabolic activity (Lyon & Davis, 2002; Lyon & King, 1997), vascular supply (Ishiyama, 2009; Lyon & Wanamaker, 1993), and changes in central vestibular relays, including degeneration of the vestibular nuclei and vestibular portion of CN VIII (Alvarez et al., 2000; Johnson, 1971; Lopez, Honrubia, & Baloh, 1997).

It is interesting to note the role of genetics in this study. As alluded to previously, the contribution of *Ahl* on structural elements has never been examined among aging mouse strains. In this study, we found that those mice exhibiting *Ahl* appeared to maintain structural elements across the lifespan. However, CE/J mice lose gravity receptor function at a significantly faster rate when compared to the C57BL/6J strain. This finding is in contrast to our structural data for the CBA strain (a mouse strain which represents normal aging) in which hair cells and synaptic ribbons declined by the oldest age group measured while gravity receptor function also exhibited a decline with age, but not to the extent of the CE/J strain.

Maintenance of pre-synaptic and post-synaptic structures with age for mouse strains harboring *Ahl* is a novel finding. One would expect that mice carrying *Ahl* would experience structural declines at least to the extent of those observed in the CBA/CaJ mouse strain given that CBA/CaJ mice represent a normal aging model. However, this was not the case, as synaptic structures remained stable with age in C57BL/6J and CE/J mice. This finding suggests that some genetic component of our *Ahl* mouse strains measured acts as a protective mechanism, prohibiting aging effects on the structural vestibular organs. The role of genetics should be considered in further examinations of structure with age.

In the future, it may be beneficial to examine structural aging in additional mouse strains that carry *Ahl*. In addition, it may be beneficial to design a mouse model to examine the relationship between *Ahl3* and structural maintenance at the hair cell level, given the disparities between function for a mouse strain which carries both *Ahl* and *Ahl3* (C57BL/6J) and a mouse strain which carries *Ahl* only (CE/J). Examination of a mouse strain which only carries *Ahl3* may help to elucidate the role of *Ahl* on gravity receptor function across the lifespan.

Broad Impact

The effects of age-related dizziness and imbalance are significant, in that older individuals with vertigo are ten times more likely to fall compared to those without symptoms (Walther & Westhofen, 2007). In addition, 50% of all accidental deaths among the elderly in the United States are related to falls (National Institutes on Deafness and other Communication Disorders, 2001). 2.3 million injuries among geriatric patients were reported and treated by emergency rooms in 2010. Over 20 thousand deaths in 2009 were related to unintentional falls (Centers for Disease Control, 2012).

Structural changes within human temporal bones have been observed across the lifespan. Merchant et al. (2000) observed a decline in type I and type II hair cells for all five vestibular organs with age. Similarly, Rauch et al. (2001) estimated that, at younger ages, average total hair cell density at birth in humans is 76-79 hair cells/0.01mm^2 in the cristae, 68 cells/0.01mm^2 in the utricle, and 61 cells/0.01mm^2 in the saccule. At older ages, the cristae lost type I hair cells at a significantly faster rate than the macular organs while type II hair cell losses occurred at an equal rate for all 5 vestibular organs. These data are consistent with quantitative hair cell counts observed for the CBA/CaJ strain with age; however, hair cell counts for the C57BL/6J and CE/J strains remained stable with age. To our knowledge, there have been no studies examining additional age-related changes in structural elements within the vestibular system in human temporal bones.

Vestibular functional declines have been observed in humans. Reports of vestibular function generally rely upon measures such as VOR, calorics, optokinetic nystagmus (OKN), vestibular-evoked myogenic potentials (VEMPs), and posturography testing. Declines in gain (ratio of eye velocity to head velocity) for VOR, OKN, and visual-VOR (VVOR) have been

reported in humans (Baloh, Jacobson, & Socotch, 1993; Kerber, Ishiyama, & Baloh, 2006; Paige, 1992, 1994). For example, Baloh and colleagues (1993) measured VOR, OKN, Velocity Step, and VVOR on individuals over the age of 75. Decreasing VOR gains were observed among the elderly when compared to young individuals as amplitude increased. Shorter time constants on velocity step testing were observed among older subjects when compared to their younger counterparts. In addition, OKN and VVOR revealed decreases in slow-phase velocity gain and an increased phase lead of eye velocity for higher amplitude stimuli, respectively. Alternatively, Peterka, Black, & Schoenhoff (1990) found no age-related declines in VOR gain. Age-related changes on vestibular evoked myogenic potential (VEMP) testing have been documented. Individuals over the age of 60 tend to have smaller VEMP amplitudes than their younger counterparts (Basta, Todt, & Ernst, 2005; Su, Huang, Young, & Cheng, 2004). In addition, increased thresholds and longer latencies have been reported with VEMP testing (Ochi & Ohashi, 2003; Su et al., 2004). No consistent declining trend was observed during caloric testing on individuals across the lifespan (Peterka, Black, & Schoenhoff, 1990). According to Baloh and colleagues, responses on vestibular tests are more variable in older individuals; therefore, a small sample size may result in misleading data. Sensory organization testing among older individuals suggested a decline in the ability to maintain balance with age among asymptomatic individuals, beginning at the fourth decade onward. This suggests that even older individuals who report no vestibular symptoms may still exhibit a decline in the ability to maintain balance with age (Borah et al., 2007; Cohen, Heaton, Congdon, & Jenkins, 1996). Alternatively, increases in magnitude of sway were observed in altered somatosensory and visual conditions during posturography (Peterka, Black, & Schoenhoff, 1990-1991).

A growing body of research has suggested that additional factors related to age may contribute to falls among the elderly. For example, in a study of 740 individuals who sought otologic evaluation of dizziness symptoms, 21% of individuals had dizziness related to specific causes while 79% of individuals with dizziness had symptoms related to progressive disequilibrium with aging (Belal & Glorig, 1986). Many geriatric individuals develop comorbid medical conditions in addition to dizziness and imbalance such as hypertension, diabetes, neurological disorders (i.e. Parkinson's disease, dementia, Alzheimer's disease), musculoskeletal diseases (i.e. osteoporosis, muscle atrophy), vascular problems, heart disease, and arthritis (National Institutes on Aging, 2012). Proprioceptive changes with age include loss of coordination, joint flexibility, and muscle strength (Means et al., 2005). Aging may also affect the visual system, resulting in declines in visual acuity, depth perception, and cross sensitivity (Ivers, Cumming, Mitchell, Attebo, 1998; Lord & Dayhew, 2001). Changes in peripheral sensitivity (i.e. hands, feet) and reaction time also occur with age (Jacobson & McCaslin, 2008). In addition, dizziness is a reported side effect of many medications, especially those that suppress the central nervous system, such as sedatives and anti-anxiety drugs (Centers for Disease Control, 2012). Environmental factors such as dim lighting, non-carpeted floors, stairs, elevators, and uneven surfaces can also result in an increased risk for falls; however, one system cannot fully account for age-related changes. As the number of older individuals continues to rise, the need for care and treatment regarding conditions that the elderly face will become more relevant. In order for health care professionals to provide proper care and better intervention strategies, more research needs to be conducted to help us understand the etiology of observed declines in gravity receptor function with age.

In summary, age-related structural changes in the vestibular system varied among mouse strains; however, additional structures or process may be involved in age-related gravity receptor functional declines. Data supports a hypothesis that genetic background influences vestibular structural aging. The current research can provide new direction involving understanding the aged vestibular system and help furnish new strategies involved in vestibular rehabilitation. Our findings provide new insight into the structural changes which occur with aging as well as the role of genetics on the aging vestibular system. The current research has implications that further examinations aimed at genetic contributions to vestibular functional aging are warranted.

REFERENCES

Alvarez, J.C., Diaz, C., Suarez, C., Fernandez, J.A., Gonzalez del Rey, C., Navarro, A., et al., (2000). Aging and the human vestibular nuclei: morphometric analysis. *Mechanisms of Aging and Development*. 114(3), 149-172. PMID: 10802120

Baloh, R.W., Jacobson, K.M., Socotch, T.M. (1993). The effect of aging of visual-vestibuloocular responses. *Experimental Brain Research.* 95(3),509-516. PMID: 8224077

Basta, D., Todt, I., Ernst, A. (2005). Normative data for P1/N1-latencies of vestibular evoked myogenic potentials induced by air- or bone-conducted tone bursts. *Clinical Neurophysiology*. 116(9), 2216-2219. PMID: 16043396

Bloom, D & Hultcrantz, M. (1994). Vestibular morphology in relation to age and circling behavior. *Acta Oto-Laryngologica.* 114(3), 387-392. PMID: 7976310

Borah, D., Wadhwa, S., Singh, U., Yadav, S.L., Bhattacharjee, M., Sindhu, V. (2007). Age related changes in postural stability. *Indian Journal of Physiology and Pharmacology*. 51(4), 395-404. PMID: 18476394

Brown, J.N., Miller, J.M., Nutall, A.L. (1995). Age-related changes in cochlear vascular conductance in mice. *Hearing Research*. 86(1-2), 189-194). PMID: 8567416

Cohen, H., Heaton, L.G., Congdon, S.L., Jenkins, H.A. (1996). Changes in sensory organization test scores with age. *Age and Aging*. 25, 39-44. PMID: 8670527

Colclasure, J.C. & Holt, J.R. (2003). Transduction and adaptation in sensory hair cells of the mammalian vestibular system. *Gravitational and Space Biology Bulletin*. 16(20, 61-70. PMID: 12959133

Della Santina, C.C., Potyagaylo, V., Migliaccio, A.A., Minor, L.B., Carey, J.P. (2005). Orientation of human semicircular canals measured by three-dimensional multiplanar CT

reconstruction. *Journal of the Association of Research for Otolaryngology*. 6(3), 191-206. PMID: 16088383

Desai, S.S., Zeh, C., & Lysakowski, A. (2005). Comparative morphology of rodent vestibular periphery. I. Saccular and utricular maculae. *Journal of Neurophysiology*. 93(1), 251-266. PMID: 15240767

Di Palma, F., Holme, R.H., Bryda, E.C., Belyantseva, I.A., Pellegrino, R., Kachar, B., et al. (2001). Mutations in Cdh23, encoding a new type of cadherin, cause stereocilia disorganization in waltzer, the mouse model for Usher syndrome type 1D. *Nature Genetics*. 27(1), 103-107. PMID: 11138008

Dick, O., Tom Dieck, S., Altrock, W.D., Ammermuller, J., Weiler, R., Garner, C.C., et al. (2003). The presynaptic active zone protein bassoon is essential for photoreceptor ribbon synapse formation in the retina. *Neuron*. 37(5), 775-786. PMID: 12628168

Eatock, R.A., Rusch, A., Lysakowski, A., Saeki, M. (1998). Hair cells in mammalian utricles. *Otolaryngology-Head and Neck Surgery*. 119(3), 172-181. PMID: 9743073

Fernandez, C., Goldberg, J.M., Baird, R.A. (1990). The vestibular nerve of the chinchilla. III. Peripheral innervation patterns in the utricular macula. *Journal of Neurophysiology*. 63(4), 767-780. PMID: 2341875

Gleeson, M. & Felix, H. (1987). A comparative study of the effect of age on the human cochlear and vestibular neuroepithelia. *Acta Oto-laryngologica*. *Supplementum*. 436, 103-109. PMID: 2823525

Gomez-Casati, M.E., Murtie, J.C., Rio, C., Stankovic, K., Liberman, M.C., Corfas, G. (2010). Nonneuronal cells regulate synapse formation in the vestibular sensory epithelium via

erbB-dependent BDNF expression. *Proceedings of the National Academy of Sciences of the United States of America*. 107(39), 17005-17010. PMID: 20837532

Gopen, Q., Lopez, I., Ishiyama, G., Baloh, R.W., Ishiyama, A. (2003). Unbiased stereologic type I and type II hair cell counts in human utricular macula. *Laryngoscope*. 113(7), 1132-1138. PMID: 12838010

Gratton, M.A. & Schulte, B.A. (1995). Alterations in microvasculature are associated with atrophy of the stria vascularis in quiet-aged gerbils. *Hearing Research*. 82(1), 44-52. PMID: 7744712

Gratton, M.A., Smyth, B.J., Lam, C.F., Boettcher, F.A., Schmiedt, R.A. (1997). Decline in the endocochlear potential corresponds to decreased Na, K-ATPase activity in the lateral wall of quiet-aged gerbils. *Hearing Research.* 108(1-2), 9-16. PMID: 9213117

Hobbs, F. The Elderly Population. Retrieved October 15, 2008, from U.S. Census Bureau Web site: http://www.census.gov/population/www/pop-profile/elderpop.html

Igarashi, M., Saito, R., Mizukoshi, K., Alford, B.R. (1993). Otoconia in young and elderly persons: a temporal bone study. *Acta Oto-laryngologica. Supplementum*. 504, 26-29. PMID: 8470528

Ishiyama, G. (2009). Imbalance and vertigo: the aging human vestibular periphery. *Seminars in Neurology*. 29(5), 491-499. PMID: 19834860

Ivers, R.Q., Cumming R.G., Mitchell, P., Attebo, K. (1998). Visual impairment and falls in older adults: the blue mountains eye study. *Journal of the American Geriatric Society*. 46(1), 58-64. PMID: 9434666

Jacobson, G.P. & McCaslin, D.L. (2008). Assessment of falls risk in the elderly. In G.P. Jacobson & N.T. Shepard (Eds). *Balance Function Assessment and Management*. (pp.585-612). San Diego: Plural Publishing.

Jang, Y.S, Hwang, C.H., Shin, J.Y., Bae, W.Y., Kim, L.S. (2006). Age related changes on the morphology of otoconia. *Laryngoscope.* 116(6), 996-1001. PMID: 16735917

Johnson, K.R., Erway, L.C., Cook, S.A., Willott, J.F., Zheng, Q.Y. (1997). A major gene affecting age-related hearing loss in C57BL/6J mice. *Hearing Research*. 114(1-2), 83-92. PMID: 9447922

Johnsson, L.G. (1971). Degenerative changes and anomalies of vestibular system in man. *Laryngoscope*. 81(10), 1682-1694. PMID: 4255919

Jones, S.M. (2008). Vestibular sensory evoked potentials. In G.P. Jacobson & N.T. Shepard (Eds). *Balance Function Assessment and Management*. (pp.379-404). San Diego: Plural Publishing.

Jones, S.M., Johnson, K.R., Yu, H., Erway, L.C., Alagramam, K.N., Pollack, N., et al. (2005). A quantitative study of gravity receptor function in mutant mouse strains. *Journal of the Association for Research in Otolaryngology*, 6(4), 297-310. PMID: 16235133

Jones, T.A. & Jones, S.M. (2007). Vestibular evoked potentials. In R.F. Burkard, M. Don, & J.J. Eggermont. *Auditory Evoked Potentials: Basis Principles and Clinical Application*. (pp. 332-347). Baltimore: Lippincott Williams & Wilkins.

Jones, S.M., Jones T.A., Johnson, K.R., Yu, H., Erway, L.C., Zheng, Q.Y. (2006). A comparison of vestibular and auditory phenotypes in inbred mouse strains. *Brain Research*. 1091, 40-46. PMID: 16499890

Jones, T.A., Jones, S.M., Hoffman, L.F. (2008) Resting discharge patterns of macular ganglion cells in otoconia-deficient mice. *Journal of the Association for Research in Otolaryngology*. 9(4), 490-505. PMID: 18661184

Keithley, E.M., Canto, C., Zheng, Q.Y., Fischel-Ghodsian, N., Johnson, K. (2004). Age-related hearing loss and the *Ahl* locus in mice. *Hearing Research*. 188, 21-28. PMID: 14759567

Kerber, K.A., Ishiyama, G.P., Baloh, R.W. (2006). A longitudinal study of oculomotor function in normal older people. *Neurobiology of Aging*. 27, 1346-1353. PMID: 16122840

Keskin, D., Borman, P., Ersoz, M., Kurtaran, A., Bodur, H., Akyuz, M. (2008). The risk factors related to falling in elderly females. *Geriatric Nursing.* 29, 58-63. PMID: 18267178

Kevetter, G.A. & Perachio, A.A. (1986). Distribution of vestibular afferents that innervate the sacculus and posterior canal in the gerbil. *Journal of Comparative Neurology*. 254(3), 410-424. PMID: 3491843

Khimich, D., Nouvian, R., Pujol, R., Tom Diek, S., Egner, A., Gundelfinger, E.D., et al. (2005). Hair cell synaptic ribbons are essential for synchronous auditory signaling. *Nature.* 434, 889-894. PMID: 15829963

Lagziel, A., Ahmed, Z.M., Schultz, J.M., Morell, R.J., Belyantseva, I.A., Friedman, T.B. (2005). Spatiotemporal pattern and isoforms of cadherin 23 in wild type and *waltzer* mice during inner ear hair cell development. *Developmental Biology.* 280(2), 295-306. PMID: 15882574

Leonard, R.B. & Kevetter, G.A. (2007). Structural and functional changes in the cristae ampullares of aged gerbils. *Neuroscience*. 147(3), 794-802. PMID: 17561351

Li, H.S. & Hultcrantz, M. (1994). Age-related degeneration of the organ of corti in two genotypes of mice. *Journal for Oto-rhino-laryngology and its Related Specialties*. 56(2), 61-67. PMID: 8177586

Li, A., Xue, J., & Peterson, E.H. (2008). Architecture of the mouse utricle: macular organization and hair bundle heights. *Journal of Neurophysiology*. 99(2), 718-733. PMID: 18046005

Lins, U., Farina, M., Kurc, M., Riordan, G., Thalmann, R., Thalmann, I., et al. (2000). The otoconia of the guinea pig utricle: internal structure, surface exposure, and interactions with the filament matrix. *Journal of Structural Biology*. 131(1), 67-78. PMID: 10945971

Liu, K., Li, S.N., Jiang, X.J. (2009). Quantitative analysis of the ribbon synapse number of cochlear inner hair cells in C57BL/6J mice using the three-dimensional modeling method. *Science in China Series C: Life Sciences.* 52(9), 807-812. PMID: 19802738

LoGuidice, L. & Matthews, G. (2009). The role of ribbons at sensory synapses. *Neuroscientist*. 15(4), 380-391. PMID: 19264728

Lopez, I., Honrubia, V., Baloh, R. (1997). Aging and the human vestibular nucleus. *Journal of Vestibular Research*. 7, 77-85. PMID: 9057161

Lord, S.R. & Dayhew, J. (2001). Visual risk factors for falls in older people. *Journal of the American Geriatrics Society*. 49(5), 508-515. PMID: 11380741

Lundberg, Y.W., Zhao, X., Yamoah, E.N. (2006). Assembly of the otoconia complex to the macular sensory epithelium of the vestibule. *Brain Research*. 1091(1), 47-57. PMID: 16600187

Lsm 510 upgrade zen 2009 (2009). (Adobe Reader version)

Lyon, M.J. & Davis, J.R. (2002). Age-related blood flow and capillary changes in the rat utricular macula: a quantitative stereological and microsphere study. *Journal of the Association for Research in Otolaryngology*. 3(2), 167-173. PMID: 12162366

Lyon, M.J. & King, J.M. (1997). Aging rat vestibular ganglion: II. Quantitative electron microscopic evaluation. *The Annals of Otology, Rhinology, and Laryngology*. 106(9), 753-758. PMID: 9302907

Lyon, M.J. & Wanamaker, H.H. (1993). Blood flow and assessment of capillaries in the aging rat posterior canal crista. *Hearing Research*. 67(1-2), 157-165. PMID: 8340267

Lysakowski, A. & Goldberg, J.M. (1997). A regional ultrastructural analysis of the cellular and synaptic architecture in the chinchilla cristae ampullares. *Journal of Comparative Neurology*. 389(3), 419-443. PMID: 9414004

Lysakowski, A. & Goldberg, J.M. (2008). Ultrastructural analysis of the cristae ampullares in the squirrel monkey (Saimiri sciureus). *Journal of Comparative Neurology*. 511, 47-64. PMID: 18729176

Marchetti, G.F. & Whitney, S.L. (2005). Older adults and balance dysfunction. *Neurologic Clinics.* 23(3), 785-805. PMID: 16026676

Martinez-Dunst, C. Michaels, R.L., Fuchs, P.A. (1997). Release sites and calcium channels in hair cells of the chick's cochlea. *Journal of Neuroscience.* 17(23), 9133-9144. PMID: 9364060

Matthews, G. & Fuchs, P. (2010). The diverse roles of ribbon synapses in sensory neurotransmission. *Nature Reviews. Neuroscience.* 11(12), 812-822. PMID: 21045860

Means, K., Rodell, D.E., O'Sullivan, P.S. (2005). Balance, Mobility, and Falls Among Community-Dwelling Elderly Persons: Effects of a Rehabilitation Exercise Program. *American Journal of Physical Medicine*. 84, 238-250. PMID: 15785256

Merchant, S.N., Velazquez-Villasenor, L., Tsuji, K., Glynn, R.J., Wall, C. 3rd, Rauch, S.D. (2000). Temporal bone studies of the human peripheral vestibular system. Normative vestibular hair cell data. *Annals of Otology, Rhinology, & Laryngology Supplement*. 181, 3-13. PMID: 10821229

Mock, B. (2008). Functional aging of the inner ear sensory systems in mouse models of age related hearing loss. Doctoral Dissertation. East Carolina University.

Mock, B., Jones, T.A., Jones, S.H. (2011). Gravity receptor aging in the CBA/CaJ strain: A comparison to auditory aging. *Journal Association for Research in Otolaryngology*. 12(2), 173-183. PMID: 21052761

Moody, H.R. (2009). Aging: concepts and controversies (H.R. Moody, Ed.). Thousand Oaks, CA: Pine Forge Press.

Moser, T., Brandt, A., Lysakowski, A. (2006). Hair cell ribbon synapses. *Cell Tissue Research*. 326(2), 347-359. PMID: 16944206

Murayama, E., Takagi, Y., Ohira, T., Davis, J.G., Greene, M.I., Nagasawa, H. (2002). Fish otolith contains a unique structural protein, otolin-1. *European Journal of Biochemistry*. 269(2), 688-696. PMID: 11856329

Naisbitt, S., Kim, E., Cheng Tu, J., Xiao, B., Salo, C., et al. (1999). Shank, a novel family of postsynaptic density proteins that binds to the NMDA receptor/PSD-95/GKAP complex and cortactin. *Neuron*. 23, 569-582. PMID: 10433268

Naito, Y., Newman, A., Lee, W.S., Beykirch, K., Honsubia, V. (1995). Projections of the individual vestibular end-organs in the brain stem of the squirrel monkey. *Hearing Research*. 87(1-2), 141-155. PMID: 8567431

National Institute on Aging (2006). Falls and older adults. Retrieved August 6, 2009 from NIH Senior Health web site: http://nihseniorhealth.gov/falls/causesandriskfactors/02.html

National Institute on Deafness and Other Communication Disorders (2010). Presbycusis. Retrieved September 10, 2011 from NIH web site: http://www.nidcd.nih.gov/health/hearing/presbycusis.htm

Nazareth, A.M. & Jones, T.A. (1998). Central and peripheral components of short latency vestibular responses in the chicken. *Journal of Vestibular Research*. 8(3), 233-252. PMID: 9626650

Nemoto, M., Morita, Y., Mishima, Y., Takahashi, S., Nomura, T., Ushiki, T., et al. (2004). Ahl3, a third locus on chromosome 17 affecting age-related hearing loss. *Biochemical and Biophysical Research Communications*. 324(4), 1283-1286. PMID: 15504353

Nouvian, R., Beutner, D., Parsons, T.D., Moser, T. (2006). Structure and function of the hair cell ribbon synapse. *The Journal of Membrane Biology*. 209(2), 153-165. PMID: 16773499

Ochi, K. & Ohashi, T. (2003). Age-related changes in the vestibular-evoked myogenic potentials. *Otolaryngology-Head and Neck Surgery*. 129(6), 655-659. PMID: 14663431

Ouagazzal, A.M., Reiss, D., Romand, R. (2006). Effects of age-related hearing loss on startle reflex and prepulse inhibition in mice on pure and mixed C57BL and 129 genetic background. *Behavioral Brain Research.* 172(2), 307-315. PMID: 16814879

Paige, G.D. (1992). Senescence of human visual-vestibular interactions. 1. Vestibulo-ocular reflex and adaptive plasticity with aging. *Journal of Vestibular Research*. 2(2), 133-151.

Paige, G.D. (1994). Senescence of human visual-vestibular interactions: smooth pursuit, optokinetic, and vestibular control of eye movements with aging. *Experimental Brain Research*. 98(2), 355-372. PMID: 1342388

Park, J C., Hubel, S.B., Woods, A.D. (1987). Morphometric analysis and fine structure of the vestibular epithelium of aged C57BL/6NNia mice. *Hearing Research.* 28, 87-96. PMID: 3038820

Pawley, J.B. (Ed.). (2006). *Handbook of biological confocal microscopy*. New York, NY: Springer Science+Business Media, LLC.

Peterka, R.J., Black, F.O., Schoenhoff, M.B. (1990). Age-related changes in human vestibule-ocular reflexes: pseudorandom rotation tests. *Journal of Vestibular Research*. 1(1), 61-71. PMID: 1670138

Peterka, R.J., Black, F.O., Schoenhoff, M.B. (1990). Age-related changes in human vestibule-ocular reflexes: sinusoidal rotation and caloric tests. *Journal of Vestibular Research: Equilibrium & Orientation*. 1, 49-59. PMID: 1670137

Prasad, V., Semwogerere, D.,Weeks, E.R. (2007). Confocal microscopy of colloids. *Journal of Physics: Condensed Matter*. 19(11), 2-20.

Rauch, S., Velazquez-Villasenor, L., Dimitri, P.S., Merchant, S.N. (2001). Decreasing hair cell counts in aging humans. *Annals of the New York Academy of Science*. 942, 220-7. PMID: 11710464

Reisine, H., Simpson, J.I., Henn, V. (1988). A geometric analysis of semicircular canals and induced activity in their peripheral afferents in the rhesus monkey. *Annals of the New York Academy of Sciences*. 545, 10-20. PMID: 2853588

Richter, E. (1980). Quantitative study of human Scarpa's ganglion and vestibular sensory epithelia. *Acta Otolaryngologica.* 90, 199-208. PMID: 6258381

Rosenhall, U. & Rubin, W. (1975). Degenerative changes in the human vestibular sensory epithelia. *Acta Otolaryngologica.* 79, 67-80. PMID: 167544

Ross, M.D., Peacor, D., Johnsson, L.G., Allard, L.F. (1976). Observations on normal and degenerating human otoconia. *The Annals of Otology, Rhinology, and Laryngology*. 85(3 pt 1), 310-326. PMID: 937958

Rusch, A., Lysakowski, A., Eatock, R.A. (1998). Postnatal development of type I and type II hair cells in the mouse utricle: acquisition of voltage-gated conductances and differentiated morphology. *Journal of Neuroscience*. 18(18), 7487-7501. PMID: 9736667

Rzadzinska, A.K., Derr, A., Kachar, B., Noben-Trauth, K. (2005). Sustained cadherin 23 expression in young and adult cochlea of normal and hearing-impaired mice. *Hearing Research*. 208(1-2), 114-121. PMID: 16005171

Schuknecht, H.F. (1964). Further observations on the pathology of presbycusis. *Archives of Otolaryngology*. 80, 369-382. PMID: 14198699

Schmitz, F. (2009). The making of synaptic ribbons: how they are built and what they do. *Neuroscientist*. 15(6), 611-624. PMID: 19700740

Severinsen, S.A., Raarup, M.K., Ulfendahl, M., Wogensen, L., Nyengaard, J.R., Kirkegaard, M. (2008). Type I hair cell degeneration in the utricular macula of the waltzing guinea pig. *Hearing Research*. 236(1-2), 33-41. PMID: 18191927

Severinsen, S.A., Sorensen, M.S., Kirkegaard, M., Nyengaard, J.R. (2010). Stereological estimation of total cell numbers in the young human utricular macula. *Acta Otolaryngologica*. 130(7), 773-779. PMID: 20082566

Sha, S., Kanicki, A., Dootz, G., Talaska, A.E., Halsey, K. Dolan, D., et al. (2008). Age-related auditory pathology in the CBA/J mouse. *Hearing Research*. 243(1-2), 87-94. PMID: 18573325

Sheng, M. & Kim, E. (2000). The shank family of scaffold proteins. *Journal of Cell Science*. 113, 1851-1856. PMID: 10806096

Shiga, A., Nakagawa, T., Nakayama, M., Endo,T., Iguchi, F., Kim,T-S., et al. (2005). Aging effects of vestibulo-ocular responses in C57BL/6 mice: Comparison in alteration with auditory function. *Audiology & Neuro-Otology*. 10, 97-104. PMID: 15650301

Stamataki, S., Francis, H.W., Lehar, M., May, B.J., Ryugo, D.J. (2006). Synaptic alterations at inner hair cells precede spiral ganglion loss in aging C57BL/6J mice. *Hearing Research*. 221, 104-118. PMID: 17005343

Sterling, P. & Matthews, G. (2005). Structure and function of ribbon synapses. *Trends in Neuroscience*. 28, 20-29. PMID: 15626493

Su, H.C., Huang, T.W., Young, Y.H., Cheng, P.W. (2004). Aging effect on vestibular evoked myogenic potential. *Otology & Neurotology*. 25(6), 977-980. PMID: 15547429

Suzuki, H., Ikeda, K., Takasaka, T. (1997). Age-related changes of the globular substance in the otoconial membrane of mice. *Laryngoscope*. 107(3), 378-381. PMID: 9121317

Takumida, M. & Zhang, D.M. (1997). Electron probe X-ray microanalysis of otoconia in guinea pig inner ear: a comparison between young and old animals. *Acta Oto-laryngologica*. 117(4), 529-537. PMID: 9288208

Walther, L.E. & Westhofen, M. (2007). Presbyvertigo-aging of otoconia and vestibular sensory cells. *Journal of Vestibular Research*. 17(2-3), 89-92. PMID: 18413901

White, J.A., Burgess, B.J., Hall, R.D., Nadol, J.B. (2000). Pattern of degeneration of the spiral ganglion cell and its processes in the C57BL/6J mouse. *Hearing Research*. 141(1-2), 12-18. PMID: 10713491

Zenisek, D., Horst, N.K., Merrifield, C., Sterling, P., Matthews, G. (2004). Visualizing synaptic ribbons in the living cell. *Journal of Neuroscience*. 24(44), 9752-9759. PMID: 15525760

Zheng, Q.Y., Johnson, K.R., Erway, L.C. (1999). Assessment of hearing in 80 inbred strains of mice by ABR threshold analyses. *Hearing Research*.130, 94-107. PMID: 10320101

APPENDIX A. IACUC APPROVAL FORM

East Carolina University

1907-2007 CENTENNIAL

Animal Care and Use Committee
212 Ed Warren Life Sciences Building
East Carolina University
Greenville, NC 27834

252-744-2436 office
252-744-2355 fax

October 22, 2009

Sherri Jones, Ph.D.
Department of CSDI
HSB 3310
East Carolina University

Dear Dr. Jones:

Your Animal Use Protocol entitled, "Morphological Correlates of Gravity Receptor Functional Aging," (AUP #P054) was reviewed by this institution's Animal Care and Use Committee on 10/22/09. The following action was taken by the Committee:

"Approved as submitted"

Please contact Dale Aycock at 744-2997 prior to biohazard use

A copy is enclosed for your laboratory files. Please be reminded that all animal procedures must be conducted as described in the approved Animal Use Protocol. Modifications of these procedures cannot be performed without prior approval of the ACUC. The Animal Welfare Act and Public Health Service Guidelines require the ACUC to suspend activities not in accordance with approved procedures and report such activities to the responsible University Official (Vice Chancellor for Health Sciences or Vice Chancellor for Academic Affairs) and appropriate federal Agencies.

Sincerely yours,

Robert G. Carroll, Ph.D.
Chairman, Animal Care and Use Committee

RGC/jd

enclosure

APPENDIX B. RECIPES

4% Paraformaldehyde (PFA) in 0.1M Phosphate Buffer (PB)

Ingredients	Desired Final Volume					
	100 mL	200 mL	300 mL	400 mL	500 mL	1 L
Paraformaldehyde	4.0 g	8.0 g	12.0 g	16.0 g	20.0 g	40.0 g
0.2 M Phosphate Buffer	50 mL	100 mL	150 mL	200 mL	250 mL	500 mL
Distilled Water	See directions for actual volume					
Sodium Hydroxide	See directions for actual volume					

Use: Fixative for animal perfusion: post-fixative for dissected tissues

Source: Vendor: Sigma (P-6148)

Biosafety Hazard: Toxic, Flammable, Carcinogen

Safety Precautions: Prepare (use in fume hood, avoid contact or inhalation)

Disposal: 1. Liquid waste: Hazardous waste container (plastic or glass)

2. Solid waste (powder residue and saturated filter paper): Biohazard trash can

Preparation (use fume hood):

1. Heat less than ½ the desired final volume of distilled water to 60^{o}C
2. Turn off heat
3. Add Paraformaldehyde while stirring
4. Add concentrated Sodium Hydroxide drop-wise until suspension clears
5. Add 0.2 M Phosphate Buffer
6. Adjust pH to 7.2-7.4 (storage: one week at 4^{o}C)

0.01 M Phosphate Buffered Saline

Ingredients	Desired Final Volume					
	100 mL	200 mL	300 mL	400 mL	500 mL	1 L
Sodium Chloride	0.8 g	1.6 g	2.4 g	3.2 g	4 g	8 g
Potassium Chloride	0.02 g	0.04 g	0.06 g	0.08 g	0.1 g	0.2 g
Sodium Phosphate	0.144 g	0.29 g	0.43 g	0.58 g	0.72 g	1.44 g
Potassium Phosphate	0.024 g	0.05 g	0.07 g	0.10 g	0.12 g	0.24 g
Distilled Water	80 mL	160 mL	240 mL	320 mL	400	800 mL

Use: Washing buffer for dissected tissues

Source: Vendor: Sigma

Biosafety Hazard: Corrosive, Irritative

Safety Precautions: Use gloves, Eyeshields

Disposal: 1. Liquid waste: Dispose in accordance to local and state regulations

Preparation:

1. Add Sodium Chloride, Potassium Chloride, Sodium Phosphate, and Potassium Phosphate to distilled water while stirring
2. Storage: store at room temperature

0.01 M Phosphate Buffered Saline with 3% Triton (0.3% PBST)

Ingredients	Desired Final Volume					
	100 mL	200 mL	300 mL	400 mL	500 mL	1 L
0.3% Triton-X 100	0.3 mL	0.6 mL	0.9 mL	1.2 mL	1.5 mL	3 mL
0.01 M Phosphate Buffered Saline	99.7 mL	199.4 mL	299.1 mL	398.8 mL	498.5 mL	997 mL

Use: Washing buffer for dissected tissues

Source: Vendor: Sigma

Biosafety Hazard: Corrosive, Irritative

Safety Precautions: Use gloves, Eyeshields

Disposal: 1. Liquid waste: Dispose in accordance to local and state regulations

Preparation:

3. Add desired amount of 0.01 M Phosphate Buffered Saline to clean bottle
4. Add 0.3% Triton to 0.01 M Phosphate Buffered Saline while stirring
5. Adjust pH to 7.4 (storage: one to two weeks at room temperature)

10% Normal Goat Serum in 0.3% Phosphate Buffered Saline with Triton X-100 (0.3% PBST)

Ingredients	Desired Final Volume				
	10 mL	20 mL	40 mL	50 mL	100 mL
10% Normal Goat Serum	1 mL	2 mL	4 mL	5 mL	10 mL
0.3% Phosphate Buffered Saline with Triton X-100	9 mL	18 mL	36 mL	45 mL	90 mL

Use: Blocking solution for dissected tissues

Source: Vendor: Invitrogen

Biosafety Hazard: Corrosive, Irritative

Safety Precautions: Use gloves, Eyeshields

Disposal: 1. Liquid waste: Dispose in accordance to local and state regulations

Preparation:

1. Add desired amount of 0.01 M Phosphate Buffered Saline to clean bottle
2. Add 10% Normal Goat Serum
3. Stir vigorously
4. Storage: (storage: one to two weeks at 4^{o}C)

5% Normal Goat Serum in 0.3% Phosphate Buffered Saline with Triton X-100 (0.3% PBST)

Ingredients	Desired Final Volume				
	10 mL	20 mL	40 mL	50 mL	100 mL
5% Normal Goat Serum	0.5 mL	1 mL	2 mL	2.5 mL	5 mL
0.3% Phosphate Buffered Saline with Triton X-100	9.5 mL	19 mL	38 mL	47.5 mL	95 mL

Use: Blocking solution for dissected tissues

Source: Vendor: Invitrogen

Biosafety Hazard: Corrosive, Irritative

Safety Precautions: Use gloves, Eyeshields

Disposal: 1. Liquid waste: Dispose in accordance to local and state regulations

Preparation:

1. Add desired amount of 0.01 M Phosphate Buffered Saline to clean bottle
2. Add 10% Normal Goat Serum
3. Stir vigorously
4. Storage: (storage: one to two weeks at 4^{o}C)

APPENDIX C: LIST OF REAGENTS AND ANTIBODIES

Fixative

Paraformaldehyde
Source: Sigma-Aldrich

Buffer

Triton X-100
Source: Sigma-Aldrich

Blocking

Normal Goat Serum
Source: Invitrogen

Primary Antibodies

Mouse anti-CtBP2
Source: BD Transduction Laboratories

Rabbit anti-Shank1a
Source: Neuromics

Secondary Antibodies

Alexa 488 goat-anti-mouse
Source: Invitrogen

Alexa 633 goat-anti-rabbit
Source: Invitrogen

Mounting Medium

ProLong® Gold antifade reagent
Source: Invitrogen

ADDRESSES

Sigma-Aldrich

Sigma-Aldrich Corp.
3050 Spruce St.
St. Louis, MO 63103
Phone: (800) 325-3010
Email: cssorders@sial.com
Fax: (800) 325-5052

Invitrogen

Life Technologies
Attn: Customer Service
3175 Staley Road
Grand Island, NY 14072 USA
Phone: (800) 955-6288
Email: customerservice@customerservice@lifetech.com
Fax: (800) 331-2286

BD Transduction Laboratories

BD Biosciences
2350 Qume Dr.
San Jose, CA 95131
Phone: (877) 232-8995
Email: Industrial_CS@bd. Com
Fax: (410) 316-4770

Neuromics

Neuromics
5325 West 74th St.
Suite 8
Edina, MN 55439
Phone: (866) 350-1500
Email: pshuster@neuromics.com
Fax: (612) 677-3976

APPENDIX D: PROTOCOLS

Utricle Dissection

1. Take out temporal bone (TB) from scintillation vial and place on microscope dish
2. Bathe TB in solution in PBST
    a. If fresh dissection, use appropriate solution
3. Use dissecting microscope to view medial side of TB
4. Break TB on either side just superior to cochlea on the medial side
5. Remove broken piece away from rest of the TB
6. Use micro spatula to gently chip away bone over vestibule, beginning on side where utricle is (left side for right TB, right side for left TB) and extending to rostral bony shelf and superior canal
7. Identify anterior and horizontal ampullae attached to utricle near top of vestibule adjacent to boney shelf
8. Open membranous labyrinth on canal side of ampullae using micro eyelash tool
9. Remove otoconia using micro eyelash tool
10. Use #55 forceps to loosen (by grabbing nerve stump) and float utricle (with attached ampullae) out of vestibule and into bathing solution
11. Continue with histological processing

Confocal Protocol

(Staining for Hair Cells, Synaptic Ribbons, Post-Synaptic Receptor Sites for Mouse Utricle)

1. Dissect temporal bones and fix overnight in 4% Paraformaldehyde in 0.1 M Phosphate Buffer at room temperature.
2. Dissect utricle from the temporal bone, gently scraping off otoconia and otoconial membrane while bathed in 0.01 M Phosphate Buffered Saline with 3% Triton (PBST; 0.3 M Sodium Chloride, 0.3% Triton-X 100, 0.01 M Phosphate Buffer, pH 7.4).
3. Wash utricles with PBST three times for 15 minutes each at room temperature.
4. Apply blocking solution (10% Normal Goat Serum in PBST) overnight at 4˚C.
5. Incubate utricles in primary antibody cocktail (Mouse anti-CtBP2: C-terminal binding protein 2; BD Transduction Laboratories; 1:300; Rabbit anti-Shank1a: Neuromics; 1:300; 5% Normal Goat Serum in PBST) for 48 hours at 4 °C.
6. Wash utricles in PBST three times for 50 minutes each at room temperature.
7. Apply secondary antibodies in a cocktail (for CtBP2: Alexa 488 goat-anti-mouse RED-Invitrogen; 1:200; for Shank1a: Alexa 633 goat-anti-rabbit GREEN-Invitrogen; 1:200) overnight at 4°C (once secondary antibodies are applied, the specimens will be shielded from light).
8. Wash utricles three times (15 minutes each) in 0.01 M Phosphate Buffered Saline at room temperature.
9. Mount each utricle on a slide with ProLong® Gold antifade reagent (Invitrogen) and cover slip.

Confocal Protocol Table Hair Cells, Synaptic Ribbons, and Post-Synaptic Receptor Site Staining for Mouse Utricle			
Step	Recipe	Duration	Temperature
Fixative	4% PFA in 0.1M PB	Overnight	4°C
Washes	0.3% PBST	3x15 minutes each	Room temperature
Blocking	10% Normal Goat Serum	Overnight	4°C
1°Antibody	1:300 CtBP2 1:300 Shank1a	~48 hours	4°C
Washes	0.3% PBST	3 x 50 minutes each	Room temperature
2°Antibody	1:200 GAR 633 1:200 GAM 488	Overnight	4°C
Washes	0.01M PBS	3x15 minutes each	Room temperature
Mounting Medium	Prolong Gold		

List of Abbreviations

PFA: Paraformaldehyde

PB: Phosphate buffer

PBST: Phosphate buffered saline with Triton

CtBP2: C-terminal binding protein-2

GAR: Goat-anti rabbit

GAM: Goat-anti mouse

PBS: Phosphate buffered saline

Confocal Microscope Instructions

1. Turn lights off
2. If microscope not on, follow instructions above computer (turn air supply on, turn on microscope control located under microscope, turn on laser control, turn on computer)
    a. Username: micro
    b. Password: confocal
3. Open program
    a. Click on LSM 510 icon
    b. Scan new image
    c. Start expert mode
4. Choose lasers
    a. Click Configuration
    b. Multitrack
    c. Add track
        i. Apply
        ii. Excitation of 20 for each except for 633: 25
        iii. Check to make sure appropriate filters are applied. Filters should be slightly above excitation wavelength (Exp. Alexa 633: LP 650, Alexa 488: BP 505-550)
5. Turn on lasers
    a. Laser icon
    b. Argon: click standby
    c. Other/s: turn on

6. Open scan and microscope
    a. Scan
        i. Frame 512
        ii. Scan speed usually 9
        iii. In channels section, set pinhole to 1
7. Microscope
    a. Change objective to 10X
        i. When changing objective, click pinhole of 1 for each
        ii. Optical slice for each tract should be 5
8. Light beside microscope
    a. F1 stays at 100
    b. F2 should be at 35
9. Put slide in inverted
    a. All the way to one side is best so it doesn't move when you need to change objectives
10. Transmitted light
    a. Should be on 2 (filter under fluorescent light should be on *none*)
    b. Find image
    c. Turn off
11. LSM
    a. Z setting
    b. Fast X-Y
    c. Split X-Y

d. Do not keep lasers in scanning XY mode any longer than necessary as it may damage the scanning device
e. Click stop

12. Click mode button
    a. Select scanning time that works best for image (3.93 sec often good)
13. Detector gain for each channel (image brightness)
    a. Should be between 600-750 (typically 750 works best)
14. Palette
    a. Range indicator
    b. Get few red (oversaturation: change detector gain) and few blue (under saturation: change amplifier offset (background signal)) for each channel
    c. Click no palette to return to regular mode
15. Z stack
    a. Scan icon
    b. Z-stack
    c. Click fast XY
    d. Find upper limit of stack
        i. Click on mark first button
        ii. Move objective down (counterclockwise) to find lower limit of stack and click stop
    e. 10X interval: 4.0 is fine, 63X interval: 0.2 is fine: enter
    f. Mark first and last
    g. Z-slice: click on optimal settings

h. Click on z slice

    i. Click optimal interval

    ii. Close

i. Click start

16. To save:

a. New MDB

b. Exp: 1/8/10 CTBP2 GluR 2/3 as folder name

c. Then name for sample Exp. C57 10X CTBP2 GluR 2/3

d. Save to flash drive: D: Lever

17. Side notes

a. Amplifier gain shouldn't change

b. Fine focus: move towards you: outer, mover away from you: deeper

c. To put water on 63X, go to empty position

d. To put oil on 100X, go to 63X position

e. Better to do 10X and 63X or 10X, 20X, and 63X

f. Usually only do z-stacks

18. If last person for the day, turn off everything (air supply last)